Okinawa Institute of Science and Technology
Graduate University

Thesis submitted for the degree

Doctor of Philosophy

Behavioral and transcriptomic analysis of embryonic microglia during colonization and degeneration of zebrafish retina

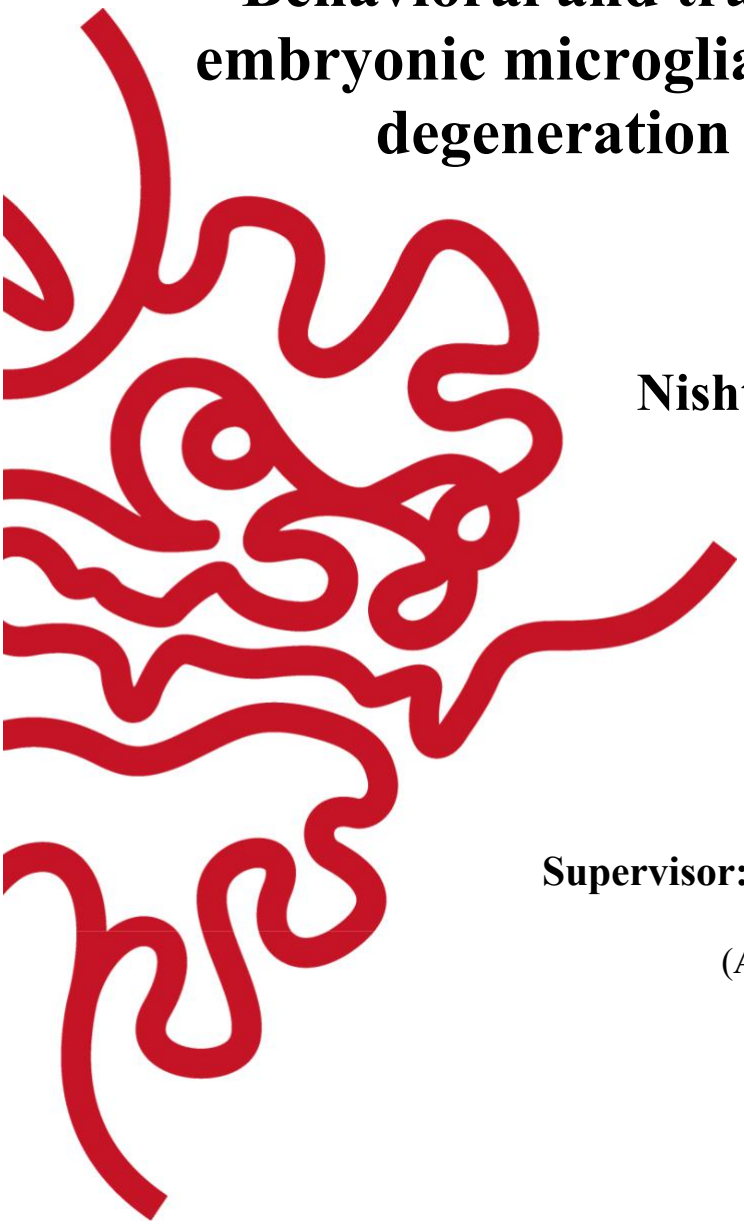

by

Nishtha Ranawat

Supervisor: Prof. Ichiro Masai

(April 2020)

Declaration of Original and Sole Authorship

I, Nishtha Ranawat, declare that this thesis entitled "Migration of embryonic microglia in zebrafish retina and changes in transcriptome therein" and the data presented in it are original and my own work.

I confirm that:

- This work was done solely while a candidate for the research degree at the Okinawa Institute of Science and Technology Graduate University, Japan.

- No part of this work has previously been submitted for a degree at this or any other university.

- References to the work of others have been clearly attributed. Quotations from the work of others have been clearly indicated, and attributed to them.
- In cases where others have contributed to part of this work, such contribution has been clearly acknowledged and distinguished from my own work.
- None of this work has been previously published elsewhere, with the exception of the following: (provide list of publications or presentations, or delete this part).

  (If the work of any co-authors appears in this thesis, authorization such as a release or signed waiver from all affected co-authors must be obtained prior to publishing the thesis. If so, attach copies of this authorization to your initial and final submitted versions, as a separate document for retention by the Graduate School, and indicate on this page that such authorization has been obtained).

Signature: (of the student) Nishtha Ranawat

Date: 13th March 2020

Behavioral and transcriptomic analysis of embryonic microglia during colonization and degeneration of zebrafish retina

1. Abstract

This work was designed to understand how embryonic microglia precursors migration relates to global processes such as blood vessel development and neurogenesis and to decipher transcriptomic signatures governing embryonic microglia behavior. The zebrafish retina provides a precise anatomical and molecularly characterized extension of forebrain to study colonization by microglia precursors. In this study we decode the mechanism driving the process of the microglia precursors colonization of developing zebrafish retina and its role in early neurodegeneration of visual system. Transgenic live imaging studies and *slbp1* mutant analysis of migrating microglia precursors into retina revealed that this migration is a step wise process depending on both retinal vasculogenesis and neurogenesis. These two key processes proceeds at the same time-scale as retinal colonization by microglia precursors. Initially microglia precursors uses emerging blood vessels system around the lens to enter the a space near basement membrane of the retina. As the wave of neurogenesis proceeds, these microglia precursors starts to migrate into retina, preferentially in neuronally differentiated neurons. Intraretinal microglia numbers decrease when retinal neurogenesis is delayed, suggesting crosstalk between early born neurons and microglia precursors. To explore microglia signaling during neurogenesis at the molecular level, we carried out a single-cell transcriptomic analysis of microglia precursors and newly matured microglia in the developing zebrafish brain.

Acknowledgements

I would like to express my sincere gratitude towards my supervisor Dr. Ichiro Masai for his constant motivation and scientific support throughout the course of my doctoral research. His supervision helped me to pursue my scientific journey as graduate student with passion and rigor. In addition, his comprehensive knowledge and more importantly, meticulous attention to minute details starting from envisioning a scientific question to devising methods to address it, has motivated me to inculcate these values in my research.

Along with my thesis advisor, I would like to thank my thesis committee members, Dr. Hiroki Ishikawa and Dr. Hidetoshi Saze, for their timely assessment and encouragement on my research.

I offer my sincere thanks to my lab members for all the support they extended during my years in the lab. A special thank you to Maria Iribarne, Yuko Nishiwaki, Yuki Takeuchi, Mai Omar and Swathy Babu for their insightful comments and constructive criticism. I could not have asked for better peers who made my graduate life simpler in many ways.

I would like to thank OIST for providing an atmosphere that stimulates interdisciplinary research. In addition to that, cultural exchange with peers and colleagues from various parts of the world, was indeed an enriching experience. I am grateful for all those moments and shall strive to make this world a better place.

I am grateful to my parents for their unconditional love, never-ending support and silent sacrifices they made to help me achieve my goals in life. I am very thankful to my partner, Hemanta Sarmah, for his love and understanding throughout my PhD. He helped me remain motivated, focused, and grounded through thick and thin.

Finally, a word of thanks to two special friends Kimberly Remund, and Christopher Pettoukhoff for extending encouragement and support throughout my research and the days of thesis writing.

List of Abbreviations

7AAD	7-Aminoactinomycin D
ALPM	anterior lateral plate mesoderm
bHLH	basic helix-loop-helix
BMP4	Bone Morphogenetic Protein 4
cDNA	complementary DNA
CMZ	ciliary marginal zone
CNS	Central nervous system
CSF1r	Colony stimulating factor 1 receptor
DNMLL1	Dynamin-like protein 1
dNTP	Deoxynucleotide triphosphates
dpc	Days of Post Coitus
dpf	days post fertilization
DRP1	dynamin-related protein 1
E. coli	*Escherichia coli*
E3	Embryo media 3
EF1a	Elongation factor 1-alpha.
EGFP	Enhanced Green Fluorescent Protein
EMPs	Erythro-myeloid progenitors
ER	Endoplasmic reticulum
EtOH	Ethanol
FACS	Fluorescence-activated cell sorting
FASTQ	FASTA and quality
FDR	False discovery rate
Fgf	Fibroblast growth factor
FP	Forward primer
FPKM	Fragments per kilo base per million mapped reads
GAPDH	Glyceraldehyde 3-phosphate dehydrogenase
GS	Goat Serum
HBSS	Hank's balanced salt solution
HDAC1	Histone deacetylase 1
HEPES	4-(2-hydroxyethyl)-1-piperazineethanesulfonic acid
Hh	Hedgehog
hpf	hours post fertilization
HSCs	Hematopoietic stem cells
ICM	inner cell mass
IL1b	Interleukin1 beta
IL2	Interleukin2
IPL	inner plexiform layer
$MgCl_2$	Magnesium chloride
microRNA	micro RNA
MO	morpholino
mpf	months post fertilization
MQ	Milli-Q grade
mRNA	messenger RNA
NaOH	Sodium Hydroxide
NaOH	Sodium Hydroxide
NSCs	Neural stem cells

OMM	Outer mitochondrial membrane
PB	Phosphate buffer
PCA	Principal component analysis
PCR	polymerase chain reaction
PFA	paraformaldehyde
PTU	phenylthiourea
qRT-PCR	quantitative real-time PCR
RBI	rostral blood islands
RGCs	retinal ganglion cells
RP	Reverse Primer
RT	room temperature
SLBP1	Stem Loop Binding Protein1
TGFb	Transforming Growth Factor Beta
tnnt2a	troponin T type 2a
TSA	Trichostatin A
TUNEL	terminal deoxynucleotidyl transferase-mediated dUTP nick-end labeling
UMAP	Uniform Manifold Approximation and Projection
VEGF	Vascular endothelial growth factor
WT	wild type

Table of Contents

List of figures

List of Tables

2. Problem statement and Aims

Retina is derived from the ventral region of the forebrain, and is the first brain region to be colonized by migrating microglial precursors from periphery. Microglial colonization of the retina was described years ago; however, many questions remain un-addressed. For instance, how is microglial migratory pathway to the developing retina determined? What kind of signals promote microglial precursors to colonize the retina? Are microglial precursors intrinsically programmed to migrate into the retina or guided by some extrinsic signal from brain microenvironment? Over the past two decades, with the advancement in imaging and microscopy, zebrafish has emerged as an excellent vertebrate animal model to study cell proliferation, cell differentiation, and cell migration during development. Here, we used zebrafish to study migration of microglial precursors from periphery into the developing retina. The current understanding of ocular development enables us to investigate the underlying cellular and molecular events related to microglial colonization into retina. Furthermore, the role of microglia in neuronal cell death was addressed using zebrafish retinal cell-death mutant. Such studies will advance our understanding of microglial contribution in neuroprotection versus neurodegeneration.

Aims of research in my PhD thesis are:

(1) to elucidate relationship between microglial colonization and ocular blood vessels.

(2) to understand microglial colonization during retinal neurogenesis.

(3) to identify role of microglia in retinal apoptosis, if any.

(4) Single cell RNAseq analysis of microglial precursors.

These research topics will advance our understanding of mechanism of microglial colonization into the retina, role of microglia in retinal apoptosis, and functional diversity of microglia.

3. Introduction: Origin of microglia in developing vertebrate embryos

3.1. Origin of microglia in vertebrates

Microglia have long been regarded as macrophages that reside within the brain and spinal cord. They constitute innate immune defense system of the central nervous system (CNS). Unlike other cells of the CNS that originate from ectoderm lineage, microglia are derived from mesoderm and migrate into the developing CNS during early embryonic stages of vertebrates (Alliot et al., 1999). Several lineage tracing experiments have been done across species to define precursors of microglia in CNS parenchyma (Ajami et al., 2007, Mildner et al., 2007, Ferrero et al., 2018).

Embryonic hematopoiesis and microglia in mammals

Two sites of embryonic hematopoiesis in mammals are : the extra-embryonic yolk-sac (YS) and the fetal liver. These sites give rise to three distinctive hematopoietic waves, namely: primitive, transient and definitive (Bertrand et al., 2005). The embryonic yolk sac is the first site of hematopoiesis in mammalian embryos. In mice the first two waves: primitive and transient waves produces primitive macrophages and prenatal erythromyeloid precursors (EMPs) respectively. YS derived primitive wave depends upon transcription factors, Pu.1, a member of ETS family of transcription factor, (Rosenbauer and Tenen, 2007) and Irf8, a heterodimeric partner of Pu.1 (Kierdorf et al., 2013). Macrophage precursors/primitive macrophages generated by first wave of hematopoiesis contributes to early macrophages throughout the embryo, including microglia precursors in developing brain (Ginhoux et al., 2010b).

The third wave originates within the embryo-proper's aorta-gonads-mesonephros region with the emergence of Hematopoietic stem cells (HSCs) at E10.5 (Medvinsky et al., 2011). With

embryonic development, EMPs and HSCs colonize the fetal liver, making it the major hematopoietic organ after E11.0. The transient and definitive wave of hematopoiesis is independent of Pu.1 but depends on c-Myb, Runx1 and Notch1. Hematopoiesis is a tightly regulated process governed by a battery of transcription factors in a timely manner. Pu.1 is involved in genesis of B-cells, macrophages and CNS parenchyma microglia (McKercher et al., 1996). IRF8 is required for microglia differentiation during development and homeostasis in adult microglia (Kierdorf et al., 2013, Masuda et al., 2012). Another transcription factor RUNX1, is a critical regulator of embryonic microglia development and proliferation of adult microglia (Ginhoux et al., 2010a, Zusso et al., 2012). Many studies have shown that primitive macrophages are the unique source of adult microglia under physiological conditions (Perdiguero et al., 2015, Kierdorf et al., 2013, Ginhoux et al., 2010b). Under steady state, like other tissue macrophages, these microglia also express surface markers such as CD11b, CD64, CD115, MerTK and F4/80 (Gautier et al., 2012). Surface markers and transcription factors only expressed by adult microglia are sialic acid-binding immunoglobulin-type lectin H (Siglec-H), Fc receptor-like S (Fcrls), and purinergic receptor P2Y G-protein coupled 12 (P2ry12) (Chiu et al., 2013, Butovsky et al., 2014).

Embryonic hematopoiesis and microglia in zebrafish

In zebrafish, successive waves of primitive and definitive hematopoiesis occurs at anatomically distinct regions. Embryonic primitive hematopoiesis starts at 11 hpf at anterior and posterior lateral plate mesoderm (Bertrand and Traver, 2009). A transient definitive wave starts at posterior blood island which gives rise to EMPS. At 26hpf, definitive wave from dorsal aorta contributes to HSCs in zebrafish embryo (de Jong and Zon, 2005, Bertrand and Traver, 2009). Around 48hpf, HSCs migrate and colonize caudal hematopoietic tissue, which is equivalent to mouse fetal liver (Kissa et al., 2008).

Microglia in zebrafish are divided into two groups: embryonic and adult microglia (Ellett and Lieschke, 2010, Jing and Zon, 2011). Embryonic microglia are generated by the primitive wave originating from anterior lateral plate mesoderm (ALPM) or rostral blood island (RBI). These primitive macrophages surround the yolk after 15 hours post-fertilization (hpf), and thereafter migrate toward the developing brain, making their way into the retina during 22 – 40 hpf (Herbomel et al., 2001b), followed by entry into the other parts of brain at 3 dpf. Similar to mammals, the first wave of microglia differentiation in zebrafish depends on Pu.1 (Lieschke et al., 2002, Bennett et al., 2001). The second wave of microglia which contributes to adult microglia, originates from the ventral wall of dorsal aorta (VDA) (Xu et al., 2015, Bertrand et al., 2007). The second wave of microglia differentiation primarily depends on Runx1 (Xu et al., 2015). From 15dpf onwards, Runx-1 dependent microglia starts colonizing the brain and replaces the RBI-derived embryonic microglia by 3 months post-fertilization (mpf). HSCs derive from endothelium of the VDA, expand and generates blood cell lineage including microglia by circulating and homing through hematopoietic organs such as kidney and liver (Bertrand et al., 2007, Jin et al., 2009). Since c-Myb is required for establishment of HSCs, it is also critical for establishment of adult microglia in zebrafish (Ferrero et al., 2018).

In zebrafish, genetic markers*: mpeg* (macrophage expressed 1, tandem duplicate 1) (Ellett et al., 2011, Walton et al., 2015) and *mfap4* (microfibril associated protein 4) (Walton et al., 2015)are commonly used to label myeloid cells including microglia. Myeloid cells start expressing *mpeg1.1* and *mfap4* from ~20hpf onwards. Based on the anatomical location of *mpeg1.1* or *mfap4* positive cells, they can be divided into specialized subtypes. *Mpeg1.1*/*mfap4* positive cells localized to brain regions and retina are identified as microglia precursors/microglia. Before maturation, the *mpeg1.1* or *mfap4* positive myeloid cells are

called microglia precursors. Microglia precursors are known to undergo differentiation into mature microglia at 60 hpf (Herbomel et al., 2001b).

3.2. Microglia in vertebrate retina under physiological conditions

Retinal microglia share similar morphological and functional properties as that of brain microglia (Ling, 1982, McCarthy et al., 2013). Retinal microglia change their morphology and location during development. In mouse, retinal microglia show amoeboid shape during postnatal stages, whereas adult retinal microglia show a ramified shape (Rathnasamy et al., 2019). Microglia are initially distributed throughout the immature retina (Ashwell et al., 1989). Accordingly as retinal cell differentiation proceeds, microglia increasingly localize in the inner plexiform layer (Santos et al., 2008). Ex-vivo studies in mice have shown that retinal microglia dynamically change cell shape, although the overall symmetrical arbor pattern and size is maintained (Lee et al., 2008). However, under normal conditions, retinal microglia do not show apparent migratory behavior, but insult to retinal microenvironment triggers their directed migration (Lee et al., 2008).

Microglia are required for neural circuit maturation and maintenance of retinal neurons. Cx3CR1 is a receptor of Cx3CL1 (Fractalkine) and specifically expressed in microglia (Liang et al., 2009, Ishizuka et al., 2017). Fractalkine-Cx3CR1 signaling promotes synapse pruning by microglia, impairment of which has been linked to Autism in humans (Ishizuka et al., 2017). Genetic knockdown of Cx3CR1 in microglia induced distorted allocation of cilia proteins and failure of outer segment elongation in retina by P17 and eventually cone photoreceptors in retina were completely depleted by P30 (Jobling et al., 2018), suggesting that Fractalkine-Cx3CR1 signaling is important for photoreceptor maturation. Few embryonic zebrafish studies have shown microglia role in proliferation and differentiation of retinal progenitors. It was

reported that knockdown of *Csf1r* delays microglia/macrophage migration from yolk to the retina , which subsequently affects proliferation of retinal progenitors (Huang et al., 2012). A growth factor, Progranulin-a, is specifically expressed in microglia and modulates photoreceptor genesis and maintenance (Walsh and Hitchcock, 2017).

4. Chapter I: Retinal blood vessels and microglial precursors

4.1. Introduction

4.1.1. Blood vessel system of embryonic zebrafish retina

In 2001, Isogai and colleagues used confocal microangiography to examine and describe vascular anatomy of the embryonic zebrafish. They described the formation of primary ocular vasculature, describing optic artery (OA), optic vein (OV), nasal ciliary artery (NCA), dorsal ciliary vein (DCV) and the choroidal ciliary vein (CVP). Fluorescent beads combined with microangiography was used to visualize lumenized vessels, hence primary vasculature formed by un-lumenized endothelial cells remained unexplored (Isogai et al., 2001). This limitation was overcame by establishment of zebrafish transgenic lines, *Tg[Fli1a:EGFP]* (Lawson and Weinstein, 2002) and *Tg[flk1:EGFP]* (Jin et al., 2005). These lines served as a strong tool for time-lapse analysis of primary vasculature formation. Taking advantage of these transgenic lines, many studies described the development of ocular vasculature in zebrafish embryos (Lawson and Weinstein, 2002, Kitambi et al., 2009, Proulx et al., 2010, Kaufman et al., 2015).

The cranial vasculature, including the ocular vessel, in zebrafish embryos is derived from two angioblast clusters: Rostral organizing center (ROC) and the midbrain organizing center (MOC) (Proulx et al., 2010, Hashiura et al., 2017). In zebrafish embryos, *Flia:EGFP* positive cells first appear within the choroid fissure and behind the medial side of lens by 24 hpf (Kitambi et al., 2009). This was confirmed by visualizing hyaloid artery (HA) reaching the optical fissure by 22 hpf (Kaufman et al., 2015). Thus, endothelial cells forming the hyaloid vasculature enter ocular region through optic fissure in early zebrafish embryos.

Zebrafish embryonic eye has a well-defined vascular system: (i) intraocular hyaloid vasculature and (ii) superficial choroidal vasculature. The hyaloid vasculature is present between posterior regions of the lens and retina, while the choroidal vasculature surrounds the optic cup (Saint-Geniez and D'Amore, 2004). Unlike mouse and human, the eye of zebrafish embryo lacks vitreous space between the lens and retina (Soules and Link, 2005). Close association between lens and hyaloid vessels has been demonstrated by fused membranes in developing zebrafish eyes (Alvarez et al., 2007).

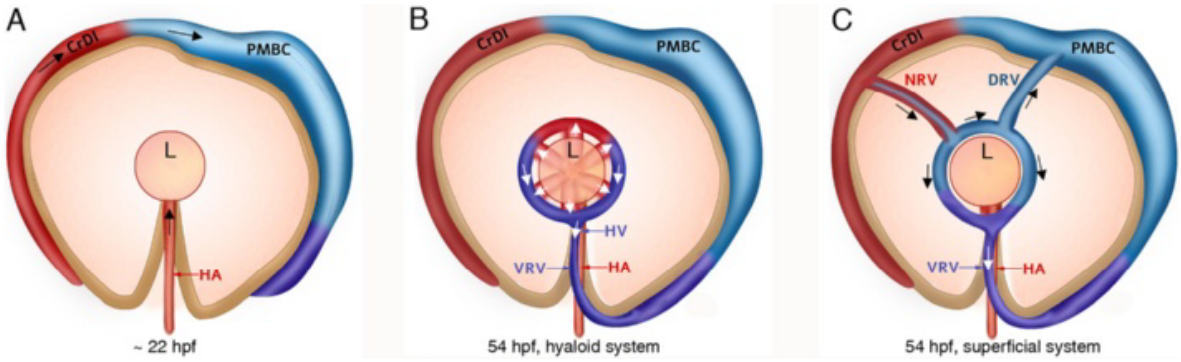

Figure 4.1: Ocular vessels origin
(A) Hyaloid artery (HA) entering through optical fissure (B) Hyaloid system around the medial side of lens (C) The complete superficial system (Kaufman et al., 2015)

Hemangioblast precursors in zebrafish are known to give rise to the hyaloid system in a VEGF dependent manner (Saint-Geniez and D'Amore, 2004, McLeod et al., 2012, Ash and Overbeek, 2000, Mitchell et al., 2006, Rutland et al., 2007). The first hyaloid cells reach the choroid fissure at approximately 18–20 hpf and migrate towards the developing lens. The primitive hyaloid artery bifurcates into nasal and temporal branches, which fuse together to form the hyaloid loop. This loop eventually gets extended into an extensively branched vessel framework encapsulating the entire posterior lens. Migration of hyaloid precursors to the ocular region is independent of lens but its maturation and maintenance has been shown to be dependent on the lens (Hartsock et al., 2014). At 2 dpf, the surface of zebrafish eye has simple superficial vessels but by 9 dpf sophisticated and elaborated choroidal vessels have replaced them. The superficial

system is made up of the nasal radial vessel (NRV), the dorsal radial vessel and the ventral radial vessel (VRV). Blood from hyaloid vessels drains into the superficial system that is of venous origin (Kitambi et al., 2009).

4.1.2. Retinal blood vessels and microglia/macrophages

Early microglia have been reported to reach brain parenchyma before vascularization (Sorokin et al., 1992, Cuadros et al., 1993, Dalmau et al., 1997, Rigato et al., 2011) . On the contrary, studies done on *Ncx 1*$^{-/-}$ mouse (Koushik et al., 2001), which lacks blood circulation due to defect in sodium calcium exchanger 1, suggests that microglia colonization into the mouse brain as blood vessel dependent event (Ginhoux et al., 2010a).

Checchin and colleagues used clodronate liposomes to deplete retinal microglia and showed loss of retinal vascular density as a consequence of it. In this study, no change in number of peripheral circulating monocytes were observed (Checchin et al., 2006). This suggests microglia-specific effect on retinal vascular development. Similar study suggested that microglia may act as a bridge during vascular sprouting (Fantin et al., 2010). This study demonstrated that absence of microglia corelates with decrease in vascular branching in hindbrain but has no effect on retinal angiogenesis. Another study demonstrated role of retinal microglia in developmental vascular remodeling where lack of retinal microglia lead to decrease in primary vascular plexus (Kubota et al., 2009). Ex-vivo studies involving retina culture have also shown that depletion of microglia in system can lead to an increase in VEGF-mediated neovascular sprouts (Unoki et al., 2010).

Extensive studies have been done on ocular blood vessels development in zebrafish embryos. But to our knowledge, there is still no detailed developmental description that links ocular blood vessel development with microglia migration. This chapter illustrates the early microglia migration in relation with the developing blood vessel system of zebrafish retina.

4.2. Materials and methods

Fish strains

Zebrafish (*Danio rerio*) were maintained using standard procedures (Westerfield, 1993). RIKEN wako (RW) was used as a wild-type strain for mutagenesis (Masai et al., 2003). Alleles of mutants, *slbp1*^{rw440} (Imai et al., 2014), and *add*^{rw399} (*hdac1*) (Yamaguchi et al., 2005), were used. Transgenic lines *Tg[ath5:EGFP]*^{rw021} were used to monitor *ath5* gene expression (Masai et al., 2005). *Tg[EF1α:mCherry-zGem]*^{oki011} (Mochizuki et al., 2014) was used for visualization of cell-cycle phases. *Tg[mfap4:tdTomato-CAAX]*^{oki058} *and Tg[mpeg1.1:EGFP]*^{oki053} were used for microglia and *Tg[kdrl:EGFP]*^{s843Tg} was employed to visualize blood vessels (Jin et al., 2005).

Solutions for rearing zebrafish egg and young larvae

E3 media composition:

34.8 g NaCl

1.6 g KCl

5.8 g $CaCl_2 \cdot 2H_2O$

9.78 g $MgCl_2 \cdot 6H_2O$

To prepare a 60X stock, dissolve the ingredients in H_2O, to a final volume of 2 L. Adjust the pH to 7.2 with NaOH. Autoclave. To prepare 1X medium, dilute 16.5 mL of the 60X stock to 1 L. Add 100 μL of 1% methylene blue (Sigma-Aldrich).

Time-lapse and time-series imaging

At 0dpf, embryos were collected from set fish crosses. After 70% epiboly stage, PTU was added to E3 media containing fertilized embryos and maintained 28.5^{0}C. Transgenic live embryos were sorted on the basis of fluorescent labels at 1 dpf and anesthetized using 5% (v/v) Tricane (3-amino benzoic acid-ethylester). Anesthetized embryos were laterally mounted using 3% methyl cellulose and 0.7-1% low melting agarose on a depression slide to image retina and

peripheral tissues. E3 media containing PTU and tricaine was then added on top of solidified low melting agarose. Water dip objective of Confocal laser scanning microscope Zeiss LSM710 (40X0.8 /1.0 W Plane Apochromat) was used for imaging. The entire ocular space was imaged from top of lens to the apical end of retina at room temperature. For snapshot of ocular space of 32-54 hpf embryos, three embryos were laterally mounted and a z-stack spanning ~110 μm (1024 x 1024, 8-bit) with serial optic sections ranging from 2-4 μm (depending on optimum step size) was captured. After z-stack image was captured at a given time-point, embryos were unmounted carefully and kept in E3 media with PTU until next time-point.

Retinal vasculogenesis and associated microglia migration was captured using time-series imaging. To optimize the gap between two time points, multiple z-stacks images were captured (512 x 512, 8-bit) using live embryos and analyzed using Imaris 9.1.2 software (Bitplane). Time interval of 5 minutes between two z-stacks was found to be optimum for time-series experiments. Anesthetized embryos were laterally mounted using 3% methyl cellulose and 0.7-1% low melting agarose on a depression slide fixed on glass bottom dish. After solidification of low melting agarose, glass dish was filled with E3 media containing PTU and tricaine. The water-dip objective was used to locate the ocular space of embryo and imaging volume was set. Before starting the imaging, a thin layer of mineral oil was added on top of E3 media to decrease evaporation of E3 media during imaging. Each time-lapse captured z-stacks every 5 minutes for 5 hours at 28.5^{0}C room temperature.

BODIPY ceramide labelling

5mM BODIPY ceramide conjugated with Alexa-488 (D3834-BODIPY™ FL C_5) solution was prepared in 2% DMSO and E3 media. Embryos were raised in E3+PTU (~0.2mM Phenylthiourea) and 0.1mM BODIPY ceramide solution was added at time points (indicated

in results). Embryos in BODIPY solution were then incubated for 30 min on slow shaking at RT. Embryos were then washed with E3 media three times and mounted for imaging.

Surface rendering

Imaris 9.1.2 software (Bitplane) was used to the reconstruct surface of microglia precursors. Source channel was selected according to transgene used to label microglia. For Surface area detail, automatically generated value was selected. Absolute intensity range (25-30) was used as threshold. For filtering, area criteria (500-5000μm^2) was used.

Morpholino experiment (tnnt2a and Pu.1)

Knockdown experiments using morpholino (MO) antisense oligos were performed. STD-MO (control) was injected in comparable concentration to test-MO concentration for each experiment. Lowest possible effective concentration of MO was chosen and special care was taken so that test-MO concentration caused no morphological abnormalities in embryos as compared to STD-MO injected embryos. In addition, developmental delays due to MO injection were also monitored for each MO experiment and concentration/morpholinoes which caused severe delays were disregarded. MO against troponin T2A (MO-tnnt2a) was designed as 5'-CATGTTTGCTCTGAT CTGACACGCA-3' (Sehnert et al., 2002). MO-Pu.1 5'-GATAT ACTGATACTCCATTGGTGGT-3' was designed. MO-tnnt2a and MO-Pu.1 were injected into fertilized eggs at 0.5 mM and 0.25 mM concentration respectively.

4.3. Results

4.3.1. Microglia/macrophage precursors reaches developing retina at 30–32 hpf

In zebrafish embryos, the very first myeloid/microglia precursors originate via primitive wave of myelopoiesis around 18 hpf. Live imaging of *Tg[mpeg1.1:EGFP]* embryos showed that

these precursors migrate and reach the choroid fissure and lens region approximately at 30–32 hpf. Majority of the microglia/macrophage precursors migrate through the choroid fissure and enter into the optic cup. During retina development in 32–54 hpf, number of microglia precursors

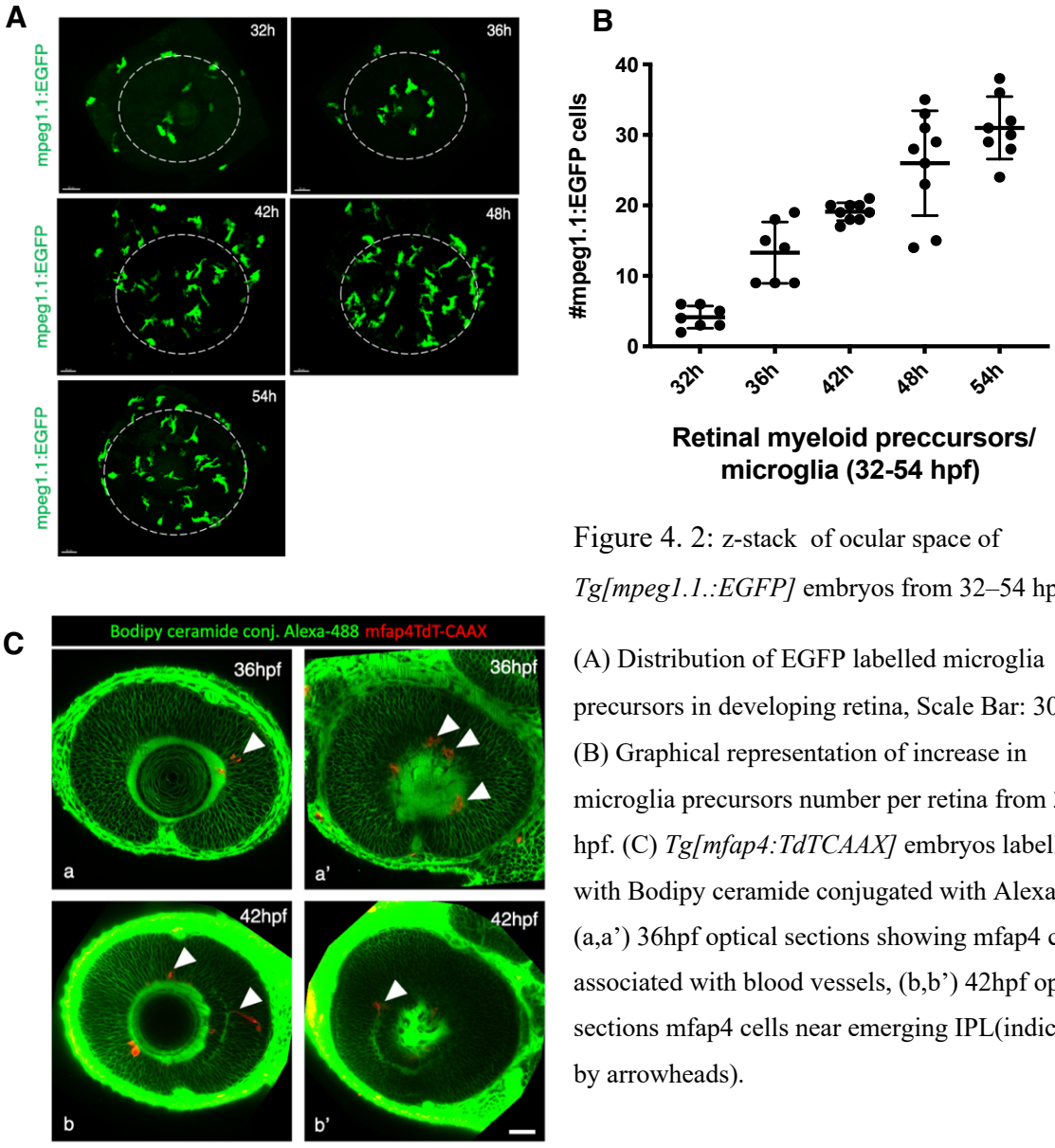

Figure 4. 2: z-stack of ocular space of *Tg[mpeg1.1.:EGFP]* embryos from 32–54 hpf

(A) Distribution of EGFP labelled microglia precursors in developing retina, Scale Bar: 30 µm (B) Graphical representation of increase in microglia precursors number per retina from 32-54 hpf. (C) *Tg[mfap4:TdTCAAX]* embryos labelled with Bodipy ceramide conjugated with Alexa-488 (a,a') 36hpf optical sections showing mfap4 cells associated with blood vessels, (b,b') 42hpf optical sections mfap4 cells near emerging IPL(indicated by arrowheads).

gradually increase within the retina. At 54 hpf, about 30–35 microglia precursors are present per retina (Fig. 4.2. A and B). To further visualize microglia precursors in optic cup, we labeled *Tg[mfap4:tdTomato CAAX]* embryos with Bodipy ceramide conjugated with Alexa 488. Bodipy ceramide labelled the retinal layer structured and mfap4 positive microglia precursors.

At 32–36 hpf, microglia precursors were associated with blood vessels located in the space between the lens and retina. At 42 hpf, mfap4 positive microglia was found near the newly emerging IPL (Fig 4.2. C)., and by 54 hpf these precursors spread throughout the fish neural retina (data not shown).

4.3.2. Microglia precursors increase by migration and not proliferation

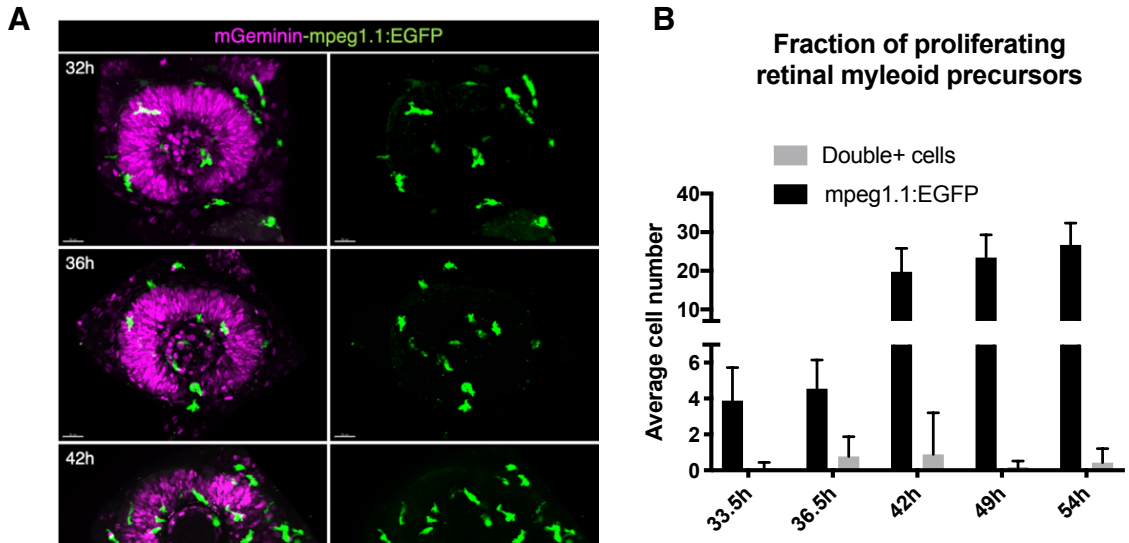

Figure 4. 3: Live imaging of *Tg[EF1α-mCherry-Geminin; mpeg1.1:EGFP]* embryos from 32–54 hpf

(A) Distribution of mCherry-Gem and EGFP labelled proliferating cells and microglia precursors respectively in developing retina, Scale Bar: 30 μm (B) Graphical representation of fraction of proliferating microglia precursor number per retina from 33–54 hpf

Based on the previous observation that microglial precursors proliferate and increase within regions of zebrafish optic tectum and midbrain regions at 4 dpf, we wanted to check whether the increase in microglia in zebrafish retina is also a result of proliferation. We established

Tg[EF1α:mCherry-Geminin; mpeg1.1:EGFP], where mCherry-Geminin marks the S/G2 phase of cell cycle and mpeg1.1 labels microglia/macrophage. Live imaging of embryos from 32–54 hpf showed that a very small fraction of cells were double positive, indicating very few microglia/macrophage cells were in S/G2 phase (Fig 4.3 A, B). Hence, the increase in microglia number in retina is majorly contributed by migration from peripheral sites/regions.

4.3.3. Microglia precursors uses blood vessels as a scaffold

Similar to microglial precursors, developing hyaloid blood vessels enter the vitreous space between lens and the neural retina via choroid fissure; however, its entry is 12 hours earlier than that of microglial precursors, suggesting guidance role of blood vessels in microglial

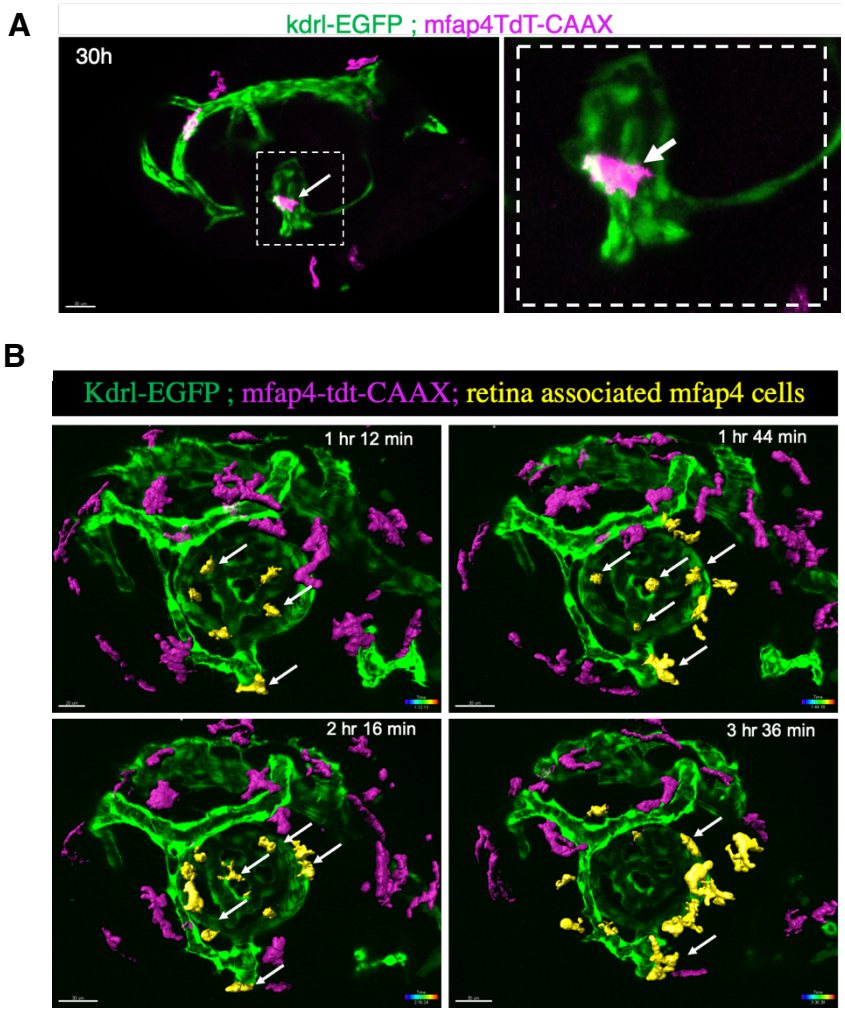

Figure 4. 4: Microglia precursors uses blood vessels as scaffold

(A) Live imaging of *Tg[Kdrl:EGFP;mfap4TdTomato-CAAX]* retinas at 30 hpf. The right panel indicates higher magnification of dotted square of the left panels. Microglial precursors and blood vessels are indicated in magenta and green color. The first microglia precursors (arrow) enters the vitreous space via choroid fissure in close association with hyaloid vessels. Scale Bar: 30 µm

(B)Live imaging of *Tg[Kdrl:EGFP;mfap4TdTomato-CAAX]* retinas at 36 hpf for 4 hours. Microglial precursors and blood vessels are indicated in magenta and green color. Microglial precursors associated with hyaloid vessels (marked as yellow) increased over time and eventual infiltrate the retina. Scale Bar: 30 µm

colonization of retina. Hyaloid blood vessels loop around the developing lens at 18–20 hpf. To study the interaction of blood vessels and microglia precursors, we established *Tg[Kdrl:EGFP;mfap4:TdTomato-CAAX]*, in which EGFP and TdTomato-CAAX label vessel endothelial cells and membrane of microglia precursors, respectively. Live image of this transgenic retinas shows that the first microglia precursor was associated with hyaloid loop around the lens at 30 hpf (Fig 4.4 A).

Live imaging of *Tg[Kdrl:EGFP;mfap4:TdTomato-CAAX]* for 4 hours demonstrated that microglia precursors are associated with ocular hyaloid blood vessels, then enter the vitreous space between the lens and the neural retina along ocular hyaloid blood vessels, and eventually infiltrate the retina. In the surface rendering analysis of live imaging data, we marked mfap4 positive microglial precursors associated with ocular hyaloid vessels as yellow and the rest of mfap4 positive cells as magenta (Fig. 4.4). In Fig 4.4 B, around 37 hpf, only 4–5 yellow cells are present on hyaloid vessel surface. Within 40 mins, the number of yellow cells increased to 10–11 and few cells could be seen infiltrating the retina. Over next 2 hours, yellow cells associated with hyaloid blood vessel were increased and infiltrated the retina. This rapid increase in the number of microglia precursors may be due to their migration from periphery or activation of microglial cell proliferation by shortening of cell cycle length; however, the latter possibility is very unlikely because the fraction of microglial precursors in S phase is very low (see Fig. 4.3). Hence, we infer that migrating microglial precursors use ocular hyaloid vessels as a scaffold to enter optic cup and eventually infiltrate retina.

Analysis of live imaging data of 30 hpf *Tg[Kdrl:EGFP;mfap4:TdTomato-CAAX]* embryos showed an interesting behavior of early mfap4 positive cells entering the optic cup (Fig 4.5). One or two mfap4 positive cells once entered the optic cup, but did not stay within 2 hours, and exited from the optic cup via the choroid fissure. This behavior was observed only in the

early stage 32 hpf, and we did not observe mfap4 positive cells exiting the optic cup later during development.

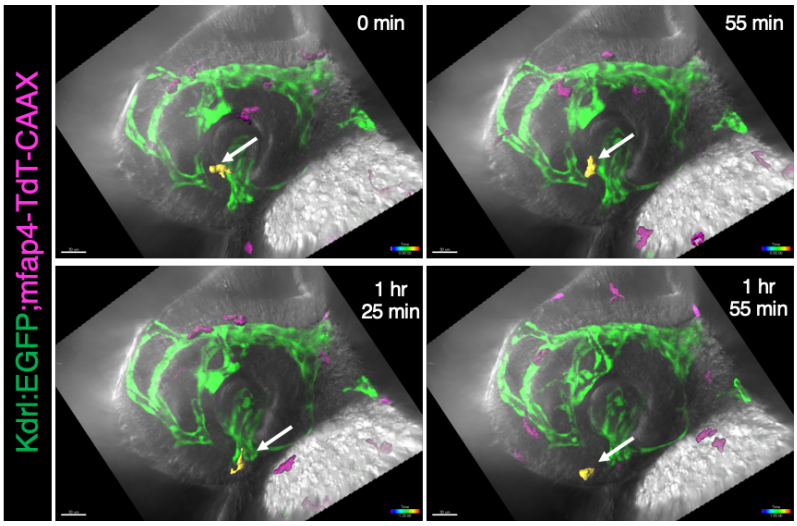

Figure 4. 5: Live imaging of *Tg[Kdrl:EGFP;mfap4TdTomato-CAAX]* retinas at 30 hpf. Microglial precursors and blood vessels are indicated in magenta and green respectively. Microglial precursor cell exiting the optic cup within 2 hours is labeled by surface rendered yellow and arrow. Scale Bar: 30 µm

4.3.4. Blocking circulation and regression of blood vessels decrease microglia precursors in retina

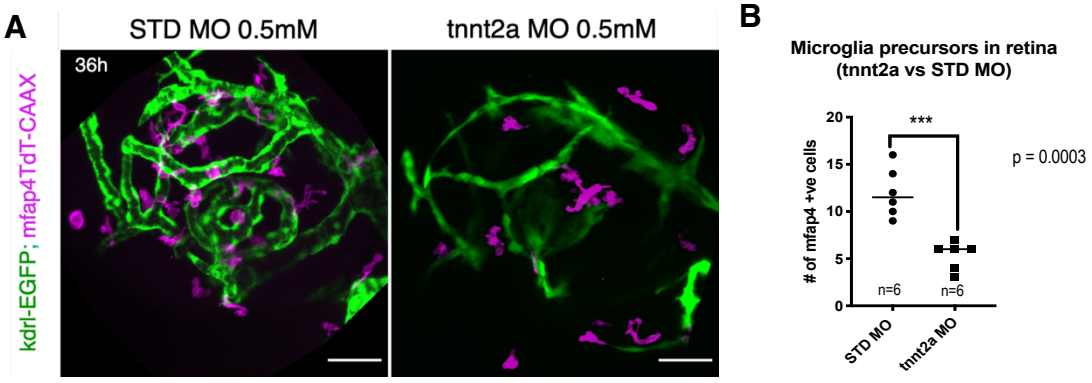

Figure 4. 6: Circulation block in 36 hpf *Tg[Kdrl:EGFP;mfap4TdTomato-CAAX]* embryos

(A) *tnnt2a* morphants compared to control morphants showing decrease in microglial precursors (magenta) in the retina. Green indicates ocular blood vessels. Scale Bar: 30 µm
(B) Histogram of the number of microglial precursors in *tnnt2a* and control morphants. The number of microglial precursors significantly decreased in *tnnt2a* morphants.

To confirm the role of blood vessels and circulation in microglial colonization of zebrafish retina, we designed experiments to pharmacologically inhibit vessels development. All major chemical inhibitors of blood vessel development such as SU5416 block VEGF receptor signaling, and simultaneously compromises myelopoiesis as side effect. Here we focused on troponin T type 2a (tnnt2a), whose knockdown is known to impair heart contraction in *tnnt2a* mutants, *silent heart* (*sih*) (Sehnert et al., 2002). We blocked blood circulation in zebrafish *Tg[Kdrl:EGFP;mfap4TdTomato-CAAX]* embryos injected with morpholino antisense against *tnnt2a*. As blood flow is indispensable for vasculogenesis in zebrafish (Chen et al., 2012), blood circulation blockage caused regression of superficial and hyaloid blood vessel system in zebrafish retina. In *tnnt2a* morphants, microglial precursors significantly decreased in number at 36 hpf, although the morphology of microglial precursors was comparable to control morphants (Fig 4.6).

4.3.5. Retinal blood vessels develop normally in absence of primitive myeloid precursors

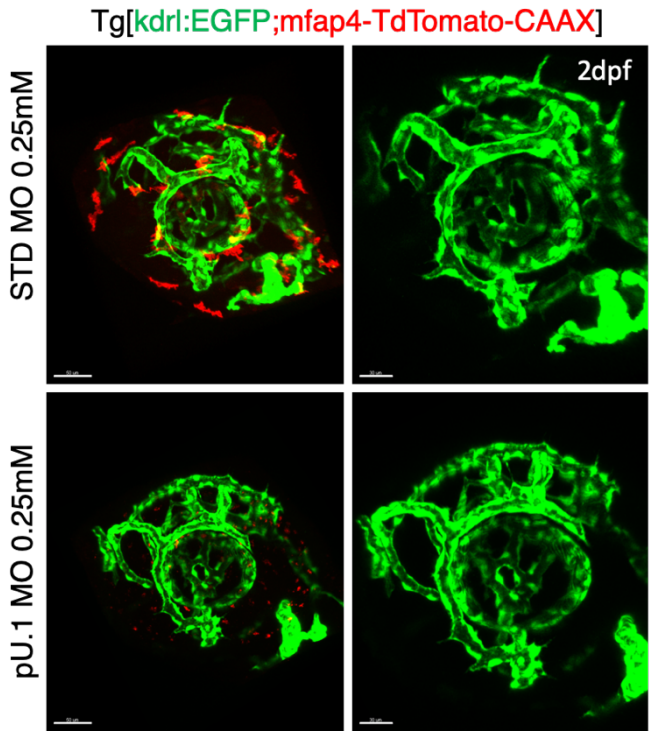

Figure 4. 7: Blood vessel formation in zebrafish *pu.1* morphants *Tg[Kdrl:EGFP;mfap4TdTomato-CAAX]* embryos at 2 dpf shows normal formation of superficial and hyaloid blood vessels in absence of primitive wave of microglial precursors. Scale Bar: 30 µm

Previous studies in mice have shown that microglia are indispensable for blood vessels formation in retina (Lobov et al., 2005, DiezRoux and Lang, 1997). However, in the zebrafish retina, the hyaloid vessel forms 10 hours prior to the entry of the first microglia precursor into the optic cup. To confirm that blood vessels development is normal in absence of microglia precursors, we inhibited *pu.1* using its morpholino in *Tg[Kdrl:EGFP;mfap4:TdTomato-CAAX]* embryos. In *pu.1* morphants, we observed normal ingression of hyaloid vessels into the choroid fissure and their morphological integrity comparable to control morphants at 2 dpf (Fig. 4.7). Hence, the absence of microglia precursors does not affect retinal blood vessels formation.

4.4. Discussion

Microglial colonization of brain, which consists of migration and seeding of microglia precursors from periphery into developing brain, is commonly observed across vertebrates. Many studies in zebrafish model have traced the path of migrating microglial precursors from periphery into midbrain, especially the optic tectum. Molecular mechanisms including p53 dependent neuronal apoptosis (Casano et al., 2016b), long-range Ca^{2+} waves, and ATP release have been suggested to colonize microglia in the optic tectum (Sieger et al., 2012b); however, mechanism that promotes microglial colonization of zebrafish developing retina has not been investigated. We show that the first microglia precursor arrives as early as 30 hpf at choroid fissure in the optic cup. These precursors are associated with ocular blood vessels and migrate into the vitreous space between the lens and retina along ocular blood vessels. During retinal development, the number of ocular microglial precursors progressively increase. After microglia enter the optic cup, they are associated with ocular blood vessels around the lens and start to infiltrate the neural retina after 42 hpf (see Fig. 4.1C).

Migration of microglia precursors into the optic tectum around 4 dpf is independent of blood circulation in zebrafish (Herbomel et al., 2001a, Rossi et al., 2015). However, the migration of

microglial precursors into the optic cup depends on ocular blood vessel system. Inhibition of ocular blood circulation in zebrafish significantly reduces the number of ocular microglia precursors. Because blood flow is critical for proper formation of blood vessels, inhibition of ocular blood circulation leads to regression of ocular blood vessel framework. Therefore, the reduction in ocular microglial precursors could be caused by defects in blood circulation and blood vessel formation. Our data strongly suggests that microglial precursors uses developing blood vessels as a scaffold to enter the optic cup from periphery.

5. Chapter II: Neurogenic state and migration of microglia precursors into retina

5.1. Introduction

5.1.1. Neurogenesis in vertebrate brain

Neurogenesis is the process by which proliferative neural progenitors gives rise to post-mitotic neurons (Schmidt et al., 2013, Appel and Chitnis, 2002). Neural development consists of four major steps: (1) induction of neural plate, (2) patterning of different brain subdomains, (3) neurogenesis and neuronal cell differentiation, and (4) neural circuit formation. BMP4 is prominently expressed in the ventral side of blastula embryos in vertebrate animals and promotes epidermis fate in ectoderm (Sasai and DeRobertis, 1997, Wilson et al., 1997, Wessely et al., 2001). Neural plate is induced in dorsal ectoderm by Noggin and Chordin, which directly bind BMP4 ligands and inhibit BMP signaling pathway to confer neural fate in ectodermal cells (Lumsden and Krumlauf, 1996). After neural plate forms, neurogenic program is initiated in three striped regions, which are aligned along anterior-posterior axis in neural plate and generates motor neurons and interneurons in the spinal cord. Neurogenesis is generally regulated by a group of proneural basic helix-loop helix (bHLH) transcription factors, which are vertebrate homologues of *Drosophila achaete-scute* complex and *atonal* genes, two membrane proteins Delta and Notch, which are homologues of *Drosophila* neurogenic genes, and anti-neurogenic bHLH transcription factors HES, which are vertebrate homologue of *Drosophila hairy* and *enhancer-of-split* complex (Blader et al., 1997, Korzh and Strahle, 2002, Allende and Weinberg, 1994). A diverse but specific neuronal cell types are generated in each of brain subregions by specific genetic programs and environmental cues (Spemann and Mangold, 2001, Lumsden and Krumlauf, 1996, Doniach and Musci, 1995). From later stages of embryonic development, neural stem cells (NSCs) are specified in the ventricular zone of

the brain and continue to generate neural progenitor cells, which subsequently generate post-mitotic neurons (Streit et al., 2000, Streit et al., 1997, Wilson et al., 2001, Rentzsch et al., 2004). Neurogenesis was thought to occur only in embryonic stages of mammals; however, neurogenesis also occurs in a very few restricted regions of the adult brain in mammals (Lois and Alvarezbuylla, 1993, Kuhn et al., 1996, Eriksson et al., 1998, Gould, 2007). Neural stem cells are dictated by extrinsic factors such as Wnt and FGF families. FGF induces expression of *soxB1* family, which specifies neuroectodermal fate intrinsically (Streit et al., 1997, Sasai, 1998). Both neural stem cells and neural progenitors expresses Sox2 which is required for maintenance of progenitor fate. Pou2/Oct4 and Sox2 cooperatively suppress neuronal inhibitory factors like *her3* (Okuda et al., 2010, Reim and Brand, 2006). During neurogenesis, neural progenitors undergo three cell-division modes: (1) proliferative symmetric cell division, (2) asymmetric neurogenic cell division and (3) symmetric neurogenic cell division. Proliferative symmetrical division generates two proliferative progenitor daughter cells. Asymmetric neurogenic cell division generates one proliferative progenitor daughter cell and the other post-mitotic neuron. This asymmetric fate determination is believed to be regulated by Notch signaling (Del Bene et al., 2008). In the last mode of neurogenesis, symmetric neurogenic cell division majorly occurs to consume a pool of progenitor cells.

5.1.2. Extrinsic and intrinsic mechanism of neurogenesis in zebrafish retina

In developing zebrafish retina, neurogenesis is initiated in region adjacent to the optic stalk around 25 hpf (Masai et al., 2000). Neurogenesis starts at ventro-nasal retina from a cluster of cells called ventro-nasal patch and then propagates to dorsal region in a wave like manner. After sweeping neurogenic events from the central retina to the peripheral retina, neurogenesis wave reaches temporal end of the retina (Masai et al., 2000, Hu and Easter, 1999). Laser ablation experiments of optic stalk in zebrafish demonstrated that optic stalk acts as a source

of factors which initiates retinal neurogenesis (Masai et al., 2000). Further studies established that optic stalk expresses Fgf3 and Fgf8 that are required for the initial induction of retinal neurogenesis (Martinez-Morales et al., 2005). A proneural bHLH gene *ath5* (also referred to as *atoh7*) expression is initiated in retinal progenitor cells undergoing in G2 phase just prior to their final mitosis, which generate post-mitotic neurons (Poggi et al., 2005) *ath5* expression continues in newly differentiating post-mitotic neurons (Masai et al., 2000). So, *ath5* expression represents retinal neurogenesis and also promotes retinal ganglion cell (RGC) differentiation (Kay et al., 2001).

It was reported that spatial progression of retinal neurogenesis is severely delayed in zebrafish *hedgehog* (*hh*) pathway mutants (Neumann and Nuesslein-Volhard, 2000). Drawing parallels with mechanism of *Drosophila* compound eye development, a sequential-induction model was suggested to explain spatial propagation of retinal neurogenesis in vertebrates, in which newly differentiated RGCs provide Shh for self-propagation of neurogenesis wave (Neumann and Nuesslein-Volhard, 2000, Zhang and Yang, 2001, Masai et al., 2000). However, explant experiments in chick suggested that production of RGCs does not depends on pre-existing RGCs (McCabe et al., 1999). Interestingly, forskolin treatment, which inhibits Hh signaling, markedly inhibited progression of retinal neurogenesis without altering initial induction of retinal neurogenesis at the ventronasal retina (Masai et al., 2005). It was also suggested that midline CNS tissue-derived Shh is involved in propagation of *ath5* expression in retina (Stenkamp and Frey, 2003). Although the role of Hh in retinal neurogenesis is not perfectly specified, FGF and Hh are required for spatial and temporal patterning of zebrafish retinal neurogenesis.

Previous studies have identified zebrafish mutants, in which retinal neurogenesis is compromised. In zebrafish *histone deacetylase 1* (*hdac1*) mutants, retinal progenitor cells fail to generate post-mitotic neurons but rather over-proliferate (Yamaguchi et al., 2005). HDAC1

promotes retinal neurogenesis by suppressing Wnt and Notch signaling pathway, which promotes retinal progenitor cell proliferation and inhibits neurogenesis, respectively. Thus, acetylation status of histone is also important for decision between proliferation and neurogenesis in zebrafish.

5.1.3. Laminar structure of zebrafish retina

During retinal neurogenesis, progenitor cells divide at apical position of retinal neuroepithelium subsequently moves basally, and form stratified retinal layers (Baye and Link, 2005). Neurogenesis gives rise to five major-classes of retinal neurons and Müller glia, which together form three nuclear layers, separated by two plexiform layers (Cepko et al., 1996, Livesey and Cepko, 2001). Classical cell lineage analyses demonstrated that RGCs are the first born retinal neurons (Hu and Easter, 1999, Rapaport et al., 2004, BeleckyAdams et al., 1996), followed by amacrine cells and cone photoreceptors. Later horizontal and bipolar cells, and rod photoreceptors differentiate. A schematic representation of retinal layers is shown in Fig.5.1.

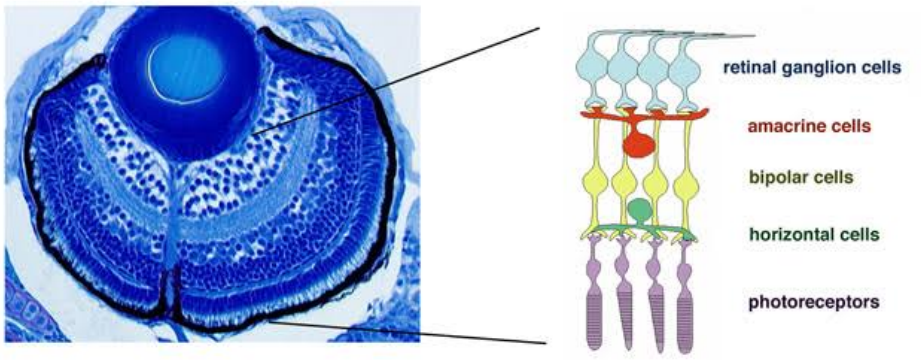

Figure 5. 1: Neuronal layers in 4 dpf zebrafish retina

5.1.4. Retinal neurogenesis is delayed in zebrafish *slbp1* mutant

Retinal neurogenesis is severely delayed in *stem-loop binding protein 1* (*slbp1*) mutant (Imai et al., 2014). Slbps are known to bind to a stem-loop structure at 3' end of histone mRNAs

(Marzluff, 1992). Binding of Slbps to histone mRNAs is required for pre-mRNA processing and assist in shuttling these mRNAs from nucleus to cytoplasm for translation (Mullen and Marzluff, 2008). Histone proteins are essential for cell-cycle progression as they play structural roles in chromatin assembly. Many studies have shown that Slbp1 is essential for histone protein translation during cell-cycle progression. In the zebrafish retina, cell-cycle progression is tightly coupled with neurogenesis. In zebrafish *slbp1* mutants, interference in histone genesis delays retinal progenitor cell proliferation, which retards retinal neurogenesis (Fig. 5.2).

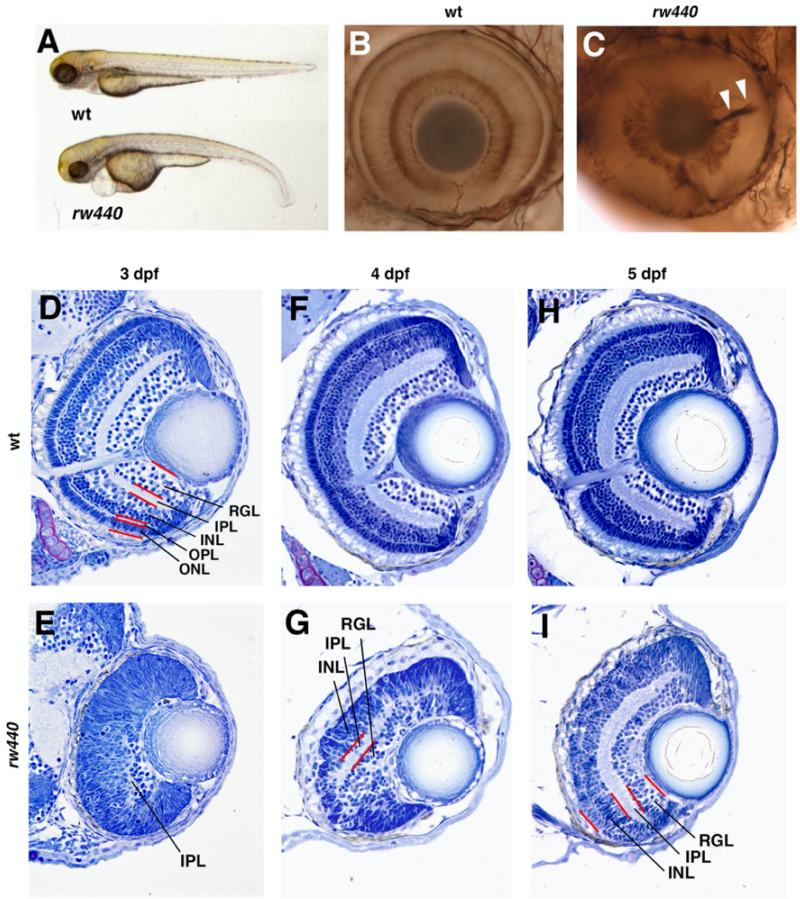

Figure 5. 2: *slbp1* (*rw440*) mutant phenotype
(A) *slbp1* embryos at 3dpf shows small eye, curled body phenotype (B,C) Staining with anti-acetylated α-tubulin shows retinal lamination defects and misrouted retinal axons within retina in *slbp1* mutant as compared to sibling and (D-I) retinal lamination delay in *slbp1* mutant as compared to sibling from 3 to 5 dpf (Adopted from (Imai et al., 2014))

In *slbp1* mutants, cell proliferation becomes slow and proliferation of retinal stem cells ceases around 2 dpf, indicating that *slbp1* is required for retinal stem cell maintenance. On the contrary, retinal progenitor cells continue to proliferate slowly in central retina and continue to generate neurons around 5dpf. Notch signaling maintains the proliferative state of retinal progenitors in *slbp1* mutants. Thus, Notch and Slbp1 are required for progenitor cell proliferation and

subsequent neurogenesis. In addition to delayed neurogenesis, *slbp1* mutant exhibits retinal axons failure to exit from optic cup and impaired choroid fissure closure.

5.1.5. Neurogenesis and microglia

Many mammalian studies showed that microglia can modulate adult neurogenesis (Gebara et al., 2013, Aarum et al., 2003, Bachstetter et al., 2011). Existence of neural progenitor cells in adult mammalian brain raised questions regarding cells or factors directing maintenance and proliferation of neural progenitor cells. Presence of microglia cells in a proximity of neural progenitor cell niches made them a prime candidate. Aarum and colleagues showed that soluble factors released from mouse microglia cell can direct migration of CNS neural progenitor cells. Microglia also holds the capacity to influence both adult and embryonic derived neural progenitor cells (Aarum et al., 2003). It was reported that microglia activation via Fractalkine-CX(3)CR1 signaling pathway and subsequent release of IL-1β are essential for survival and proliferation of neuronal progenitor cells (Bachstetter et al., 2011). A non-mammalian study suggested role of microglia in retinal neurogenesis during zebrafish development. This study showed that delaying microglia migration into developing zebrafish retina by knocking down *Csf1r,* causes delay in cell-cycle exit in retinal progenitors and absence of neuronal differentiation (Huang et al., 2012).

Presence of microglia in neural stem cell niche like subventricular zone and sub-granular zone of dentate gyrus in hippocampus also rose the possibility that neural progenitor cells could influence microglia behavior present in neurogenic niches. An elegant study showed that neural progenitor cells produce factors like tissue inhibitor of metalloproteinase type-1 (TIMP-1), VEGF, haptoglobin, which are known modulators of microglia functions (Mosher et al., 2012). These studies suggest reciprocal and context-dependent communication between neuronal

progenitors and microglia. Here we studied zebrafish retina to decipher the correlation between microglia colonization and neurogenesis.

5.2. Materials and methods

Time-lapse imaging

As previously described in Chapter I. Transgenic live embryos were anesthetized using 5% (v/v) Tricane (3-amino benzoic acid-ethylester) and laterally mounted using 1% low melting agarose on a depression slide to image retina. Confocal laser scanning microscope Zeiss LSM710 (40X0.8 /1.0 W Plane Apochromat) was used for live imaging.

Cryosections

PTU treated embryos at desired developmental stages were fixed with 4% PFA overnight. Samples were washed in Phosphate Buffer (PB) and transferred to 12.5%, 20% and 30% serial dilution of sucrose at room temperature. Samples were kept in 30% sucrose overnight at 4^0 C. Following day samples were embedded in OCT and stored at -80^0 C. OCT blocks were used to cut 7–10 μm sections using cryostat.

Transplant experiment

Reagent required: Ringer solution recipe

NaCl (MW: 58.44 gm)	13.65 gms
KCl (MW: 74.55 gm)	0.432 gms
CaCl2.2H2O (MW 147.01 gm)	0.530 gms
HEPES (MW 238.31 gm)	2.38 gms
MilliQ H2O	Make up volume to1000 mL

Embryos with synchronized developmental stage were collected from pair-wise crosses of both donor and host strains. Donor embryos were injected with Dextran-488 at 1 – 4 cell stage. Around blastula stage (~256 cells), donor embryos with strong dextran-488 signal were selected to be used for cell transplantation experiments as donor. Labelled donor embryos were dechorionated using Pronase in glass dish and placed on agarose-coated plastic dish containing 1/3xRinger solution. Host embryos were dechorionated and placed on agarose-coated plastic dish. Both donor and host embryos were transferred into an agarose-made embryo holding mould. Using transplantation needle on manipulator, 4–5 cells were taken from donor embryos and transplanted into host embryos. Cells from one wildtype donor embryos were transplanted into 5 or 6 host embryos. Host with transplanted cells were sorted at 70% epiboly by monitoring dextran-488 expression and transferred to PTU-containing E3 media. Host embryos with donor retinal columns were sorted and used for live imaging at desired developmental stage using a confocal laser scanning microscope.

Immuno-histochemistry

Five to seven μm cryosections were prepared by cryostat and air-dried for 30 mins. Sections were washed with PO_4 Buffer (PB) at room temperature and transferred to blocking solution (PB with 0.1% Triton (PBT) + 10% goat serum) for 1 hour. Zn5 antibody in PBT+ 1% goat serum was applied at 1:50 to sections overnight at 4^0 C. Slides were washed with PBT four times at 15 minutes interval. Secondary antibody was applied at 1:500 with TO-PRO3 (0.1% v/v) (Thermo Fischer) at RT for 2 hours. Slides were washed in PBT and mounted with Fluoromount medium for observation.

RNA sequencing

Seven–ten heads of 48 hpf zebrafish embryos were cut and collected in an eppendorf containing 100 µl Sepasol kept on ice. Heads were homogenized using hand homogenizer (~20 pulses). 20µl $CHCl_3$ was added to samples and mixed gently. After centrifugation at 15000g for 15 minutes, aqueous phase was collected and mixed with 100µl isopropanol. 1µl of RNase free glycogen was added to samples. After incubating at room temperature for 10 minutes, samples were centrifuged at 15000g at 4^0 C for 15 minutes. Supernatant was removed and pellet was washed with 500 µl 75% of ethanol three times at 8000g at 4^0 C. The pellet was then resuspended in desired amount of Nuclease free water and stored at -80^0 C. RNA concentration and purity of samples were determined using Nanodrop.

Bulk RNA sequence analysis

RNA samples with RIN >7 were subjected to pair-end sequencing using Illumina HiSeq4000 platform. First quality check was performed using FastQC and read trimming was done by Trimomatic. PRINSEQ lite was used for PolyA trimming and quality filtering. The trimmed sequences were then mapped to zebrafish reference genome (GRCz11) using hisat2.1.0. Using R package (EdgeR) differentially expressed genes with FDR values <0.05 were extracted for analysis.

cDNA synthesis and qPCR analysis

Using Toyobo cDNA kit, total RNA (500 ng) was reverse transcribed by following steps:

RNA (500 ng)	X µl	Keep at 65^0 C for 5 min. Add 4DN
4DN	2 µl	Keep RNA+4DN at 37^0 C for 5 min
Water	(8-X) µl	
5X RT MM II	2 µl	Add water and 5X RT MM II to RNA+4DN (Total=10µl)

cDNA was synthesized using following steps in thermocycler:

Temperature	Time
37^0 C	15 min
50^0 C	5 min
98^0 C	5 min
4^0 C	∝

q-RT PCR analysis

Extracted RNA from 48 hpf *slbp1* sibling and mutant embryos was used to prepare cDNA using Toyobo ReverseTra Ace® qPCR RT master mix with gDNA remover. Expression level of *il34* mRNA was evaluated by quantitative PCR using following primers. mRNA of cytoplasmic actin β2, namely *actb2* (ZFIN), was used for normalization.

Forward primer for *il34* mRNA: 5'- TGGTCCAGTCCGAATGCT-3'

Reserve primer for *il34* mRNA: 5'- GCTGCACTACTGCACACTGG -3'

Forward primer for *actb2* mRNA: 5'- TGTCTTCCCATCCATCGTG -3'

Reserve primer for *actb2* mRNA: 5'- TGTCTTCCCATCCATCGTG-3'

5.3. Results

5.3.1. Microglia precursors positioned preferentially in differentiating neural retina

Retinal neurogenesis is initiated at ventro-nasal patch, adjacent to the optic stalk around 25 hpf (Masai et al., 2000). To study microglia precursor migration in context of retinal neurogenesis, we used two transgenic lines: (1) *Tg[EF1α:mCherry-zGeminin;mpeg1.1:EGFP]*, in which mCherry-zGem marks all proliferative cells undergoing in S and G2 phases (Mochizuki et al., 2014) and EGFP marks microglial precursors and mature microglia, and (2) *Tg[ath5:EGFP;mfap4:tdT-CAAX]*, in which EGFP marks postmitotic neurons and TdT-

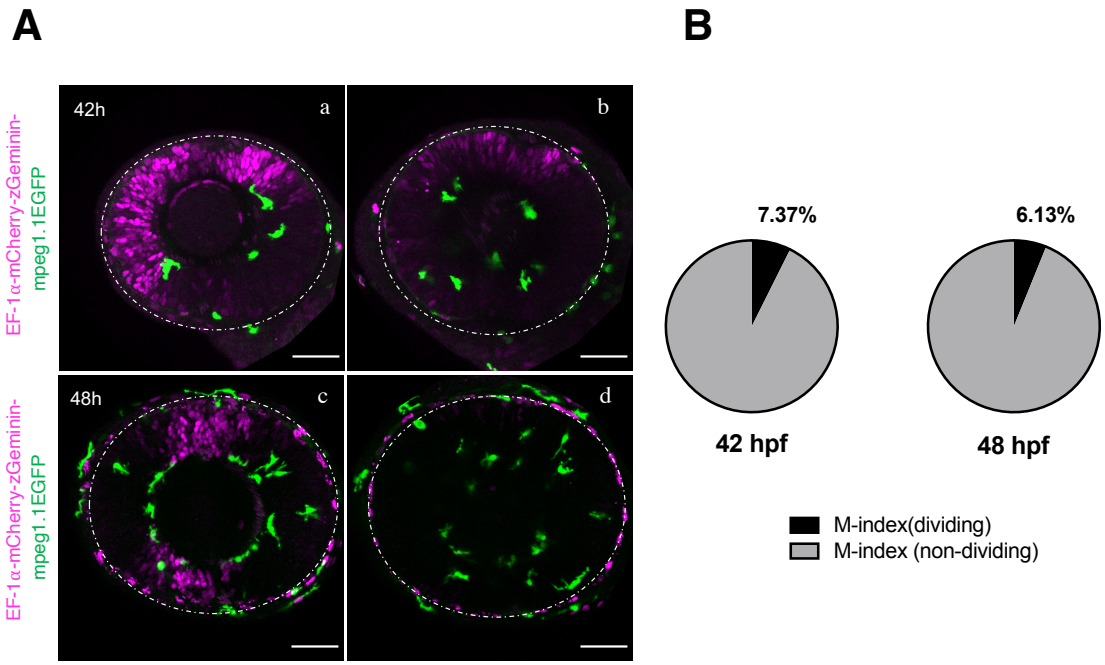

$$\text{M-index(dividing)} = \frac{\text{(\#of microglia precursors/mCh-mGem positive area)}}{\text{(\#of microglia precursors/mCh-mGem positive area + \# of microglia precursors in total area)}}$$

Figure 5. 3: Microglia precursors avoids regions of proliferation
(A) Live images of developing retina of Tg(EF1α:mCherry-zGem; mpeg1.1:EGFP) embryos at 42 hpf (a) basal (b) apical optical section and at 48hpf (c) basal (d) apical optical section. (B) M-index at 42 and 48 hpf

CAAX labels membrane of microglia precursors and mature microglia. We scanned retinas of *Tg[EF1α:mCherry-zGeminin;mpeg1.1:EGFP]* embryos from 36 – 48 hpf, and found that microglia precursors infiltrating the neural retina avoided S/G2 cell area marked by mCherry-mGem (Fig. 5.3A). To quantify the percentage of microglial precursors associated with mCherry-mGem-positive S/G2 cell region and mCherry-mGem-negative G1 or post-mitotic region, we calculated M-index combining three different optical sections within one retina (Fig. 5.3A). In total 18 sections from 6 retinas were used for calculating M-index, which is defined as shown in Fig. 5.3B.

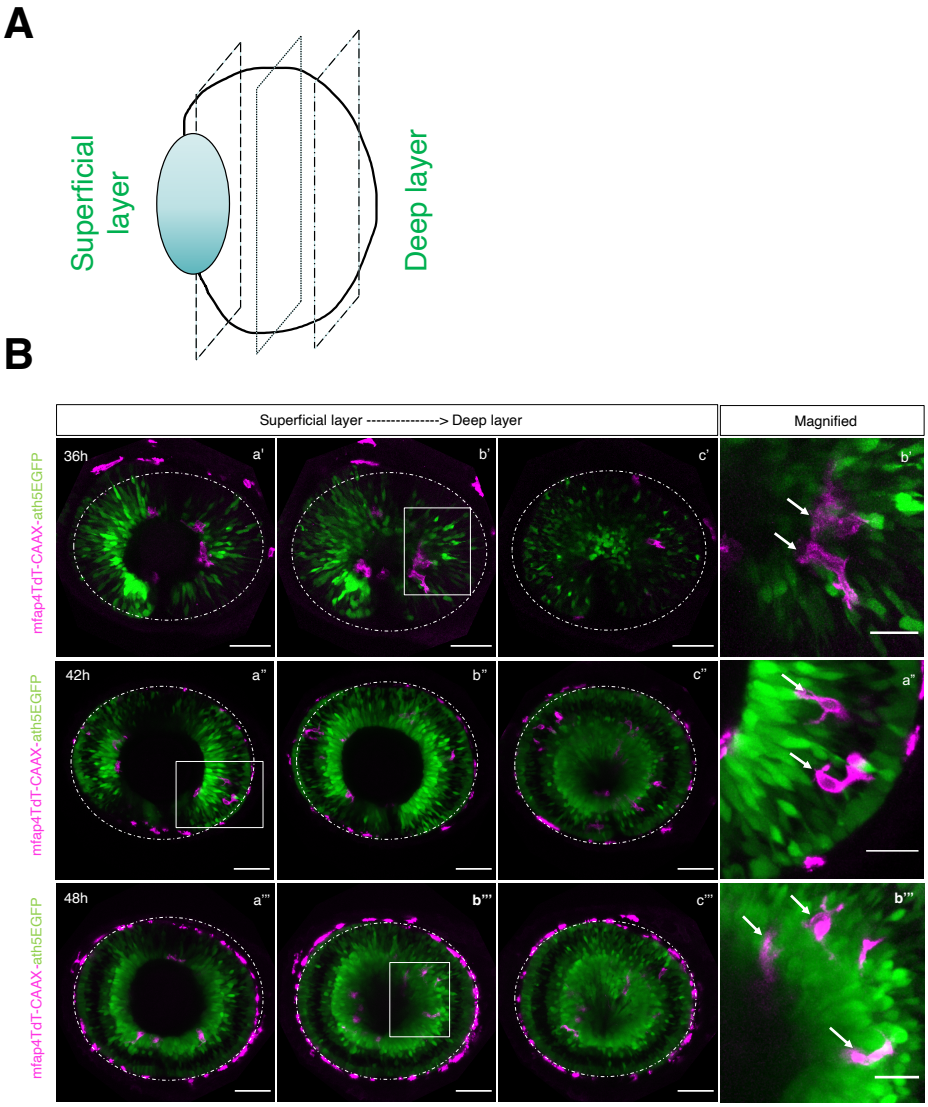

Figure 5. 4: Microglia precursors associate with differentiating neurons
(A) Cartoon showing optical sections depiction from superficial layer to deep layer (basal to apical) in a z-stack as a, b, c. (B) Optical sections from basal to apical of live images of *Tg(ath5:EGFP;mfap4TdTomato-CAAX)* retinas at 36 hpf (a', b', c'), 42 hpf (a", b", c") and 48 hpf (a"', b"', c"'). Magnified images (b', a'', b"") shows mfap4 positive cells are in close association with neurogenic ath5 positive area (arrows).

Since the fraction of G1 retinal cells is very small, these data suggest that microglial precursors preferentially infiltrate the neural retina through neurogenic area. To confirm this possibility, we scanned retinas of *Tg[ath5:EGFP;mfap4:tdt-CAAX]* embryos from 36 – 48 hpf (Figure 5.4). At 36 hpf, we observed the presence of mfap4 positive cells at the basement membrane of

differentiating neurons. From 42 – 48 hpf, mfap4 positive cells were mostly distributed in ath5 positive areas, suggesting that microglial precursors preferentially infiltrate the neural retina through neurogenic area. These observations suggest that microglial precursors colonization into the neural retina depends on neurogenic status in developing retina.

5.3.2. Microglia precursors decreases in a neurogenesis-defective mutant slbp1

To further examine whether retinal neurogenesis is required for microglial infiltration of the neural retina, we inhibited retinal neurogenesis. In zebrafish *slbp1* mutants, retinal neurogenesis is severely delayed (Imai et al., 2014). We combined *slbp1* mutants with *Tg[ath5:EGFP;mfap4:tdT-CAAX]*. Live imaging analysis showed significant difference in number of mfap4 positive cells between wild-type sibling and *slbp1* mutants retinas (Fig. 5.5A, C). There were only 4 – 5 microglia precursors in *slbp1* mutant retina as compared to 15 – 20

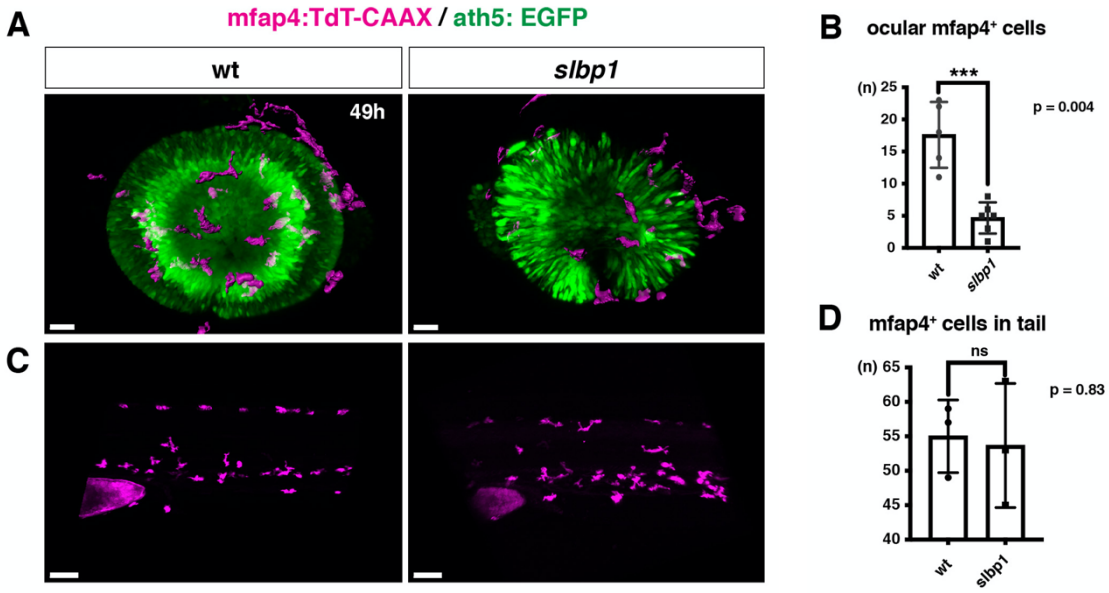

Figure 5. 5: Microglia in delayed neurogenesis mutant *slbp1*
(A, C) Live images of wild-type and *slbp1*mutant retinas (A) and tail region (C) with *Tg[mfap4TdTomato-CAAX;ath5:EGFP]* at 49 hpf. The number of mfap4+ cells (magenta) is reduced as compared with wild-type siblings. (B, D) Histogram of mfap4+ cells in wild-type sibling and *slbp1* mutant at 49hpf in retina (B) and tail region (D). mfap4+ cells are reduced in *slbp1* mutant retina as compared to sibling, whereas there is no difference in tail region.

microglia precursors in wild-type sibling retinas. Expression of *ath5:GFP* and number of mfap4 positive cells in 48 hpf *slbp1* mutant retina is comparable to 35-36 hpf wild-type retina. To exclude the possibility that *slbp1* mutation affects myeloid cell population number in peripheral regions, we examined mfap4 positive cells in tail region of *slbp1* mutants. There was no significant difference in number of peripheral macrophages between wild—type sibling and *slbp1* mutants. Although, there was no accumulation of mfap4 cells in peripheral tissues, slightly more mfap4 cells were distributed over yolk in *slbp1* mutants at 2dpf. These data support that microglial infiltration of the neural retina depends on neurogenic state of retinal cells.

5.3.3. Cxcl12/CxcR4 signaling in slbp1 mutants

In *slbp1* mutants, *cxcl12a* mRNA expression is reduced in optic stalk (Fig. 5.6). *Cxcr4b*, the cognate receptor of *cxcl12a* is known to present on microglia (Oosterhof et al., 2017).

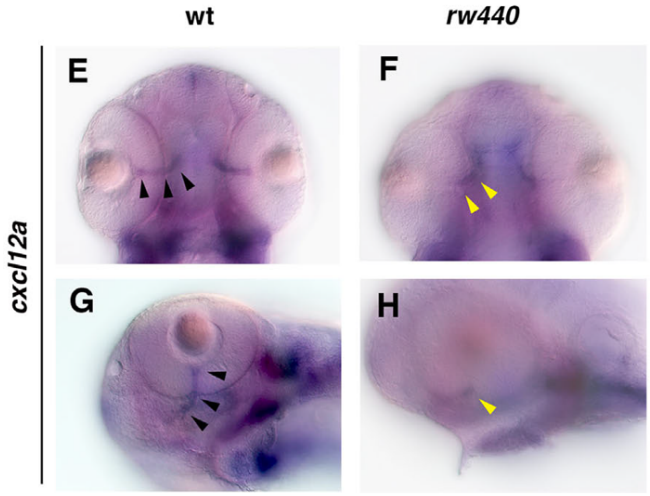

Figure 5. 6: Wildtype and *slbp1* (*rw440*) mutant *cxcl12a* in-situ hybridization at 60 hpf (Adapted from (Imai et al., 2014).

To confirm whether absence of *cxcl12a* causes the decrease in microglial precursor number in *slbp1* mutant, we injected *cxcl12a* morpholino into embryos of *Tg[mpeg1.1:EGFP]*. Live

imaging of *cxcl12a* morphants at 2 dpf showed no decrease in mpeg1.1 positive cells in retina as compared to control morphants (Fig. 5.7), indicating that *cxcl12a-cxcr4b* signaling does not play a role in microglia precursors colonization of the neural retina.

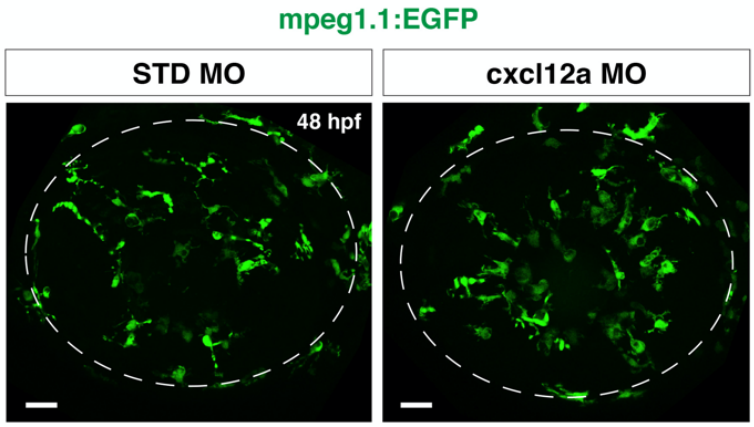

Figure 5. 7: mpeg1.1 positive cells in 2 dpf retina of cxcl12a and control morphants

5.3.4. Pharmacological blocking of progression of retinal neurogenesis

HDAC1 promotes retinal neurogenesis in zebrafish by suppressing Wnt and Notch signaling pathways (Yamaguchi et al., 2005). To confirm our hypothesis that retinal neurogenesis drives infiltration of microglial precursors into the neural retina, we used a HDAC1 inhibitor, Trichostatin A (TSA), to inhibit retinal neurogenesis. We examined

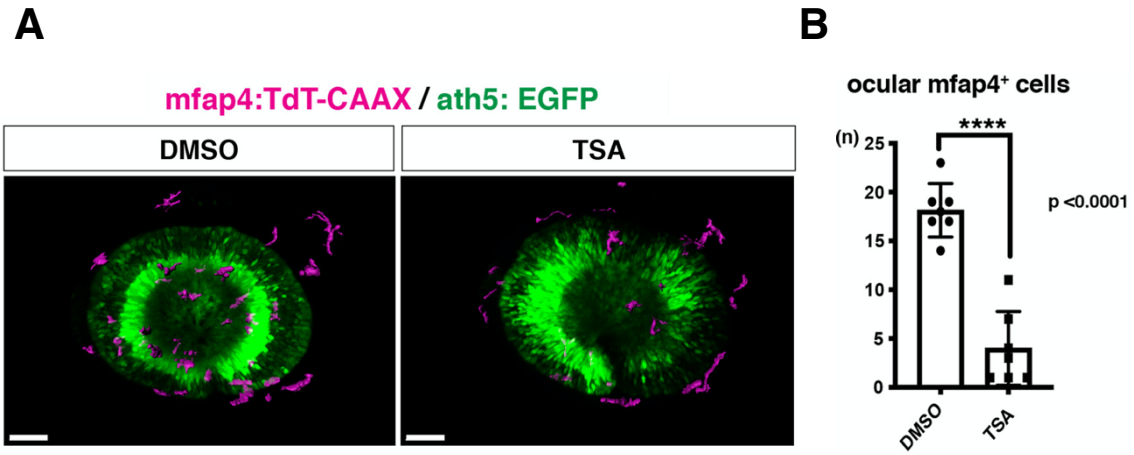

Figure 5. 8: TSA treated retinas at 49hpf

(A) Live images of TSA treated retinas of 49 hpf *Tg[mfap4TdTomato-CAAX;ath5:EGFP]* embryos. (B) Histogram of the number of mfap4+ cells in retina of DMSO and TSA treated embryos at 49hpf

Tg[ath5:EGFP;mfap4:tdT-CAAX] embryos with TSA from tail-bud stage to 50 hpf. TSA caused severe delay in retinal neurogenesis and it also significantly reduced the number of ocular microglial precursors (Fig. 5.8). This observation strengthens the possibility that neurogenic state of the retina act as a cue for microglial precursor infiltration of the neural retina.

5.3.5. Microglia are decreased in retinas lacking RGCs

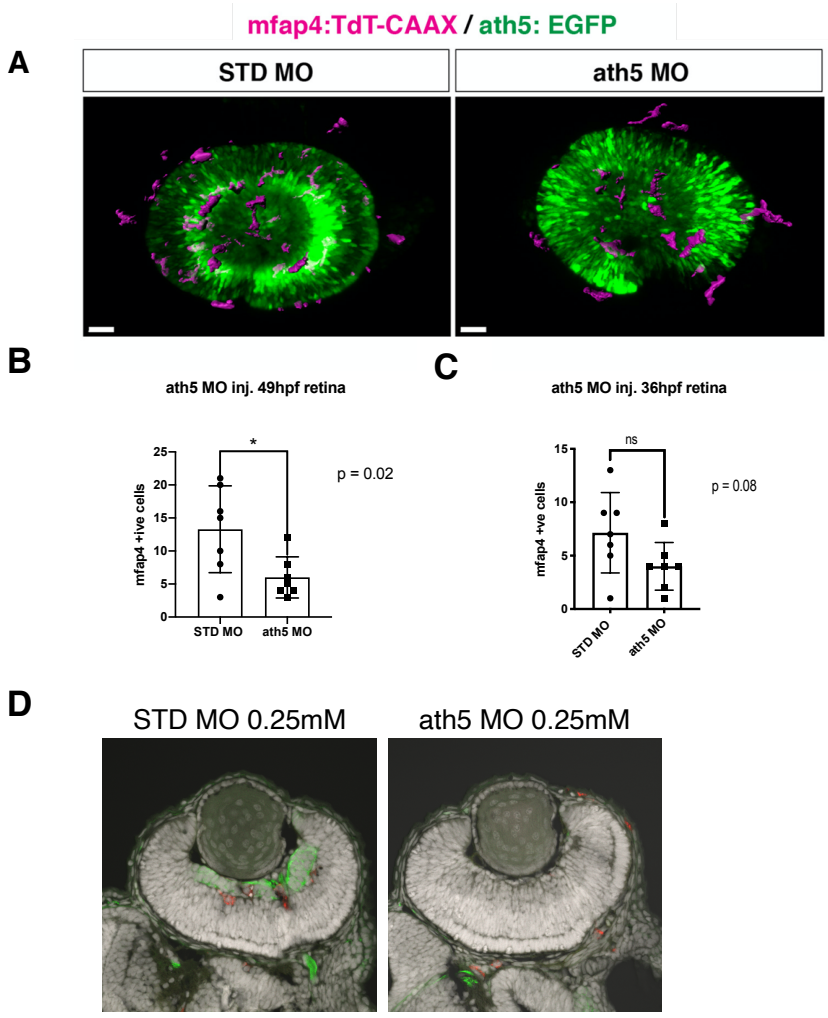

Figure 5. 9: Microglia decreased in absence of RGC's

(A) Live images of ath5 morphant retinas with *Tg[mfap4TdTomato-CAAX;ath5:EGFP]* at 49 hpf. (B, C) Histogram of mfap4+ cells in standard and ath5 morphants at 49 hpf (B) and at 36 hpf (C). (D) standard and *ath5* morphant retinas labelled with zn5 antibody at 3dpf. zn5 signals (green) label RGC.

RGCs are the first born neurons in developing retina. To examine whether blockade of RGC genesis affects microglial infiltration of the neural retina, we used antisense morpholino against ath5, which normally promotes RGC differentiation. In *ath5* morphants, microglial precursors entered the optic cup on time and in comparable numbers to control morphant embryos at 36 hpf (Fig. 5.9 C) but the number of microglial precursors was decreased at 48 hpf (Fig.5.9 A, B). These data suggest that differentiated RGC contributes to the infiltration of microglial precursors in the neural retina. To confirm that RGCs were completely absent in *ath5* morphants, we applied zn5 antibody, which labels RGC. *ath5* morphant showed complete absence of RGC layer (Fig. 5.9D).

5.3.6. *Slbp1* mutant neurogenic status at transcription level

Histological analysis of *slbp1* mutant clearly shows the delay in neurogenesis. To further investigate neurogenesis status of *slbp1* mutant brain at 2 dpf, we performed bulk RNA sequencing analysis. Lots of genes were up/downregulated in *slbp1* mutants as compared to

A **B**

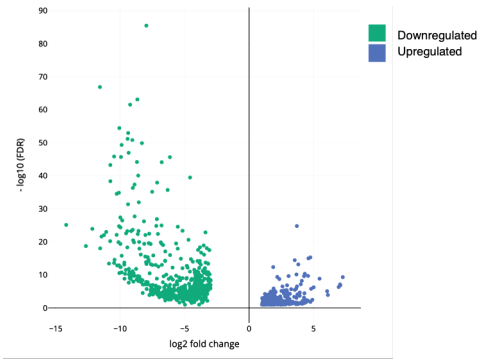

11	Homophilic cell adhesion via plasma membrane adhesion molecules
29	Nervous system development
22	Neurogenesis
26	Cell development
4	Gamma-aminobutyric acid transport
4	Dendrite self-avoidance
19	Neuron differentiation
32	Cell differentiation
7	Neurotransmitter transport
14	Cell adhesion
41	System development

Figure 5. 10: *Slbp1* mutant neurogenic status at transcriptional level
(A) Volcano plot showing upregulated genes (blue) and downregulated genes (green) in *slbp1* mutants as compared to wilds-type siblings at 48 hpf, (B) Table of number of downregulated genes related to neurogenesis, neurotransmitter transport and other vital functions in *slbp1* mutants.

wild-type siblings (Fig 5.10A). Genes related to neurogenesis, nervous system development, and neuronal differentiation was significantly downregulated in *slbp1* mutants (Fig 5.10B).

To further confirm that retinal neurogenesis in *slbp1* mutants is compromised at transcription level, we compared the expression of essential genes involved in photoreceptor differentiation between *slbp1* mutants and wild-type siblings. The transformed expression analysis of *neurod1*, *neurod2*, *neurod6a*, *neurod6b* (Fig 5.11A) and *crx* (Fig 5.11B) genes shows that these genes are downregulated in *slbp1* mutants, confirming that retinal neurogenesis is delayed in *slbp1* mutants.

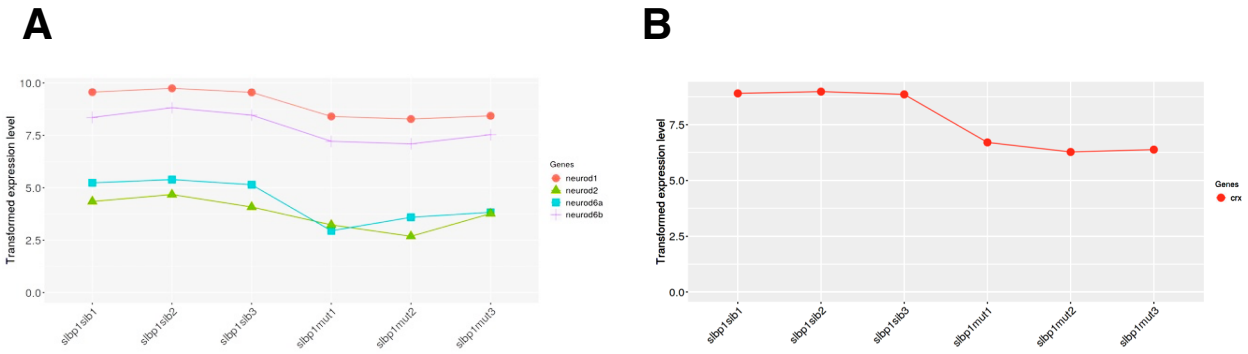

Figure 5. 11: Transformed expression level analysis of *slbp1* mutants and WT siblings at 48 hpf
(A) *neurod1, neurod2, neurod6a* and *neurod6b* expression level. (B) *crx* expression level.

5.3.7. Microglia associates with transplanted donor wild-type retinal columns in *slbp1* mutant host retinas

To clarify whether microglia precursors have a higher affinity towards differentiating neurons than retinal progenitor cells, we conducted cell transplantation experiments. At blastula stage, wild-type donor cells and labeled with dextran-Alexa 488 and transplanted into wild-type or *slbp1* mutant host embryos with *Tg[mfap4:tdT-CAAX]* transgene. Wild-type and *slbp1* mutant

host embryos, in which wild-type donor retinal cell columns were introduced, were selected at 1 dpf and scanned using confocal LSM at 2 dpf (Fig. 5.12A). Host microglia precursors were visualized with mfap4:TdT-CAAX fluorescence.

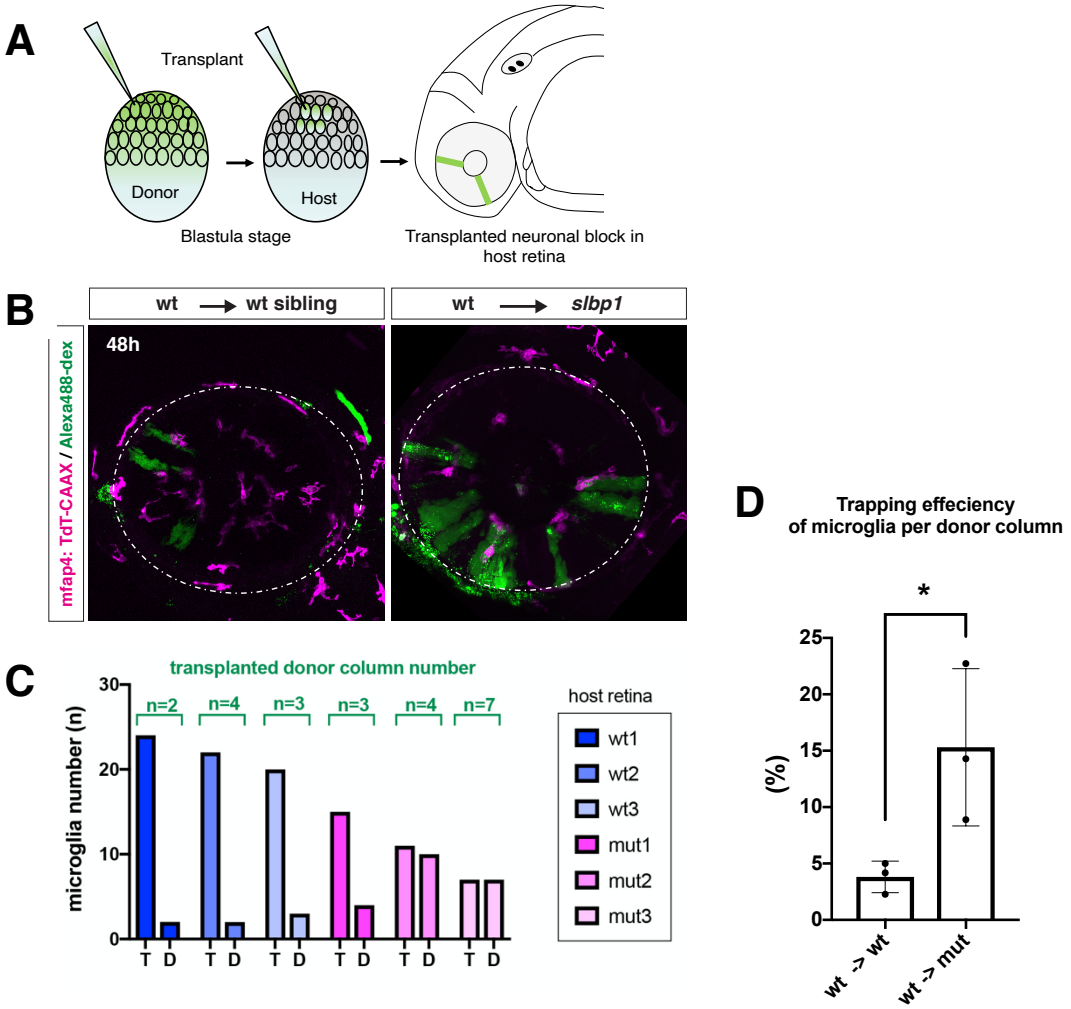

Figure 5. 12: Microglia associated with transplanted WT retinal columns in *slbp1* mutants (A) Schematic drawing of cell transplantation experiments (B) Live images of *slbp1* mutant retinas with transplanted wild-type donor retinal cell columns at 48 hpf. Donor wild-type retinal cell columns are labeled with Alexa-488 dextran (green). Host microglial precursors are visualized with the transgene *Tg[mfap4:tdTomato-CAAX]* (magenta). (C) Histogram of numbers of microglial precursors associated with donor retinal columns (D) and total number of microglial precursors (T) in host retina. Three sets of wild-type and *slbp1* mutant host samples are indicated by bars with different colors. (D) Histogram of the trapping efficiency of mfap4-positive microglial precursors per donor column.

In *slbp1* mutant host retinas, microglial precursors were likely to be associated with donor wild-type retinal columns more frequently than in wild-type host retinas (Fig. 5.12B). To analyze the data numerically, we compared three sets of transplanted eyes from wild-type donors to wild-type hosts with those from wild-type donors into *slbp1* mutant hosts (Fig. 5.12C). Microglial precursors associated with donor retinal columns accounted for 72.53% of all retinal microglial precursors in *slbp1* mutant host retinas at 48 hpf, whereas it was only 10.18% in wild-type sibling host retinas, suggesting that microglial precursors are more attracted by wild-type donor neurogenic retinal columns than surrounding *slbp* mutant proliferative retinal cells. Since the fraction of microglial precursors associated with donor retinal columns in total microglial precursors may depend on the number of donor retinal columns incorporated into host retinas, next, we estimated trapping efficiency of microglia per donor column by dividing the fraction of microglia associated with donor columns with transplanted donor column number in each eye (Fig. 5.12D). Trapping efficiency of microglia per donor column was 15.30% and significantly higher in *slbp1* mutant host retinas than in wild-type sibling host retinas (3.813 %) (Fig. 5.12D). So, it is likely that *slbp1* mutant host-derived microglial cells are preferentially associated with donor-derived wild-type retinal cells than with host-derived *slbp1* mutant retinal cells at 48 hpf. Thus, microglial precursors are preferentially attracted by differentiating neurons.

5.3.8 CSF1Ra-IL34 signaling is not affected in slbp1 mutants

Recent studies suggested the role of *Csf1ra-il34* signaling in microglial colonization of zebrafish midbrain (Wu et al., 2018), where IL34 expressed in developing brain attracts microglia expressing its receptor, *Csf1ra*. To examine whether *il34* expression is compromised in *slbp1* mutants, we performed qPCR amplification of *il34* mRNA in *slbp1* mutants and wild-

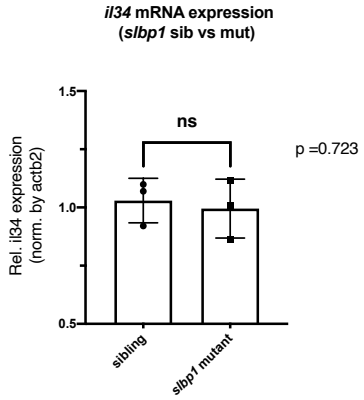

Figure 5. 13: Comparable *il34* mRNA expression in slbp1 mutant heads relative to WT

type siblings. There was no significant change in *il34* expression relative to *actb2* between *slbp1* sibling and mutant (Fig.5.13), indicating that *Csf1ra-il34* signaling is not involved in reduction of ocular microglial precursor number in *slbp1* mutants. To further elucidate the role of *il34* expression in microglial colonization of developing retina, we overexpressed *il34* under the control of retinal progenitor-specific *rx1* promoter. Overexpression of *rx.1:il34* did not increase the number of ocular microglia at 48 hpf (Fig.5.14). These data also exclude the possibility that *Csf1ra-il34* signaling is involved in microglial colonization of zebrafish retinas.

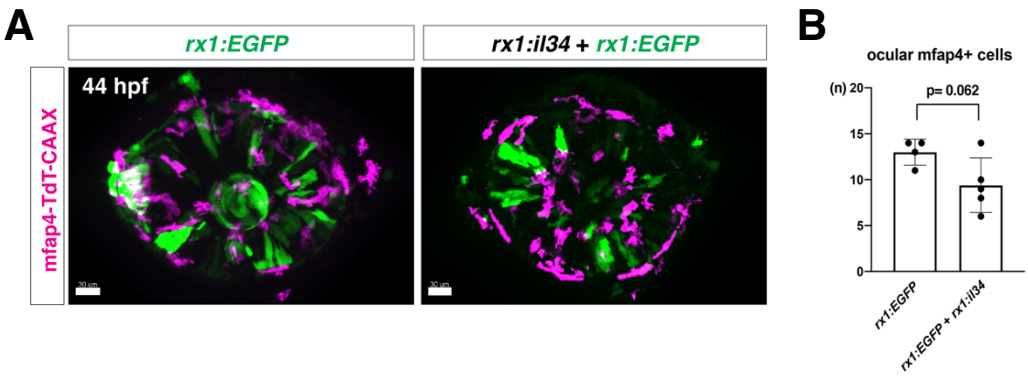

Figure 5. 14: Overexpression of *il34* in retina

(A) Confocal images of *Tg[mfap4:tdTomato]* transgenic retinas injected with *rx1:EGFP* expression construct and a mixture of expression construct of *rx1:EGFP* and *rx1:il34* (B) Histogram of the number of ocular microglial precursors in non-injection control, retinas expressing *rx1:EGFP*, and retinas expressing a mixture of *rx1:EGFP* and *rx1:il34*.

5.4 Discussion

We found that microglial precursors preferentially infiltrate the neural retina through neurogenic area. Furthermore, we found that microglial colonization of the neural retina is affected in retinal *slbp1* mutants, in which retinal neurogenesis is severely delayed. In *slbp1* mutants, microglial precursors enter the optic cup along ocular blood vessels, but fail to infiltrate the neural retina. HDAC1 inhibition also decreased the number of ocular microglial precursors. Thus, neurogenic state of retinal cells functions as a gateway for microglial precursors to infiltrate the neural retina. We also observed that the number of microglia in the neural retina is diminished in *ath5* morphant retinas, suggesting that blockade of RGC differentiation compromises infiltration of microglia into the neural retina. At present, we cannot say whether neurogenesis or RGC maturation is more responsible for microglial infiltration of the neural retina. There are at least three possible mechanisms for this infiltration. First, the basal region of retinal progenitor cells may function as a physical barrier that inhibits microglial infiltration of the neural retina. Second, microglia are attracted to the surfaces of retinal neurons or ganglion cells. Third, retinal neurons or ganglion cells release a specific attractant for microglia. There are several candidate molecules which may suggest the third possibility. In adult mice, RGCs express IL34, which attracts microglia and retains them around the IPL niche (O'Koren et al., 2019). However, we found that *il34* mRNA expression is comparable in *slbp1* mutants and their wild-type siblings. Furthermore, overexpression of *il34* mRNA in retinal progenitor cells did not increase the number of ocular microglial precursors, so IL34 seems unlikely to promote microglial infiltration of the retina. It was also reported that apoptosis attracts microglia in zebrafish developing brain (Casano et al., 2016a, Xu et al., 2016). However, we found microglial colonization of the retina is normal in zebrafish *tp53* morphant retinas (data not shown), suggesting that apoptosis is not required for microglial colonization of the retina prior to 54 hpf. It was reported that mouse brain cortex colonization

by microglia depends on the Cxcl12a-Cxcr4 signaling axis (Arno et al., 2014). We previously reported that *cxcl12a* expression in optic stalk is absent in *slbp1* mutants (Imai et al., 2014). However, microglial colonization in retina is normal in zebrafish *cxcl12a* morphant retinas, suggesting that Cxcl12a-Cxcr4 signaling is not involved in microglial colonization of retina. In this study, we conducted cell transplantation experiments, in which wild-type donor retinal cells were incorporated into *slbp1* mutant host retinas. Interestingly, microglial precursors were preferentially associated with the basal domain of wild-type donor cell columns in *slbp1* mutant host retinas at 48 hpf. Since most *slbp1* mutant retinal cells were still proliferative at 48 hpf, it is likely that microglia are preferentially attracted by wild-type donor neurogenic retinal cells, supporting the first or second possibilities. Further studies will be necessary to unveil the molecular mechanism underlying microglial infiltration into neural retina.

6. Chapter III: Retinal microglia and DNA damage signals

6.1. Introduction

6.1.1. Pinball eye mutant

The *pinball eye* (*piy*) mutant was isolated as part of large-scale mutagenesis experiment conducted at RIKEN. In *piy* mutants, almost all retinal neurons undergo apoptosis soon after neurogenesis (Yamaguchi et al., 2008) (Fig.6.1). TUNEL revealed that only the central retina undergoes apoptosis in 2 dpf *piy* mutant retina, where mostly differentiated neurons are located (Fig.6.1 BC). Retinal stem cells that normally localize in peripheral regions of the retina also known as the the ciliary marginal zone (CMZ), are not affected in *piy* mutants. This suggests that retinal stem cells are maintained and continue to proliferate in *piy* mutants until 5 dpf (asterisks in Fig. 6.1.C) (Yamaguchi et al., 2008).

Cloning of the *piy* mutation locus showed that a missense mutation in the small subunit of DNA primase, namely Prim1, is responsible for defects in *piy* mutants (Yamaguchi et al., 2008). DNA primases are important for DNA replication on lagging strands in vertebrates.

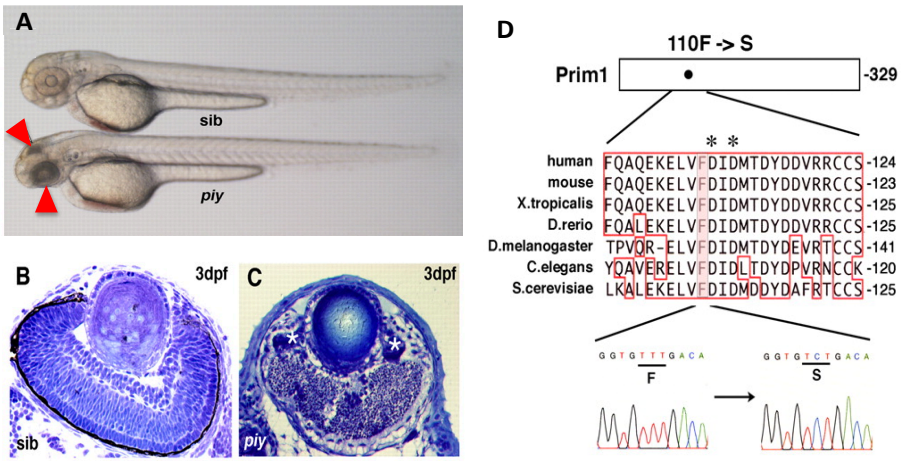

Figure 6. 1: Defects in *piy* mutant vs. sibling
(A) Neuronal debris accumulation in *piy* mutant (shown by arrows), (B,C) Retinal neuronal cell death in 3dpf *piy* mutant, (D) Missense mutation occurred in the *prim1* gene in the *piy* mutant. The transversion from T to C replaces phenylalanine (F) 110 with serine (S) (Yamaguchi et al., 2008).

DNA synthesis on lagging strand depends on RNA primers whose synthesis is catalyzed by DNA primase. Although DNA primase is involved in the synthesis of Okazaki fragments on the lagging strand, this missense mutation does not affect retinal cell proliferation but rather causes apoptosis of differentiating retinal neurons.

The integrity of DNA replication is normally monitored by DNA replication checkpoints, whose major regulator is Ataxia telangiectasia mutated and rad3 related (ATR). ATR-dependent DNA checkpoint relies on DNA primase (Marini et al., 1997, MacDougall et al., 2007). ATR also cross-talks with another DNA damage checkpoint regulator, Ataxia telangiectasia mutated (ATM), which activates downstream molecules Check point kinase 2 and tumor suppressor p53 (Jazayeri et al., 2006, Myers and Cortez, 2006). Stabilized p53 halts the cell-cycle progression and promotes the repair of DNA damage. However, in case where DNA damage cannot be repaired ,p53 induces apoptosis (Pettmann and Henderson, 1998).

6.1.2. Mitochondria-dependent apoptosis pathway

Apoptosis in eukaryotic cells is initiated by various cellular stress signals, for example, DNA damage, infection and deprivation of growth factors. These types of cellular stress leads to activation of Bax. Under normal conditions, Bax is inhibited by anti-apoptotic Bcl2 family of proteins such as Bcl2. However, cellular stress suppresses Bcl2-mediated Bax inhibition, and activates Bax, which then translocates to outer mitochondrial membrane (OMM) to form multimeric Bax protein complex. This process leads to formation of large channels on mitochondria, increasing OMM permeabilization. Increase in OMM permeabilization causes release of cytochrome-c from mitochondria into cytosol through Bax channels. Cytochrome-c binds to an adaptor protein Apaf-1 and Caspase 9 to form a complex known as the apoptosome. In turn, the apoptosome activates the executioner protease Caspase 3 (van Loo et al., 2002). In zebrafish, many Bcl2 paralogues such as, Bax1, Bax2, Boka, Bokb, Mcl-1a, Mcl-1b , Bmf1

and Bmf2 (Kratz et al., 2006, Cory and Adams, 2002) exist due to genomic duplication. It was also reported that Bcl2 proteins have non-apoptotic roles like regulation of cell migration during early zebrafish development (Cory and Adams, 2002). Although the presence of zebrafish apoptosome has not been confirmed, zebrafish genome contains all functional components that are required for apoptosome (Inohara and Nunez, 2000).

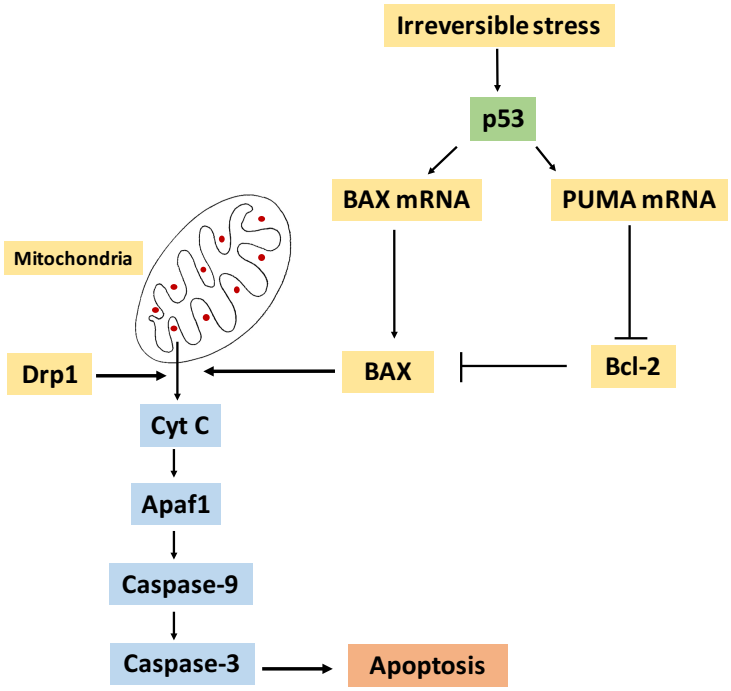

Figure 6. 2: A schematic of p53-mediated apoptotic pathway
p53 is stabilized by irreversible stress, promotes pro-apoptotic BAX and PUMA. PUMA is a BH3-only protein and activates Bax by releasing it from Bcl2-mediated inhibition. Bax cooperates with Drp1 to release cytochrome C (Cyt C) from the mitochondria. Cyt C, Caspase 9 and Apaf1 forms apoptosome and activates effector caspases including caspase 3, leading to cell death.

In *piy* mutant retinas, neuronal apoptosis have been shown to depend on DNA damage response elements such as ATM , Chk2 and p53 (Yamaguchi et al., 2008). A possible explanation to be this can be seen in terms of *prim1* mutation leading to compromised functional integrity of DNA replication, subsequently activating ATR, a PI3 kinase family protein. Activated ATR

phosphorylates Check point kinase 1 (Chk1), which inhibits M phase entry post DNA replication. ATR may activate ATM, which subsequently activates Chk2. Under normal condition, p53 is unstable due to a rapid ubiquitin-dependent proteasomal degradation. This degradation is mediated by MDM2, an E3 ubiquitin ligase (Kubbutat et al., 1997). However, under stress conditions, Chk2 phosphorylates Ser18 of p53, and MDM2 does not interact with

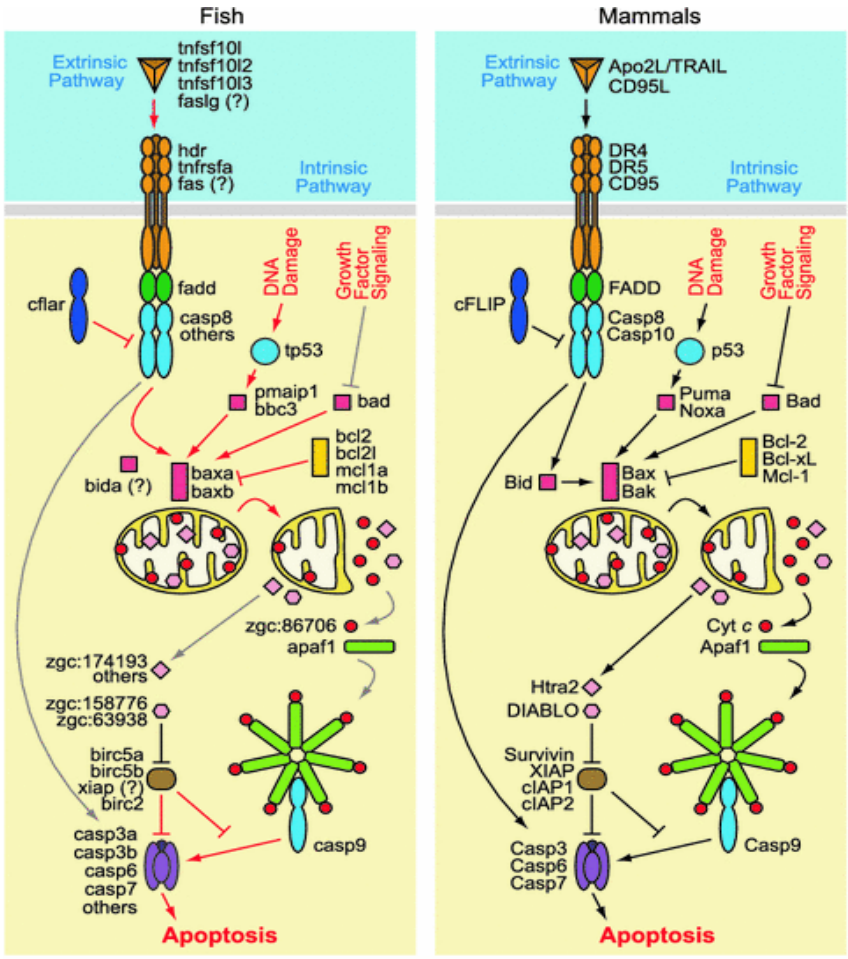

Figure 6. 3: Comparison of apoptotic pathway in zebrafish and mammals
Adapted from (Eimon and Ashkenazi, 2010)

this phosphorylated p53, leading to stabilization of p53. Stabilized p53 induces transcription of cell-cycle arrest genes such as a cdk inhibitor p21 and pro-apoptotic proteins such as Bax and a BH3-only protein PUMA (Yuan et al., 1996, Meek, 1997). PUMA binds to an anti-apoptotic protein, Bcl2, and relieves Bax from Bcl2-mediated Bax inhibition. Activated Bax

protein translocates into the mitochondrial outer membranes and promotes release of cytochrome c from mitochondria (Saelens et al., 2004, Schuler and Green, 2001). It was reported that a mitochondria-fission regulator, dynamin-related protein 1 (Drp1), is required for apoptosis (Friedman et al., 2011, Jagasia et al., 2005). Drp1 was reported to cooperate with Bax to promote cytochrome c release from mitochondria(Jahani-Asl and Slack, 2007). Released cytochrome c forms the apoptosome complex with adaptor proteins Apaf1 and Caspase 9 (Chinnaiyan, 1999, Hill et al., 2004). The apoptosome complex activates downstream effectors such as Caspases 3 and 7 and leads to cell death. A section of the apoptotic pathway has been summarized in Figure 6.3.

It was reported that DNA damage response activates other molecular targets, which bypass p53, and induce cell death (Sidi et al., 2008). In zebrafish, gamma radiation stress bypasses p53

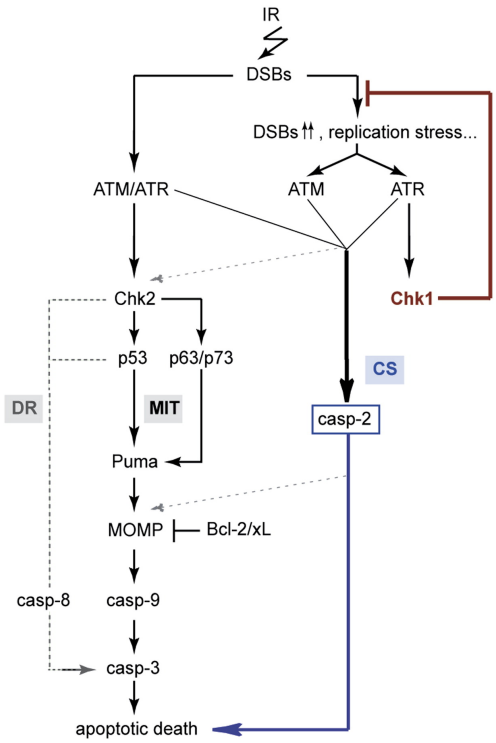

Figure 6. 4: Illustration showing p53-independent pathway stimulated with DNA-damage signals ATM/ATR
Adapted from (Sidi et al., 2008).

activation and activate novel Caspase-2 dependent apoptosis via Chk1. Caspase-2 dependent apoptosis is not rescued by p53 inhibition or Bcl2 overexpression (Figure 6.4).

6.1.3. Microglia in *piy* mutant retina

Microglia is responsible for clearance of apoptotic neurons during development. Few studies have proved that apoptotic cells do not release soluble signals for microglial response (Savill et al., 1993), instead cell-cell contact drives microglia activity (Tanaka et al., 1998). Cell surface components specific to dying cells suggested as "eat-me signals" were required for identification by microglia cells. Phosphatidylserine (PS), a phospholipid component of cell membrane, is flipped to outer surface of apoptotic neurons. Pros1, an extracellular protein, binds to PS and activates a tyrosine kinase receptor, MERTK, on microglia to initiate phagocytosis (Graham et al., 2014). Change in status of glycosylation of membrane proteins such as Lectin and Integrin on apoptotic neurons also mediates recognition and phagocytosis by microglia (Witting et al., 2000). Previously, it was reported that injured neurons attract microglia by a long-range Ca^{2+} wave via glutamate dependent process (Sieger et al., 2012a). However, the precise mechanism that attracts microglia towards dying neurons in *piy* mutants remains to be elucidated.

6.2. Materials and methods

Transgenic lines

Alleles of mutants *piy*^{rw255} (Yamaguchi et al., 2008), *dnm1l*^{sa24668} (Stemple lab), *tp53*^{zdf1} (Berghmans et al., 2005) were used. *Tg(ath5:GFP)*^{rw021} (Masai et al., 2005) was used to monitor *ath5* expression. *Tg[mfap4:tdTomato-CAAX]*^{oki058} was used to visualize microglial precursors.

Plastic sections and Toluidine staining

1. Embryos of appropriate age were dechorionated and fixed with 4% PFA at 4^0 C overnight.

2. Washed with PBS 3 x 5 minutes at RT.
3. PBS was serially replaced with 100% ethanol.

%Ethanol	Wash Time (RT)
30%	2 min
50%	2 min
70%	2min
100%(twice)	2min

4. Embryos were then transferred to 100% Ethanol/JB4 solution (1:1) for 3 hours at RT and then to JB4 solution overnight at 4^0 C.
5. Embryos were then embedded in a mould using JB4 (A+B) solution. After adjusting the embryos in correct orientation, the mould was covered with transparent cellophane paper to cut air supply. In cases of bubbles in solution, aspirator was used for 5 min.
6. After 1 hour, once the solution has solidified, sample was trimmed and mounted on wooden block.
7. The mounted sample was then cut into 5 μm thin sections using microtome.
8. Each section was then arranged on distilled water on a slide and dried on a hot plate.
9. After drying, the slide was immersed in 0.1% toluidine solution for 2 min.
10. Slides were washed with distilled water until excessive toluidine blue dye is removed from tissues.
11. Slides were then dried on hot plate and mounted with inclusion reagent.

Morpholino experiments

Morpholino name	Sequence	Rescue/ Other observations
p53	5′-GCGCCATTGCTTTGCAAGAATTG-3′	Yes, small head
bbc3/PUMA	5'-TGCTTTCCATCTCTGGTCGGGCCAT-3'	NO

Bax1+Bax2	5'-TGAAAATAAGCGAACTGAAGAAGAC-3' 5'-ATTTTTCGGCTAAAACGTGTATGGG-3'	NO
Drp1	5'- ACAGGAATAAGAGCCTCCATCGCGT-3'	Yes, small head
Caspase 9	5′-GAATCTGTCTGTGTTTCTGCTCCAT-3′	NO
Caspase 8	5′-ACAGGGTTTTAACTCACAGTAGATC-3′	NO
Caspase 3a	5' - TTGCGTCCACACAGTCTCCGTTCAT - 3'	NO

Table 1. 1: List of morpholino sequences used for knockdown experiments

Live imaging

Sorted embryos were anesthetized in E3 medium containing Tricaine and PTU. The embryos were then kept on 3% methyl cellulose on plastic mounting plate and aligned (lateral/ventral view). 50 µl of 1-1.5% low melting agarose (maintained at 45-55^0 C) was added to cover the embryo. The embryo with agarose was then left for 10-15 minutes to set. The sample was then mounted on confocal microscope stage (LSM710) and E3 medium with Tricaine +PTU was added to cover the space between agarose-embedded embryo and water immersion objective lens. Desired z-stacks were obtained.

DNA extraction for Genotyping

The appropriate stage embryos were dechorionated and fixed in 4% PFA overnight. Next day, embryos tails were cut and transferred to 1x PBS. After 2 hours, PBS was replaced with 50 µl lysis buffer. Following steps were performed:

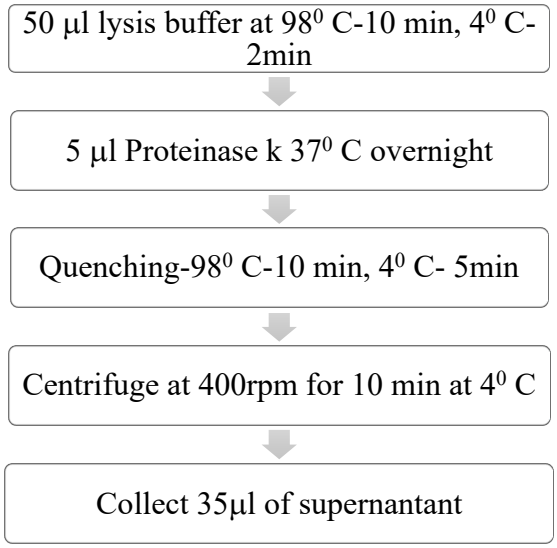

RNA extraction

1. Heads from 2dpf embryos were dissected and transferred to 100 µl Sepasol. The heads were then stored at - 80^0 C or RNA was extracted immediately.
2. 20 µl $CHCl_3$ was added to samples in Sepasol and mixed vigorously, followed by incubation at RT for 10 min.
3. Samples were then centrifuged at 4^0 C for 15000g for 15 min.
4. Aqueous was then transferred to 1.5ml eppendorf and 100 µl of isopropanol was added.
5. This solution was incubated at RT for 10 min and centrifuged at 4^0 C for 15000g for 15 min.
6. Supernatant was discarded and the pellet was washed twice with 75% EtOH at 8000g for 5 min at 4^0 C.
7. EtOH was removed completely and the pellet was air-dried for 5 min.
8. The pellet was resuspended in 10-15 µl Nuclease free water and RNA concentration was measured using NanoDrop.
9. RNA was stored at - 80^0 C.

cDNA synthesis

1. 5 µl of RNA(500ng) was kept at 65^0 C for 5 min.
2. 2 µl 4DN (Tyobo kit) was added to all RNA samples.
3. After incubation at 37^0 C for 5 min, 2 µl 5x RT Master Mix II + 1 µl Milli Q water was added to the samples (in total 10 µl reaction mix).
4. cDNA was synthesized using the following thermo cycler program.

Temperature	Time
37^0C	15 min
50^0C	5 min
98^0C	5 min
4^0C	∝

Quantitative Real Time PCR

Extracted RNA from 48 hpf *piy* siblings and mutants embryos was used to prepare cDNA using Toyobo ReveresTra Ace® qPCR RT master mix with gDNA remover. Expression level of apoptosis related genes was evaluated by quantitative PCR using following primers. mRNA of cytoplasmic actin β2, namely *actb2* (ZFIN), was used for normalization.

Gene name	Primers
p21	5'-AAGCGCAAACAGACCAACAT-3' 5'-AAGCGCAAACAGACCAACAT-3'
PUMA/bbc3	5'-CTGAGGAGGACCCCACACT-3' 5'-TCTCCAGTTCTGCCAGTGC-3'
tp53	5'-GAGGTCGGCAAAATCAATTC-3' 5'-GAGGTCGGCAAAATCAATTC-3'

ATM	5'-CCTCAAGGCTGTGGAGAACT-3' 5'-CCTCAAGGCTGTGGAGAACT-3'
RIPK1L	5'-CCTCAAGGCTGTGGAGAACT-3' 5'-TCACAGATATTGGAACCGTCAC-3'

Table 1. 2: Primers used for quantitative real-time PCR analysis

RNA sequencing and analysis

RNA samples with RIN >7 were subjected to pair-end sequencing using Illumina HiSeq4000 platform. First quality check was performed using FastQC and read trimming was done by Trimomatic. PRINSEQ lite was used for PolyA trimming and quality filtering. The trimmed sequences were then mapped to zebrafish reference genome (GRCz11) using hisat2.1.0. Using R package (EdgeR) differentially expressed genes with FDR values <0.05 were extracted for analysis.

6.3. Results

6.3.1. Microglia precursors in *piy* mutant retina

Previous *piy* study indicated that apoptosis occurs in *piy* mutants at 2 dpf (Yamaguchi et al., 2008). So, we examined whether the number of ocular microglial precursors is increased at 32 hpf due to predisposition of retinal neurons to undergo apoptosis at 2 dpf. To confirm this, we performed in-situ hybridization of wild-type sibling and *piy* mutant embryos at 32 hpf, using *L-plastin* antisense RNA probe, which labels both microglia/macrophages and neutrophils (Fig. 6.5A). Quantification showed significant increase in *L-plastin* positive cells in *piy* mutant retinas as compared to wild type sibling (Fig. 6.5B).

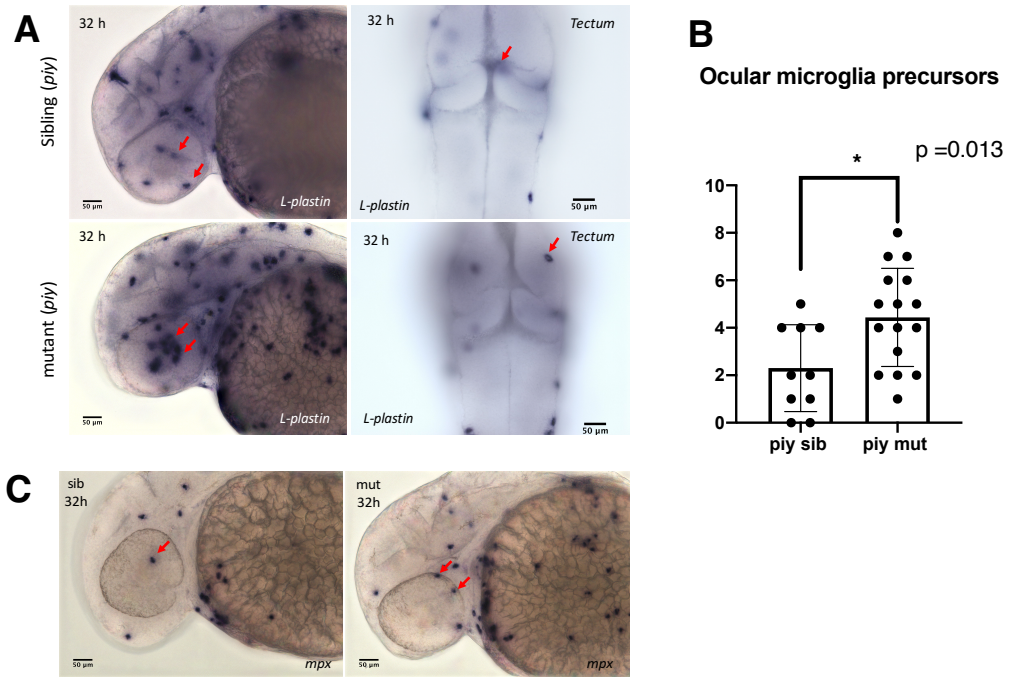

Figure 6. 5: Myeloid precursors in 32 hpf *pinball eye* embryos

(A) *L-plastin* in-situ hybridization of 32 hpf wild-type sibling head and tectum (top panel) and *piy* mutant head and tectum (bottom panel).

(B) Quantification of ocular microglia precursors in wild-type sibling and *piy* mutant at 32 hpf.

(C) *mpx* in-situ hybridization of wild-type sibling and *piy* mutant at 32 hpf.

To confirm the increase of microglia in *piy* mutant retinas, we conducted live imaging of 33 hpf *piy* mutant retina with a transgene *Tg[mfap4:TdT-CAAX*], which specifically visualizes microglial precursors. There was a significant increase in *mfap4* positive cells in *piy* mutant retinas. Combining previous results, we hypothesized that microglia precursors in *piy* mutant could respond to "find-me signals" generated by neurons predisposed to undergo cell death via p53 dependent apoptosis, even before apoptosis. To confirm that increased *L-plastin* cells in *piy* mutants are microglia/macrophages precursors and not neutrophils, we performed in situ hybridization using *mpx* antisense RNA probe (neutrophil marker) on 32 hpf *piy* mutants. There was no change in number of neutrophils in *piy* mutants retina as compared to wildtype sibling (Fig. 6.5C).

6.3.2. Cell-death at 1.5dpf in *piy* mutant retina

Abnormally round cells and accumulation of cloudy dead cell debris, are indications of apoptosis in embryonic zebrafish retina. At 1.5 dpf, none of these features were observed in

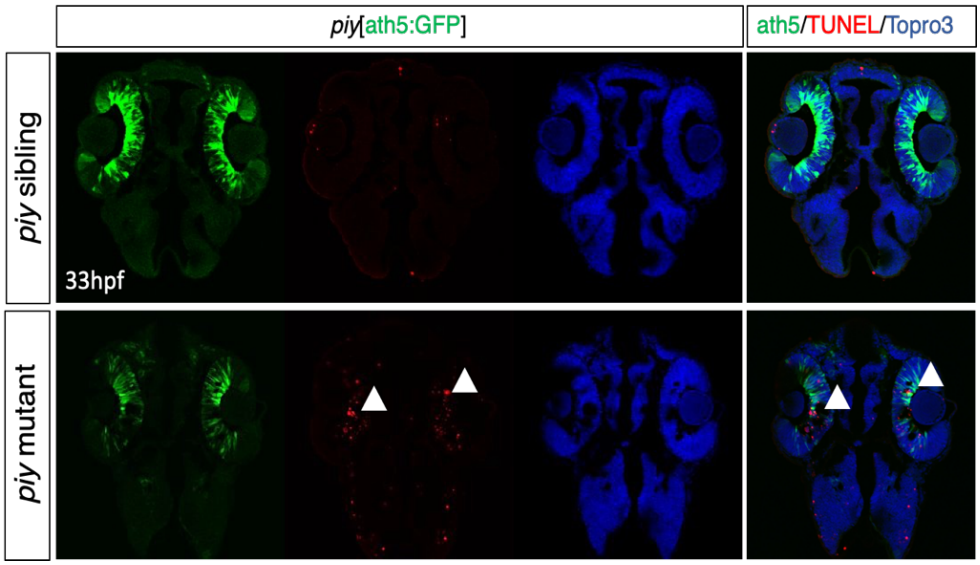

Figure 6. 6: TUNEL staining of *piy* mutant retinas with *Tg[ath5:EGFP]* at 33hpf
Wild-type sibling (top panel) and *piy* mutant (bottom panel) embryos were labelled with ath5:EGFP for early differentiated neurons (green), TUNEL for dead cells (red) and TOPRO3 for nucleus (blue). Arrowheads (bottom panel) indicates dead cells.

piy mutant retinas under dissecting microscope. To check the presence of dead cells at 33 hpf, we performed TUNEL on cryosections *piy[ath5:EGFP]*. We observed increased TUNEL positive signal in *piy* mutant retina at 33 hpf as compared to wild-type siblings (Fig. 6.6). This result indicated that cell death in *piy* mutant retinas starts as early as 33 hpf, leading to an increase in microglial precursor, which was not observed and reported in previous publication. Given this observation, we modified our "Find-me signal" hypothesis and started to investigate which intermediate steps in classical p53-dependent apoptosis pathway in *piy* mutants, could generate signals to attract microglia precursors before the initiation of activation of terminal caspases in *piy* mutants retina.

6.3.3. Microglial precursors at 2 dpf in *piy* mutant retina

Live imaging of 2 dpf *piy* mutant embryos with *Tg[ath5:GFP;mfap4:tdt-CAAX]* clearly showed reduction in *ath5* expression and round-shaped mfap4 positive cells in retina as

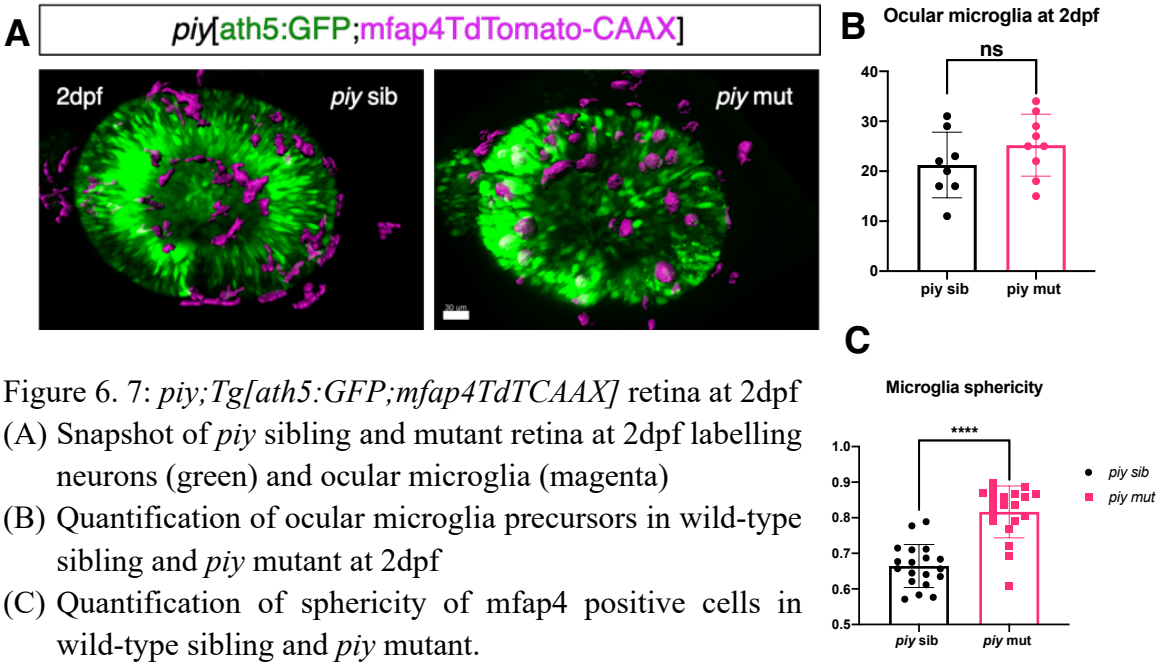

Figure 6. 7: *piy;Tg[ath5:GFP;mfap4TdTCAAX]* retina at 2dpf
(A) Snapshot of *piy* sibling and mutant retina at 2dpf labelling neurons (green) and ocular microglia (magenta)
(B) Quantification of ocular microglia precursors in wild-type sibling and *piy* mutant at 2dpf
(C) Quantification of sphericity of mfap4 positive cells in wild-type sibling and *piy* mutant.

compared to its WT sibling. There was no significant change in microglia precursors number in in *piy* mutant retina (Fig.6.7.B) but retinal microglia precursors had characteristic amoeboid morphology (Fig.6.7.A) of activated microglia. To further confirm this, we calculated the sphericity of mfap4 positive cells in wild-type siblings and *piy* mutants, using Imaris software (Fig.6.7.C). The average sphericity of microglia precursors in wild-type sibling was 0.65, whereas in *piy* mutants it was 0.85, suggesting phagocytosis of dead neurons by retinal microglia precursors in *piy* mutants. In zebrafish, the microglia/macrophages precursors are known to undergo differentiation at 60 hpf and act as primary immune effector cells in brain (Herbomel et al., 2001b). In degenerating *piy* mutant retina, the immature retinal microglia precursors show reactivity towards excessive cell death and attain morphology comparable to mature microglia possibly to remove dead cell debris.

6.3.4 Absence of microglia precursors leads to excessive neurodegeneration

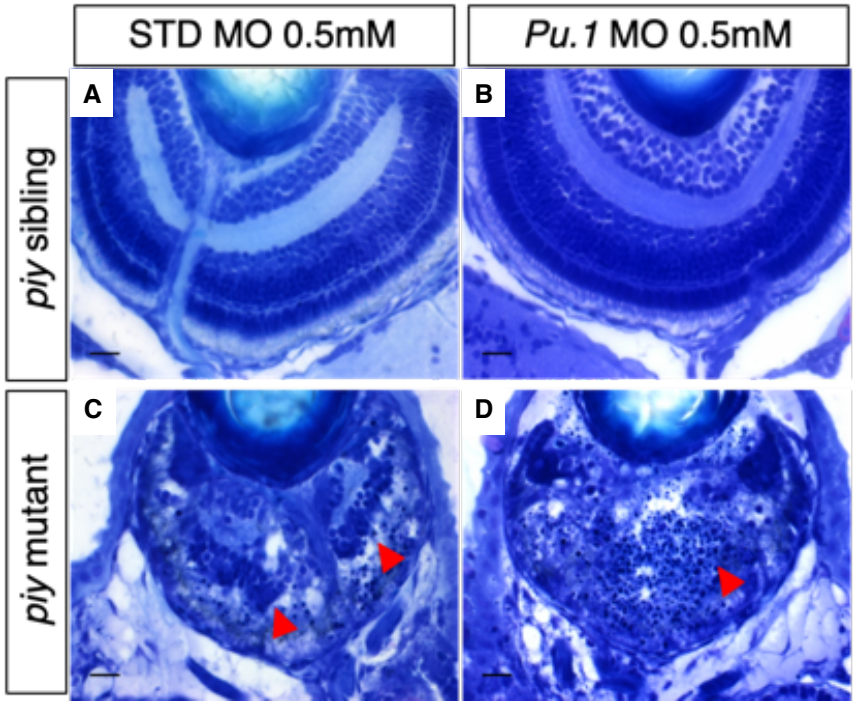

Figure 6. 8: *Pu.1 pinball eye* morphants at 3dpf
(A) Plastic sections of *piy* embryos injected with standard morpholino (A,C) and *Pu.1* morpholino (B,D). Red arrows in *piy* mutant (C) indicates residual neuronal layer due to ongoing cell death. In *Pu.1* morphant *piy* mutant (D) red arrows indicate complete lack of neuronal layer in absence of microglia.

To examine whether microglia precursors play a neuroprotective or neurodegenerating role in in *piy* mutant retinas, we removed microglial precursors by a knockdown approach. Using *pu.1* morpholino, we removed microglia precursors contributed by the first wave of hematopoiesis. First, we compared the plastic sections of *pu.1* MO- injected 3 dpf wild-type sibling and *piy* mutant retinas (Fig.6.8). In *pu.1* morphants of *piy* wild-type sibling background (Fig.6.8.B), no apparent change in retinal lamination was observed. On the contrary, retinal sections of *pu.1* morphants of *piy* mutants (Fig.6.8.D) showed complete loss of retinal lamination as compare to its standard control *piy* mutant retina. This data suggests that absence of microglia increases neurodegeneration in retina of *piy* mutants.

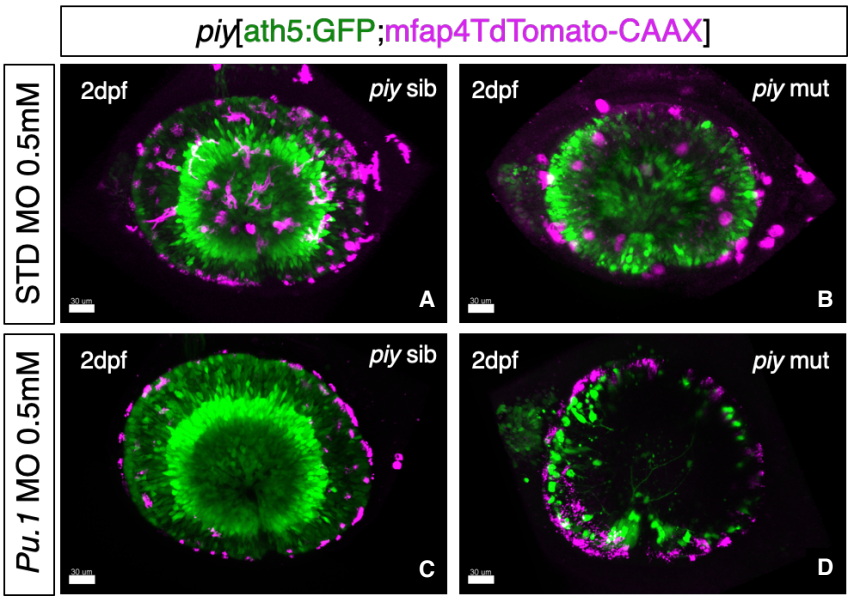

Figure 6. 9: Live images of *Pu.1* morphants

Live images of *piy; Tg[ath5:GFP;mfap4TdT-CAAX]* embryos injected with standard morpholino (A, B) and *Pu.1* morpholino (C, D) at 2 dpf. Pu.1 MO injected retina completely lacks mfap4 positive cells (C, D). Comparing *piy* mutant retinas with standard and morphant (B, D) clearly shows the reduction in ath5:EGFP expression in absence of microglial precursors.

To further confirm whether the absence of microglial precursors leads to acceleration of neurodegeneration in *piy* mutant retinas, we performed live imaging of pu.1 morphants of *piy; [ath5:GFP;mfap4:tdT-CAAX]* background at 2dpf. In Fig.6.9. Upper panels show standard control morphants of wild-type sibling and *piy* mutant retinas, where piy mutant retina clearly have activated microglial precursors as compared to WT sibling. Lower panels show wild-type sibling and *piy* mutant retinas lacking mfap4 positive cells. The comparison of *piy* mutant retina with (Fig.6.9.B) and without microglial precursors (Fig.6.9.D) shows complete absence of *ath5* signal in *pu.1* morphant retina, indicating complete loss of newly differentiated neurons in *pu.1* morphant *piy* mutant retina . These data suggest that microglial precursors may play a neuroprotective role in *piy* mutant retina.

6.3.4. Targeting molecular components in p53-dependent apoptosis pathway

To elucidate molecular components of p53-dependent apoptosis pathway in *piy* mutants, we knockdown key molecules that are known to function in apoptosis. Most of the morpholinos used in this study were previously published (the list is shown in Material and Method, Morpholino experiments). Out of seven morpholinos, only two morpholinos, *p53* MO and *Drp1/dnm1l* MO showed complete rescue of cell death in *piy* mutants. As previously published (Yamaguchi et al., 2008), *p53* knockdown showed complete rescue of cell-death phenotype in

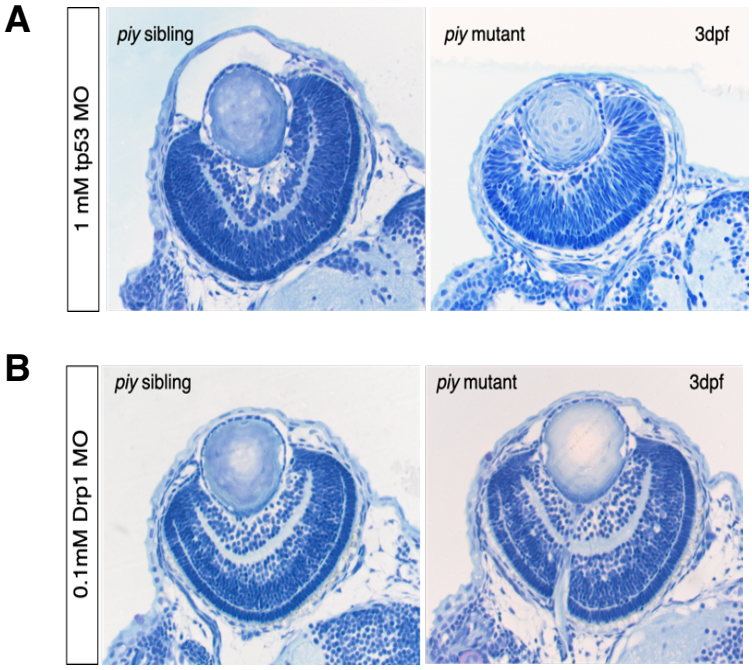

Figure 6. 10: Rescue experiment
(A) Plastic sections of 3 dpf *piy* mutant embryos injected with 1mM *p53* MO showing rescue of *pinball* eye phenotype.
(B) Plastic sections of 3 dpf *piy* mutant embryos injected with 0.1mM *Drp1/dnm1l* MO showing rescue of cell death in *pinball* eye mutant.

piy mutant retinas. In addition to decrease in retinal cell death in *piy* mutants, *p53* morphants also exhibited delay in retina development (Fig.6.10A). Similarly, knockdown of GTPase, *Drp1/dnm1l* (dynamin like-1 protein), also rescued *piy* mutant cell death phenotype at 2 dpf (Fig.6.10B). Knockdown of downstream molecular targets of p53 such as *bbc3/PUMA*, *Bax1, Bax2, Casp9, Casp8 or Casp3a* could not rescue *piy* mutant cell death phenotype even at high concentrations (data not shown).

As p53 MO rescued cell death phenotype in piy mutant, we generated *piy; p53* double mutants, to study microglia precursors behavior in *piy* mutant with *p53* mutant background. The rationale was to minimize micro-injection effects and find if molecules between DNA-damage and p53 activation could communicate with microglia precursors. To confirm genetic knockout of *p53* could rescue piy mutant phenotype, , we performed toluidine staining of plastic sections of 2 dpf retinas of *piy; p53;[ath5:GFP;mfap4TdTCAAX]* embryos. The *piy-p53* double mutants plastic sections showed clear retinal neurodegeneration similar to *piy* mutants (Fig.6.11A), suggesting the possibility of either genetic compensation by p53 homologues such as p63 and p73, or activation of p53-independent extrinsic cell death pathway, which may bypass ATM-Chk2-p53-dependent apoptosis in *piy; p53* double mutants.

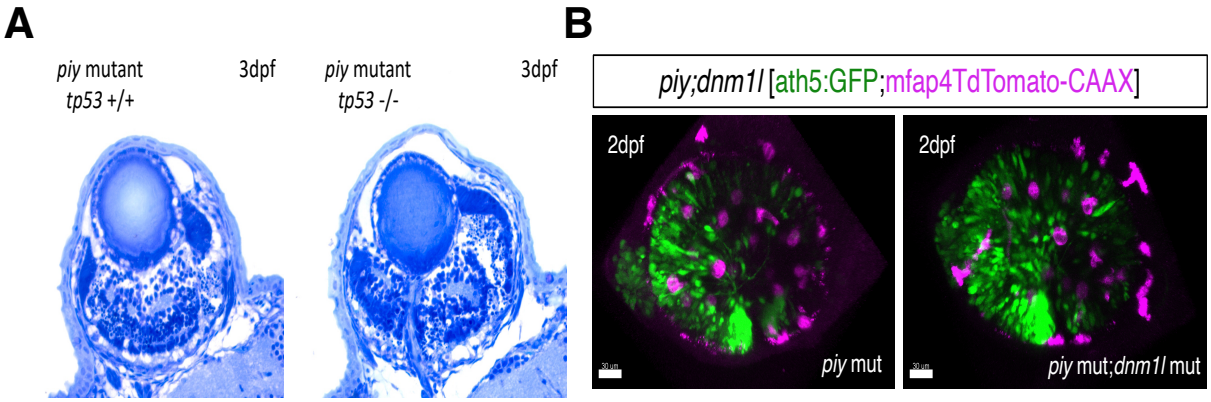

Figure 6. 11: Analysis of *piy-/-;tp53*+/+ and *piy-/-;dnm1l-/-*

(A) Plastic sections of 3 dpf *piy-/-;tp53*+/+ and *piy-/-;tp53-/-* embryos showing extensive cell death of retinal neurons in both *piy-/-* and double genetic mutant of *piy-/-;p53-/-*.
(B) Live images of *piy; dnm1l;* Tg[ath5:GFP;mfap4-TdTCAAX] showing retinal cell death and round activated mfap4 positive cells in both *piy-/-* and *piy-/-;dnm1l-/-* mutants.

On similar lines, we generated double mutant *piy; dnm1l; Tg[ath5:GFP;mfap4TdTCAAX]* to study microglia behavior in *piy* where mutant phenotype is rescued by genetic mutation in *dnm1l*. Analysis of live images of *piy; dnm1l* double mutants showed no rescue of cell death in double mutants at 2 dpf (Fig.6.11B). This result raise a possibility that genetic compensation

mechanism may also bypass apoptosis in *piy; dnm1l* double mutants. Further investigation is necessary to explain this phenotypic difference between *p53* or *dnm1l* morphants and their genetic mutants.

6.3.5. RNA sequencing data

As knockdown experiments did not provide concluding results, we performed bulk RNA sequencing analysis of wild-type sibling and *piy* mutant brain at 2 dpf to decipher the detailed molecular mechanisms behind the retinal cell death. Many genes were up/downregulated in *piy* mutants as compared to wild-type siblings. Genes related to cell-cycle arrest, apoptosis, inflammation were upregulated in *piy* mutants as compared to siblings. Analysis of RNA sequencing data of *piy* mutants showed significant increase in expression of genes which play

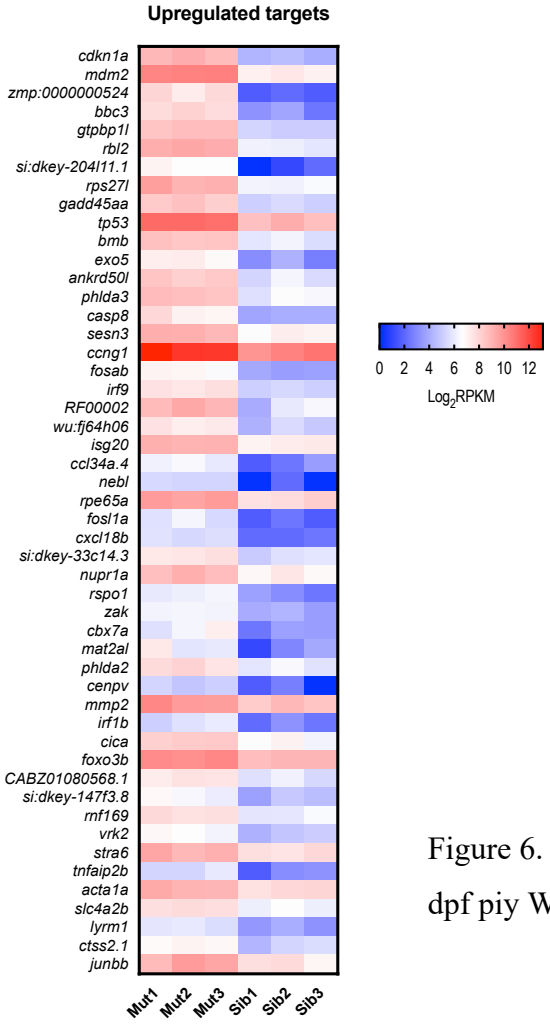

Figure 6. 12: Heatmap of RNA sequencing of 2 dpf piy WT siblings and mutants

critical roles in cell-cycle arrest. *Ccng1, mdm2, parp3, g0s2* were significantly upregulated, indicating that cell-cycle arrest and DNA damage repair are activated in *piy* mutants. In addition, pro-apoptotic genes such as *p21, tp53, bbc3(PUMA), Casp8* were also upregulated.

Interestingly, *Caspase 8* was upregulated in *piy* mutant, which is known to be involved in extrinsic cell death pathway independent of *p53* signaling. *Caspase 8* is also known to bypass

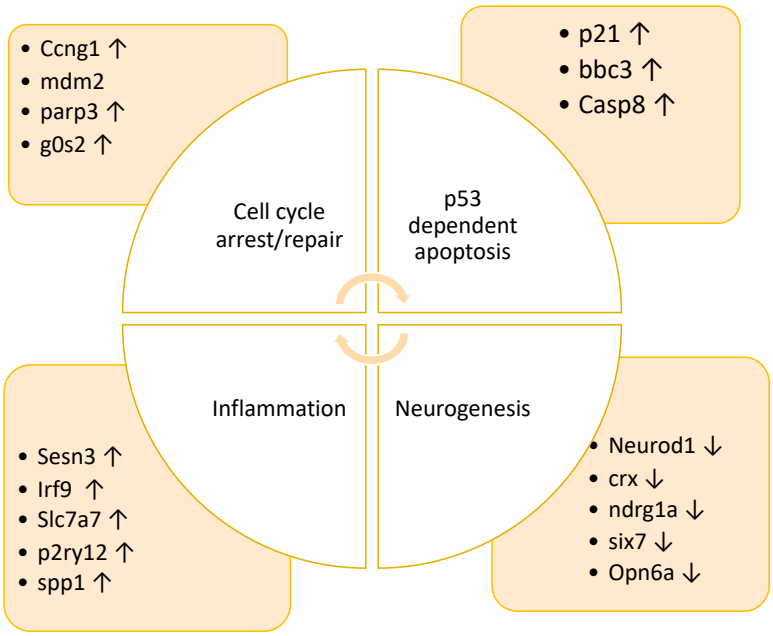

Figure 6. 13: Altered process in 2dpf *piy* mutants.

p53 pathway in presence of activated ATM/ATR which can cause apoptosis (Sidi et al., 2008). Altogether , the data indicates that the retinal cell death in *piy* mutants could be a combination of p53-dependent and independent pathway. Further investigation will be required to address role of extrinsic cell death pathway, involving *Caspase 8*, in retinal apoptosis in *piy* mutants.

PUMA (bbc3) was another pro-apoptotic gene, which was upregulated in *piy* mutants. *bbc3* is known to be a key player in p53-dependent apoptosis; but is also involved in ER-stress induced

cell death mechanisms. We validated genes involved in cell-cycle arrest and apoptosis using quantitative PCR. Caspase 8 and PUMA were consistently high in transcriptomic study and quantitative mRNA analysis (Fig.6.14).

Bulk RNA analysis also revealed that many major retinal related neurogenesis genes were downregulated in *piy* mutants. *Neurod1, six7, crx, Opn6a,* markers of differentiated retinal neurons in zebrafish were significantly downregulated suggesting either neurons failed to differentiate or neuronal loss due to cell death. Bulk RNA sequencing data also showed upregulation of microglia specific markers like *slc7a7, p2ry12*. Expression of genes involve in

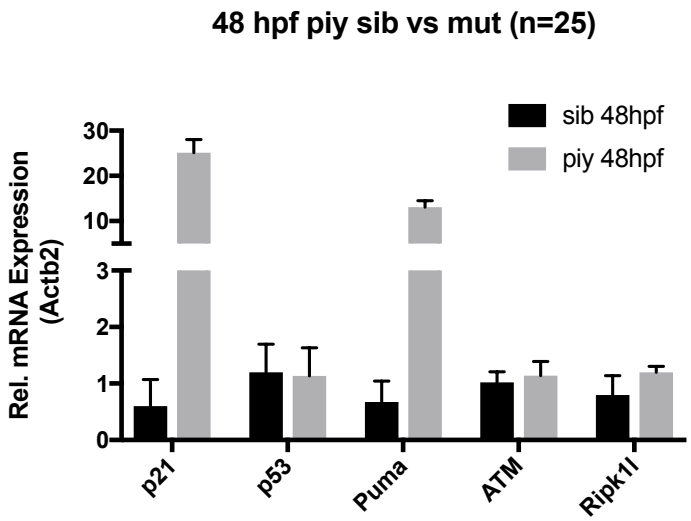

Figure 6. 14: Relative mRNA expression of *p21, p53, PUMA, ATM* and *Ripk1l* in piy mutants at 48hpf (2dpf).

microglia attraction such as *Sesn3, Spp1,* was also upregulated. This data explains the increase in microglia and confirms heightened immune response in piy mutants at 2dpf at molecular level as compared to its WT sibling.

6.4 Discussion

Microglia respond to cell death, injury and accumulation of cell debris in zebrafish brain similar to their counterparts in mammalian systems. An elegant study in zebrafish have revealed cross talk between neuronal regeneration and immune responses within the retina (Mitchell et al., 2019). This study also suggested that resident microglia and peripheral macrophages instruct Müller glia to initiate neuronal regeneration in response to retinal damage. Thus, embryonic zebrafish retina provides an excellent model system to elucidate communication between damaged neurons, microglia and Müller glia. For understanding the role of embryonic microglia in neuronal degeneration and regeneration, I studied zebrafish *piy* mutants, where retinal neurons are pre-disposed to undergo apoptosis due to *prim1* mutation.

In *piy* mutants, extensive cell death is observed in highly proliferating region such as the retina and optic tectum, whereas other brain regions were relatively unaffected. Previous study from the our laboratory demonstrated that differentiating retinal cells in *piy* mutant undergo ATM-Chk2-p53 dependent apoptosis at 48hpf (Yamaguchi et al., 2008). However, the behavior and response of microglia in *piy* mutant retinas under conditions of severe degeneration was not investigated. To demonstrate the behavior of embryonic microglia and identify "Find-me signals", I counted the number of ocular microglial precursors in *piy* mutants before induction of apoptotic cell death. I found that microglial cell number was marginally yet significantly increased at 32 hpf in *piy* mutant retinas. TUNEL signal was also marginally higher in *piy* mutant retina at 33 hpf. To further elucidate behavior of microglial precursors in *piy* mutant retinas, I studied microglial precursors number and morphology in progressively degenerating retina at 48hpf. Interestingly, the number of microglial precursors in *piy* mutants retina was not significantly altered relative to WT siblings. Having said that, I noticed a stark difference in shape and size of microglia precursors in mutant retinas, suggesting that microglial precursors

were actively involved in removal of dying or dead retinal neurons via phagocytosis. Quantification of sphericity microglial precursors in *piy* mutants retina correlated their activated state. Removal of microglial cells in piy mutants showed increased neurodegeneration in *piy* mutant retinas. A step-wise knockdown analysis of targets involved in DNA-damage response and apoptosis inducing molecular machinery, uncovered the existence of non-classical mechanisms of cell death. In addition, transcriptome analysis of *piy* mutants also showed upregulation of *Caspase 8*, a protease involved in extrinsic apoptotic pathway, which is independent of *p53* signaling.

In conclusion, apoptosis of retinal neurons commences in *piy* mutant retina as early as 33hpf. Extensive cell death in *piy* mutant retina activates phagocytic activity of ocular microglial cells, but does not accelerate recruitment of microglial precursors from periphery into the developing retina. Furthermore *piy* mutants also don't exhibit cell proliferation of existing ocular microglial precursors. However, this remains to be seen if microglial precursors in *piy* mutants are steadily being replenished from periphery during the course of retinal neurodegeneration.

Activated immune cells like microglia (Tang and Le, 2016, Keren-Shaul et al., 2017) or employed peripheral macrophages and T-cells have been implicated in promoting neurodegeneration in many disease models (Harms et al., 2013). Elimination of embryonic microglial precursors in *piy* mutants by knock down of transcription factor *Pu.1*, has demonstrated enhanced neurodegeneration *piy* retinas. This indicates that ocular microglial precursors have neuro-protective function in *piy* retinas. One plausible scenario is that, activated microglial precursors eliminate neuronal debris from *piy* mutants retina. However, absence of microglial precursors leads to accumulation of dead cells in retina which in-turn

fast-tracks neuronal cell death. In order to relate molecular events with observed microglial behavior in *piy* mutants, in-depth investigation is required.

In retina of *piy* mutants, embryonic microglial precursors exhibit morphology of activated matured microglia. This signifies that microglial precursors can attain accelerated maturity depending on environmental cues. Further detailed and stepwise investigation of cell-death pathway in *piy* model system could assist in finding molecules that prime embryonic microglia to get an activated state.

7. IV. Single cell RNA seq analysis of microglia precursors

7.1. Introduction

7.1.1. Transcription profile of microglia/macrophage in vertebrates

Under steady state conditions, myeloid cells are localized within parenchymal space of CNS. In addition, the CNS contains other subpopulation of myeloid cells such as leptomeningeal, perivascular and choroid-plexus macrophages, that localize within non-parenchymal space (Goldmann et al., 2016). Together these myeloid cells belong to the family of mononuclear phagocytes and therefore share some similar transcriptomic features. Differences in transcriptome however arise based on changes in environment and niche (Lavin et al., 2014).

In mice, microglial precursors appear between E7.0 to E8.0 dpc, within regions of extraembryonic yolk sac as part of primitive wave of hematopoiesis. The second wave of microglia is generated as part of the definitive hematopoiesis wave at ~E10.5 from regions within the embryo-proper. Microglia generated as part of this wave, migrate into developing CNS until the blood brain-barrier is formed by E13.5 (Fig.7.1) (Matcovitch-Natan et al., 2016, Crotti and Ransohoff, 2016).

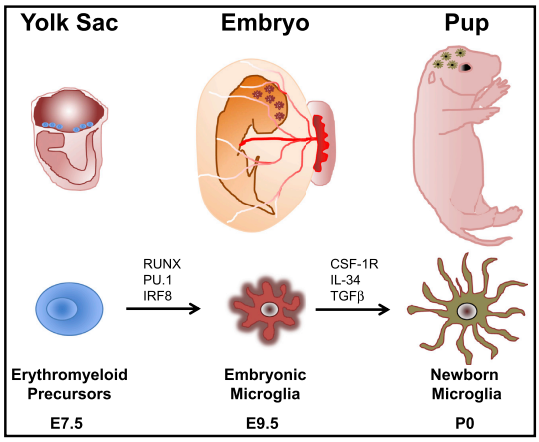

Figure 7. 1: Microglia origin in mouse embryos

Adapted from (Crotti and Ransohoff, 2016)

Over the past decade few transcriptome wide studies, both at bulk and single-cell resolution have shed light on characteristic gene expression profiles/networks of embryonic and adult microglia in mammals (Mitchell et al., 2019, Mathys et al., 2017, Matcovitch-Natan et al., 2016, Butovsky et al., 2014, Hickman et al., 2013). Based on these studies, mouse microglia are characterized as cells expressing markers such as *Hexb, Cx3cr1, P2ry12, Tmem119, Socs3, Gpr34, Siglech, Trem2* and *Gpr84*. In mice, adult microglia are known to originate in a *Pu.1* and *Irf8* dependent manner. Microglia sensome was first described in 2013 (Hickman et al., 2013). This study compared the transcriptome profile of microglia with macrophages derived from adult and aged mice. A battery of genes encoding receptors involved in pattern recognition and chemoattraction were found to be enriched in microglia compared to peripheral macrophages. *DAP12* and *Trem2* transcripts were shown to be important regulators of microglia sensing functions. Furthermore, expression levels of *DAP12* and *Trem2* differed in adult vs. aged microglia (Hickman et al., 2013).

In 2014, Butovesky and colleagues compared transcriptome of adult microglia vs. peripheral myeloid and immune cells in mice. The study identified 239 unique genes and 9 microRNAs specific to adult microglia. For instance, combination of miR-342-3p, miR-125b-5p and miR-99a were distinctly present only in adult microglia. They also found TGF-β1 as a major differentiation factor for adult microglia. These cells showed high expression level of *Tgfb1* and *Tgfbr1*. In addition, this study revealed that microglia signature genes were absent in microglia cell lines, hence suggesting that microglia-based culture studies might not be the true representation of *in-vivo* scenario (Butovsky et al., 2014).

In 2016, Matcovitch and colleagues revealed an extensive temporal expression profile of mouse microglia captured by RNA-seq, CHIP-seq, ATAC-seq and sc-RNAsequencing. On the basis of development time and transcription, microglia was described as (i) Early microglia: enriched in cell cycle and differentiation genes (*Mcm5*, *Dab2*) (ii) Pre-microglia: enriched in

genes related to neuronal development like synapse pruning (*Csf1*,*Cxcr2*) and (iii) Adult microglia: enriched in immune homeostatic genes (*Cd14*, *Mef2a*). At a given developmental time point, single-cell RNA sequencing showed high homogeneity in microglia population. Transcription factor *MAFB* was shown to regulate adult microglia homeostasis along with known TFs like *Pu.1* and *Irf8*. This study traced microglia development in germ-free mice and in immune system activated pregnant mice, putting impetus on environmental cues in shaping the immune profile of CNS (Matcovitch-Natan et al., 2016, Lavin et al., 2014).

In zebrafish, lack of specific markers for microglia has made it difficult to distinguish between non-parenchymal CNS macrophages and peripheral macrophages. In this model, microglial precursors originating from yolk sac, migrate to retina and other parts of brain starting at 30 hpf. These microglial/macrophage precursors undergo maturation at 54 – 60 hpf (Herbomel et al., 2001b). Over time, a second wave of microglia replaces the pool of embryonic microglia.

In 2017, Oosterhof and colleagues showed that microglia isolated from adult zebrafish brain had comparable gene expression as that of mouse and human microglia. *Mpeg* positive zebrafish microglia were enriched in microglia specific genes such as *apoeb, csfr1a, slc7a7 and irf8*. In addition, these cells showed high expression of *tlr1, tlr7, tlr21* (Toll-like receptors), *cxcr5, cxcr12a, ccr9a* (chemokine receptors), *p2rx7, p2ry12* (purinergic receptors) and MHC-II complex genes (Oosterhof et al., 2017).

Recently bulk RNA sequencing analysis of microglia from larval zebrafish also confirmed conservation of microglia genes during early zebrafish developmental stages (Mazzolini et al., 2020). To our knowledge, no study has been conducted at single-cell level in larval zebrafish to decipher transcriptomic changes accompanying the early transition of microglia precursors into mature CNS resident microglia and subtypes associated with these developmental stages.

Thus, we conducted this experiment to study transcriptomic developmental profile of microglia/myeloid precursors of embryonic zebrafish brain at single-cell resolution.

7.2. Materials and methods

Isolation of mpeg1.1 cells from zebrafish larval heads

Media required

1. E3 media: 6.4 mM KCl,0.22 mM NaCl, 0.33 mM CaCl2 2H2O, 0.33 mM MgSO4 7H2O.
2. Media A: 15mM HEPES and 25 mM D-glucose in 1x HBSS.
3. 1x DPBS.
4. Density gradient medium (100%): 9 volume of the density gradient medium in 1 volume of 10x HBSS.
5. Density gradient medium (22%): 22ml of the density gradient medium (100%) in 88ml of 1x DPBS.

Embryo collection and sorting

1. Embryos were collected immediately after fertilization at 0dpf and incubated at 28.5^0 C in E3 media.
2. 1-phenyl 2-thiourea (PTU) was added to collected embryos after 75% epiboly stage to inhibit pigmentation.
3. Embryos were sorted at 2 dpf on the basis of EGFP expression and split into sets of 20 embryos in 90mm dishes.

Dissection and Homogenization (performed at 4^0 C)

1. 1ml Tricaine was added to petri dish containing 20 embryos in 25ml of E3 media and 1.5ml PTU. Petri dishes were kept on ice to maintain temperature of 4^0 C during course of dissection.
2. Anesthetized embryos were then transferred to ice-cold E3 media with tricaine in petri dish.
3. Larval heads were transected over the yolk sac using surgical micro-scissors.
4. Dissected head were collected using the Pasteur plastic bulk pipette into a glass homogenizer kept on ice containing 1ml ice-cold Media A.
5. Ice-cold E3 media +Tricaine in petri dish and glass homogenizer was replaced every 30 mins or until the color of media started fading.
6. Once all heads were collected (~500 heads/stage), Media A in glass homogenizer was replaced by 1 ml of fresh Media A.
7. Brain tissue was thereafter disrupted with a dounce homogenizer (tight) on ice. 60 rounds of crushing wre performed on ice for 2-5 dpf larvae.
8. Media A was added to cell suspension (1ml/200 heads) to dilute cell density and reduce cell aggregation/clumps during density gradient medium separation.
9. Cell suspension was passed through 40 μm cell strainer placed on top of ice cold 50 ml falcon tube. This step was repeated 3 times.
10. 1 ml of this cell suspension was then transferred to a fresh sterile1.5ml cold Eppendorf tubes and spun at 300g for 10 minutes at 4^0 C.
11. Supernatant was removed using a 10-ml syringe attached to 23Gx1 needle.

Density gradient separation

1. Cell pellet was re-suspended in 1ml of ice-cold 22% density gradient medium. 0.5ml of ice-cold 1x DPBS was gently overlaid on cell suspension without mixing these two solutions.

2. Tubes were thereafter spin at 950 g (without brake and slow acceleration) for 30 minutes at 4^0 C. Desired cell pelleted at the bottom of the tube and supernatant was removed using 10-ml syringe + needle 23Gx1".
3. Cells were thereafter washed with 0.5ml of Media A +2% normal goat serum and centrifuged at 300g for 10 minutes at 4^0 C.
4. Approximately 80-90% of was gently discarded leaving the cell pellet for resuspension in 500 µl of 1x DPBS + 2 % NGS. 1 µl of 7AAD was also added to label dead cells in cell suspension. Cell suspension was immediately taken for sorting using BD FACSAria cell sorter.

Cell sorting

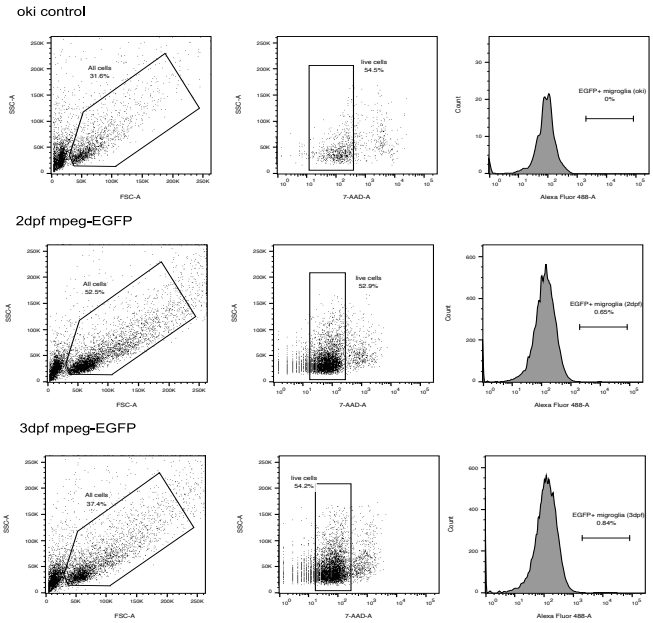

Figure 7. 2: FACS settings for live EGFP singlets from samples.

1. Analysis of cell suspension was performed using calibrated laser settings for each fluorophore/dye. Singlets were separated from doublets/multiplets by adjusting FSC and SSC settings as shown in Fig. 7.2.
2. Percent of EGFP positive cell population in WT (Oki), 2dpf-mpegEGFP and 3dpf-mpegEGFP are shown in Fig. 7.3.

	Sample Name	Subset Name	Count
	sample_mpeg-egfp low 488_001.fcs	EGFP+ migroglia (3dpf)	200
	sample_mpeg-egfp low 488_001.fcs	EGFP+ migroglia (2dpf)	139
	sample_oki-low 488_002.fcs	EGFP+ migroglia (oki)	0

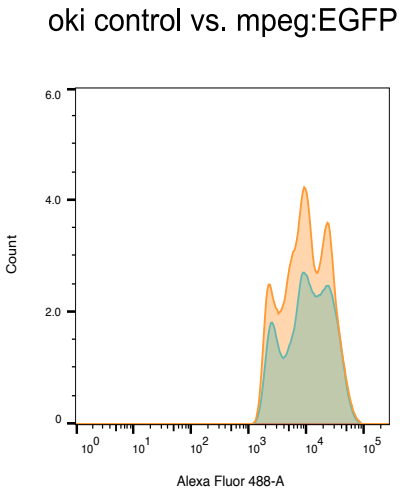

Figure 7. 3: Histogram of EGFP positive cells derived from 2dpf-mpegEGFP embryos vs. cells derived from oki embryos.

Single cell library preparation using 10X chromium platform

Reagents required

1. Single cell gel beads
2. RT reagent mix, RT primer, additive A, RT enzyme mix
3. 50% glycerol

Preparing single cell master mix and loading on Single cell A chip

1. Master mix was made as shown in the table:

Master mix	2.2 rxn (µl)
RT reagent mix	110
RT primer	8.36
Additive A	5.28
RT enzyme mix	22
Total	145.64

2. Master mix was mixed gently by pipetting 15x followed by brief centrifugation.
3. 50% glycerol was added into unused well except ones designated as recovery wells.
4. 66.2 µl master mix was added to each well of tube strip placed on ice. Appropriate amount of nuclease-free water was added to master mix.

5. Appropriate volume of cell suspension is added into each tube strip well. For ~4000 cells and 800 cells/µl, 8.7 µl cell suspension + 25.1 µl of Nuclear free water? (NFW), For ~5000 cells and 1000 cells/µl, 8.7µl cell suspension + 25.1 µl of NFW. Pipette mix 5 times on ice.
6. 90 µl master mix+ cells were dispensed into row1 of single cell chip.
7. Single Cell 3' Gel bead strip was snapped and vortexed for 30 sec. 40 µl Single Cell 3' Gel beads were added into row2.
8. 270 µl of Partitioning oil was added to row3.
9. A 10x gasket was attached such that holes on the gasket were aligned to wells on Single cell chip.
10. The assembled chip was placed in Chromium controller and Single cell A program was run.
11. 100 µl of GEMs collected in recovery well were then transferred into 8-well PCR strip and maintained on ice.
12. PCR strip was then placed into thermal cycler and following incubation program was run:

Lid temperature	Reaction volume	Run time
53^0 C	125 µl	55 min
Step	Temperature	Time
1	53^0 C	45:00
2	85^0 C	5:00
3	4^0 C	Hold

13. PCR product was stored overnight at 4^0 C.

Post GEM-RT cleanup and cDNA amplification

Reagents required

1. Additive A
2. cDNA additive
3. cDNA primer mix
4. Amplification master mix
5. Buffer sample clean up

Post GEM-RT cleanup-silane Dynabeads

1. 125 µl recovery agent was added to RT PCR product and mixed by pipetting.
2. 125 µl recovery agent was then removed and discarded. 200 µl Dynabeads cleanup mix was added to remaining solution and mixed. This solution was incubated for 10 min on H magnet.

DynaBeads cleanup mix	1x µl
Nuclease-free water	9
Buffer sample clean up 1	182
Dynabead MyOne SILANE	4
Additive A	5
Total	200

3. Supernatant was removed and pellet was washed three times with 300 µl of 80% ethanol. After complete removal of ethanol, 35.5 µl elution solution was added and incubated for 1 min on L magnet. 35µl of sample was transferred to new strip.

cDNA amplification and Cleanup-SPRIselect

1. cDNA amplification reaction mix:

cDNA amplification reaction mix	1x µl
Nuclease free water	8
Amplification master mix	50
cDNA additive	5
cDNA primer mix	2
Total	65

2. 65 µl of cDNA amplification reaction mix was added to 35µl of purified GEM-RT product. Total solution was pipette mixed and placed in thermal cycler. The following program was run.

Lid Temperature	Reaction volume	Run time
105^0 C	100 µl	30-45 min
Step	Temperature	Time
1	98^0 C	3:00
2	98^0 C	0:15
3	67^0 C	0:20
4	72^0 C	1:00
5	Go to step 2	
6	72^0 C	1:00
7	4^0 C	Hold

3. 60 µl of SPRIselect reagent was added to cDNA amplification product and incubated for 5 min on H magnet. Thereafter supernatant was removed and pellet was washed three times using 80% ethanol.
4. 40.5 µl Buffer EB was added to pellet and mixed. Followed by incubation for 2 min on H magnet. 40µl sample was transferred to new PCR strip.
5. 1µl of sample was then loaded on Agilent tape station High Sensitivity D1000 screen tape for qualitative analysis.

Library construction

Reagents required

1. Fragmentation buffer, fragmentation enzyme blend
2. Ligation buffer, DNA ligase, Amplification master mix
3. Adaptor mix
4. SI-PCR primer
5. Chromium i7 sample index plate

Fragmentation, End repair and A-tailing

1. 15 µl of fragmentation buffer was mixed with 35 µl purified cDNA. Composition of fragmentation buffer is as follows:

Fragmentation mix	1x µl
Fragmentation enzyme blend	10
Fragmentation buffer	5
Total	15

2. Chilled tube strip was then placed in pre-cooled thermal cycler and Fragmentation program was started.

Lid Temperature	Reaction volume	Run time
65^0 C	50 µl	35 min
Step	Temperature	Time
Pre-cool block	4^0 C	Hold
Fragmentation	32^0 C	5:00
End repair and A-tailing	65^0 C	30:00
Hold	4^0 C	Hold

3. 30 µl SPRIselect was added to post fragmentation solution and incubated for 5 minutes on H magnet.
4. 75 µl of supernatant was thereafter collected in a new PCR strip. 10 µl SPRI select reagent and resultant solution was mixed 15 times followed by % minute incubation on H magnet.
5. 80 µl of supernatant was removed, and the pellet was washed three times with 80% ethanol.
6. 50.5µl of Buffer EB was added to pellet, mixed and incubated for 2 min at H magnet.
7. 50 µl of sample was thereafter transferred to new tube strip.

Adaptor ligation, Cleanup-SPRIselect and sample Index PCR

Adaptor ligation mix	1x µl
Nuclease-free water	17.5
Ligation buffer	20
DNA ligase	10
Adaptor mix	2.5
Total	50

1. 50 µl adaptor ligation mix (as indicated in table above) was added to 50 µl of post fragmented, end repaired and A-tailed sample.
2. Mixed thoroughly and run through Adaptor ligation program.

Lid Temperature	Reaction volume	Run time
30^0 C	100 µl	
Step	Temperature	Time
1	20^0 C	15:00

3. To the adaptor ligated mixture, 80 µl of SPRI select reagent was added and incubated for 5 min on H magnet.
4. Supernatant was removed and the pellet was washed three times with 80% ethanol.

5. Washed pellet was resuspended in 30.5 µl Buffer EB and thereafter incubated on L magnet for 2 min.
6. 30 µl sample was collected in a new PCR tube.

Sample index PCR mix	1xµl
Nuclease free water	8
Amplification master mix	50
SI-PCR primer	2
Total	60

7. 60 µl of sample index (as indicated in table above) was added to collected sample.
8. 10 µl of aliquot of unique Chromium i7 Sample Index was added to above solution mix and pipette mixed.
9. Thereafter PCR tube was placed in thermal cycler and the following program was run for 12-14 cycles.

Lid Temperature	Reaction volume	Run time
105^0 C	100 µl	25-40 min
Step	Temperature	Time
1	98^0 C	0:45
2	98^0 C	0:20
3	54^0 C	0:30
4	72^0 C	0:20
5	Go to step 2	
6	72^0 C	1:00
7	4^0 C	Hold

Post Sample index Double sided size selection

1. After sample indexing, 60 µl SPRIselect reagent was added to sample and incubated on H magnet.
2. 150 µl supernatant was then transferred to a new strip.
3. 20µl SPRIselect reagent was further added and incubated on H magnet for 5 min.

4. Supernatant was removed and pellet was washed three times with 80% ethanol.
5. The pellet was resuspended in 35.5 µl Buffer EB and thereafter incubated on L magnet for 2 min.
6. 35 µl sample was collected in a new PCR tube.
7. 1µl of sample was then loaded on Agilent tape station High Sensitivity D1000 screen tape for qualitative analysis.

Sequencing and Analysis

Generated Single cell libraries were sequenced using paired-end and single indexing on Illumina HiSeq4000 platform. Using Cell Ranger 3.1.0 (10x chromium platform), raw base call (BCL) files generated by Illumina sequencers were demultiplexed into FASTQ files. Quality filtering, alignment, and gene counting was performed by "cellranger count" using zebrafish GRCz11 genome database as reference. Seurat v3.1 (R package for single cell genomics) was used for further analysis of single cell transcriptomic data. Mitochondrial and ribosomal protein genes are regressed out from the variables examined in the following analysis. Principle component analysis (PCA), elbow plot and JackStraw plot were used to determine the dimensionality of scRNA sequence dataset. For non-linear dimension reduction, UMAP technique was used and cell clusters were generated by Seurat's "FindNeighbors" and "Findclusters" function. Feature and expression data in cell clusters was obtained by FeaturePlot and VlnPlot.

7.3. Results

7.3.1. Single cell transcriptome analysis of 2 dpf mpeg1.1 cells using Seurat v3.1

We recovered low yield of target cells from 48 hpf embryos. Out of ~8000 sorted EGFP positive cells, only 471 cells were filtered after quality filtering and deemed good for further analysis. Marker analysis showed that only ~100 cells out of 471 were mpeg1.1/mfap4 positive. As FACS Aria has high false positive rate, it is possible that many non-EGFP cells were also sorted.

7.3.1.1. Dimension reduction of dataset

To avoid technical noise in any single feature of single cell RNA sequence data it is essential to make clusters based on PCA (Principal Component Analysis) scores. There are three main ways to determine "dimensionality" of a scRNA seq dataset: Resampling test, JackStraw plot and Elbow plot. The Principle components generated essentially represent a "metafeature", which defines the variance-covariance between the set of features using linear combinations. Fig 7.4.A,B shows the Elbow plot of 471 cells sequenced from 48hpf zebrafish embryo samples. The "elbow" in plot is achieved around PC7-8, indicating that first 7-8 PCs capture the true signals. We also checked the dimensionality of dataset using JackStraw plot , which also shows PC7-8 are significant ($P < 0.01$).

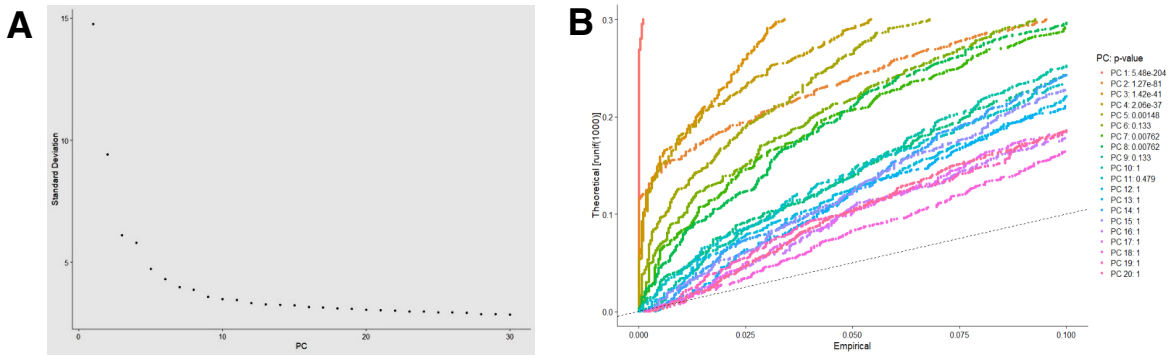

Figure 7. 4: Dimension reduction of 2dpf scRNA seq
(A) Elbow plot of cells sequenced at 48hpf, B) JackStraw plot

To perform non-linear dimension reduction, Seurat uses a novel manifold technique UMAP (Uniform Manifold Approximation and Projection) which is an alternative visualization tool to t-SNE. UMAP algorithm places similar cells of clusters in low-dimension space. We used 7 PCs as input for UMAP clustering analysis.

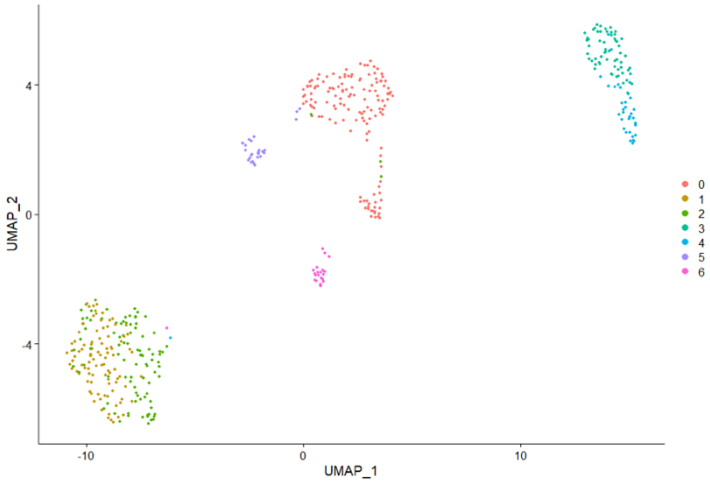

Figure 7. 5: UMAP plot showing similar cells grouped in 7 clusters in 48hpf sample

Fig 7.5. shows cluster generated by non-linear dimension reduction of 2 dpf cells. Seven cluster were obtained using UMAP algorithm. As the false positive rates in FACS sorting can be high,

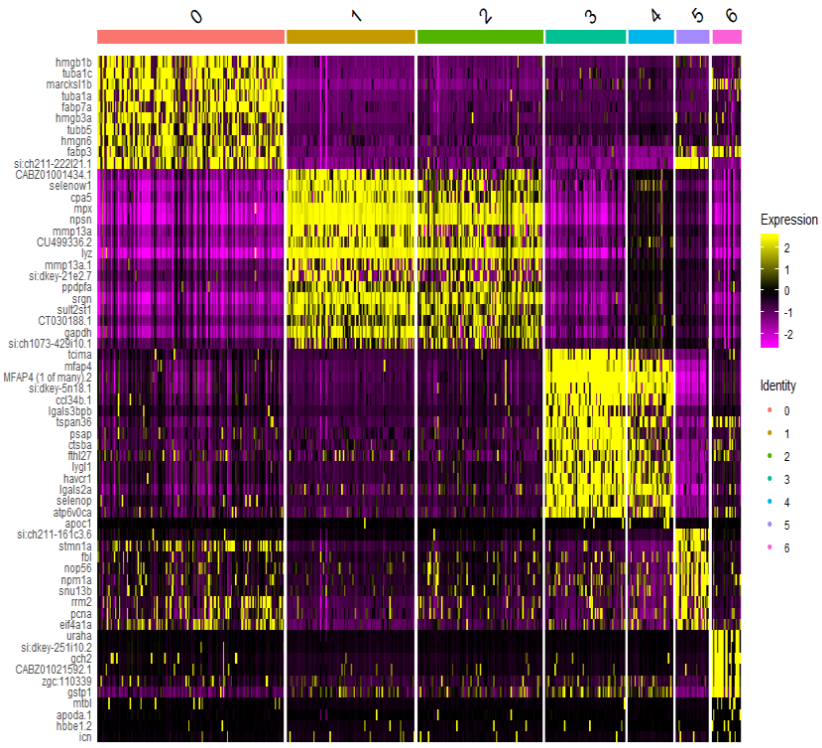

Figure 7. 6: Heatmap showing genes defining the clusters representing 48hpf data

visualizing cluster generated on basis of representative features/gene expression is necessary. Heatmap generated (Fig 7.6) visualizes 7 clusters generated on the basis of primary source of heterogeneity and top 10 markers. Cluster 0 had cells with top markers like *hmgb1b*, *hmgn6*, *hmgb3a*, *fabp3*, *marcksl1b*. These genes are mainly known to express in immature central nervous system and intermediate cell mass of mesoderm (Prieto and Zolessi, 2017). Cluster 1 and 2 showed cells expressing *mpx*, *lyz*, *mmp13a*, *ppdpfa* etc., characteristic of neutrophils. mfap4/mpeg1.1 expression was enriched in Clusters 3 and 4, indicating them to be true microglia/macrophage cell clusters.

We performed feature and expression analysis on these clusters to determine true microglia/macrophage cells. VlnPlot Fig 7.7 shows mpeg1.1 and mfap4 expression probability distribution across clusters. Similar to heatmap (Fig 7.6), only Cluster 3 and 4 represented microglia /macrophage cells sequenced from 48hpf head samples. A very small subset of mpeg1.1/mfap4 positive cells, suggests contamination of sample with non-myeloid cells.

To visualize expression of known markers of myeloid lineage cells such as, *mfap4, mpeg1.1, spi1a* and *apoeb* in a PCA plot we generated FeaturePlot (Fig. 7.8.). Feature plots visualizes feature expression in low-dimension space. Absence of *apoeb* expression in mfap4/mpeg1.1

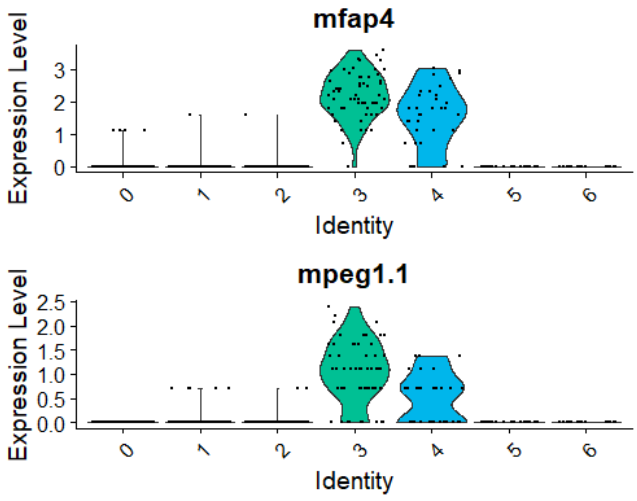

Figure 7. 7: VlnPlot showing mpeg1.1/mfap4 positive cluster (2,4) among 7 clusters in 48hpf sample

positive cluster suggests that myeloid/microglia precursors had not undergone differentiation till 48 hpf.

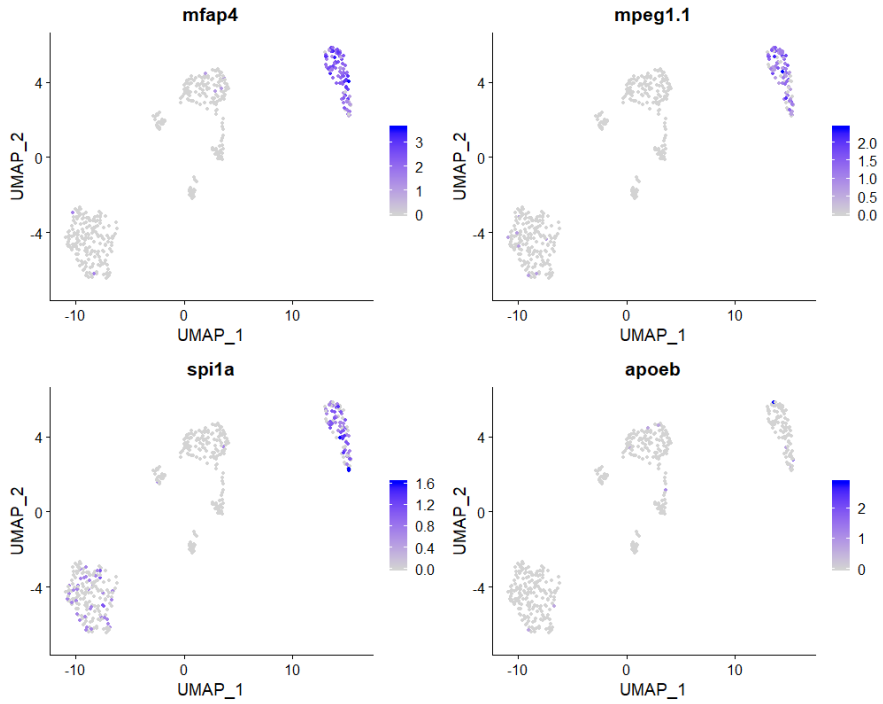

Figure 7. 8: FeaturePlot showing cluster representation of myeloid cell population in cells sequenced from 48hpf data

7.3.1.2. Cluster biomarkers

To identify differentially expressed features in mpeg.1./mfap4 clusters, we extracted cluster 3 and 4 from the dataset. To compare the gene expression of microglia/macrophage population with neutrophils, we also included cluster 1 and 2 in differentially expressed gene analysis (Fig7.9 and Fig7.10).

Many markers for microglia/macrophage cells, showed enrichment in cluster 3 and 4. In addition, we also found expression of biomarkers *tcima*, *tspan36*, *slc3a2a*, *ccl43b.1*, *slc37a2*, *selenop* corresponding to microglia/macrophage population within cluster 3 and 4. *Slc37a2*,

one of the cluster biomarker, was only enriched in cluster 3 at 48hpf (Fig7.9). *Slc37a2* has been recently shown to assist shrinkage of phagosomes in zebrafish microglia/macrophage (Villani et al., 2019). Our data shows that *slc37a2* is only expressed in one cluster of microglia/macrophage obtained by scRNA sequencing. This can be a potential candidate to distinguish between two population of microglia/macrophage at 48hpf in zebrafish embryos. Another differentially expressed gene, *slc3a2a,* known to play role in primitive myelopoiesis (Jia et al., 2019) is also expressed in mpeg1.1/mfap4 cells. Cluster 3 and 4 also show enrichment of chemokine *ccl34b.1*. To our knowledge this is the first study to shows specific expression of *ccl34b.1* in microglia/macrophage at early developmental stage of 48hpf in zebrafish.

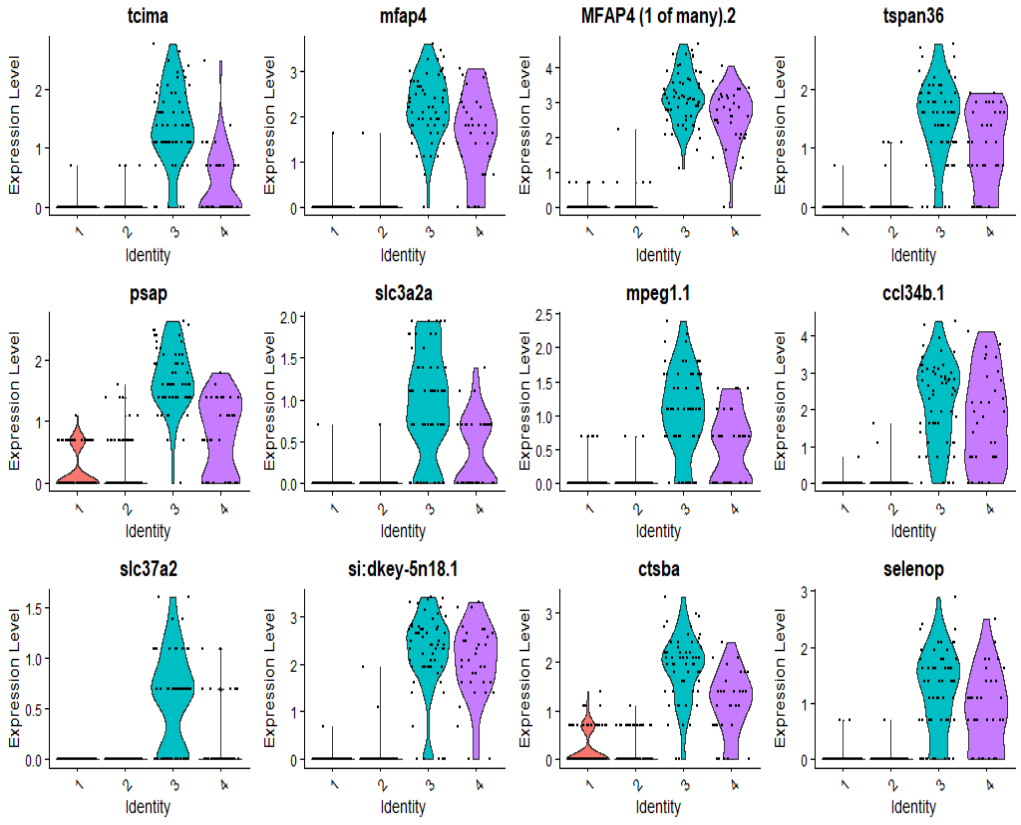

Figure 7. 9: VlnPlot showing differentially expressed genes in cluster 3 and 4.

Analysis of other biomarkers such as Lygl1 (codes lysosome g-like 1) and si:dkey-5n18.1 (codes C1q domain) showed that they were only expressed by early microglia/macrophages and not by neutrophils in zebrafish embryos. Gene *Igals2a,* also known as Drgal1-12 known to have role in regeneration in adult zebrafish retina (Craig et al., 2010), was also highly enriched in microglia/macrophage population at 48 hpf.

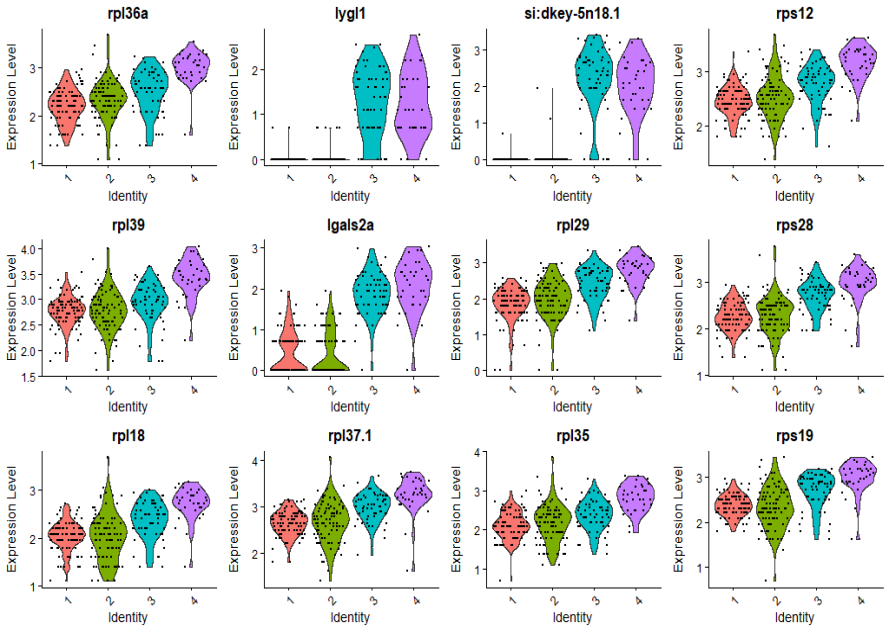

Figure 7. 10: VlnPlot showing differentially expressed genes in neutrophil and microglia/macrophage clusters

7.3.2. Single cell transcriptome analysis of 3dpf mpeg1.1 cells using Seurat v3.1

7.3.2.1. Dimension reduction of dataset

We generated ElbowPlot of 1107 cells (Fig6.9) obtained after filtration of sequenced cells on the basis of QC metrics, data normalization and scaling, and finding variable features. Same as 48hpf data, mitochondrial and ribosomal protein genes are regressed out for PCA and clustering analysis.

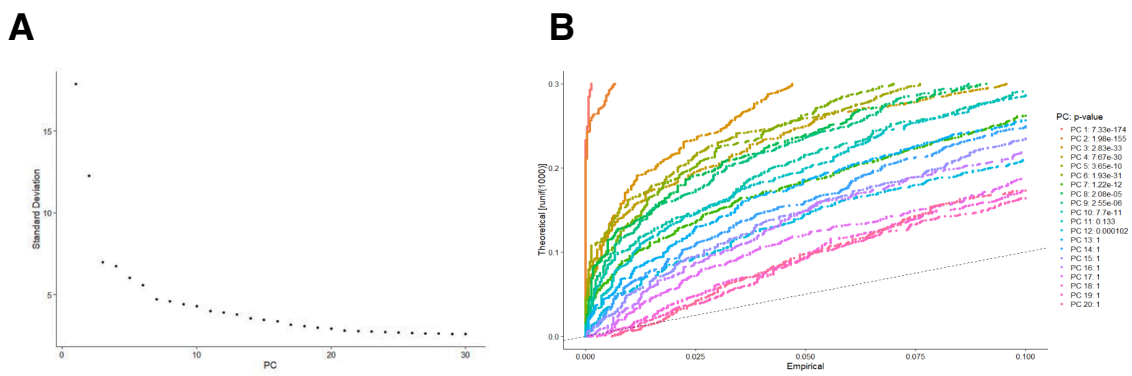

Figure 7. 11: Elbow and JackStraw plot of 1109 cells sequenced from 72hpf sample.

The "elbow" in plot is achieved around PC7-8 (Fig.7.11A), which is also significant ($P < 0.01$) in JackStraw plot (Fig.7.11B). Using the same PCs we obtained UMAP, placing cells into 11 different clusters (Fig 7.12).

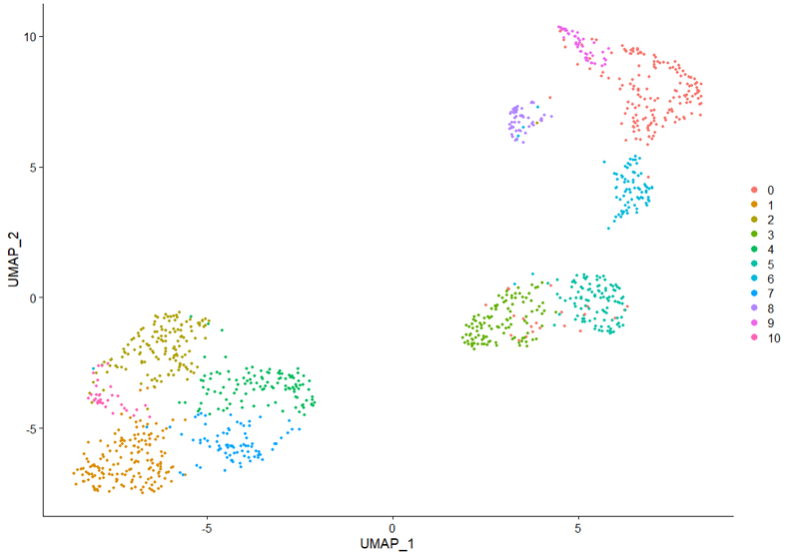

Figure 7. 12: UMAP plot showing similar cells grouped in 11 clusters in 72hpf sample

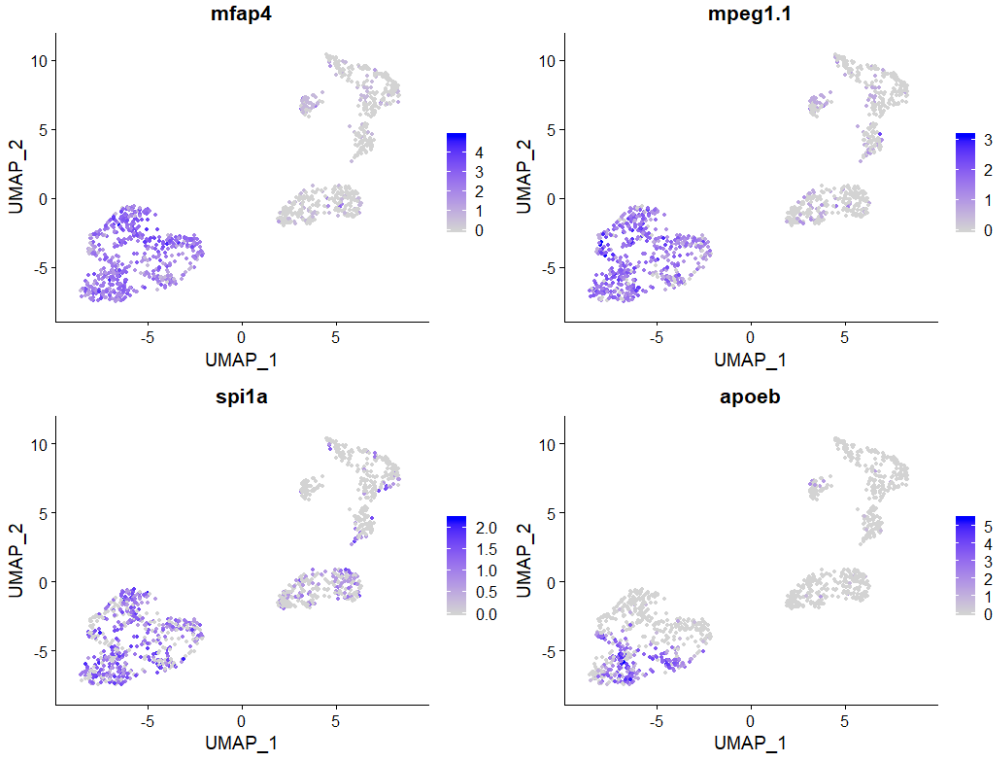

Figure 7. 13: : FeaturePlot showing expression of mpeg1.1, mfap4, spi1a and apoeb in the cluster obtained

To visualize expression of known markers of myeloid cells like, *mfap4*, *mpeg1.1*, *spi1a* and *apoeb* in specific clusters in a PCA plot, we generated FeaturePlot (Fig 7.13.). Expression of mpeg1.1 showed that only approximately half of sorted cell populations were microglia/macrophage, indicating contamination of cells with non-myeloid cells during sorting.

To further delineate the microglia/macrophage clusters from other clusters, VlnPlot was generated (Fig 7.14). VlnPlot confirmed that five clusters out of elven clusters (1,2,4,7 and 10) were true microglia/macrophage population.

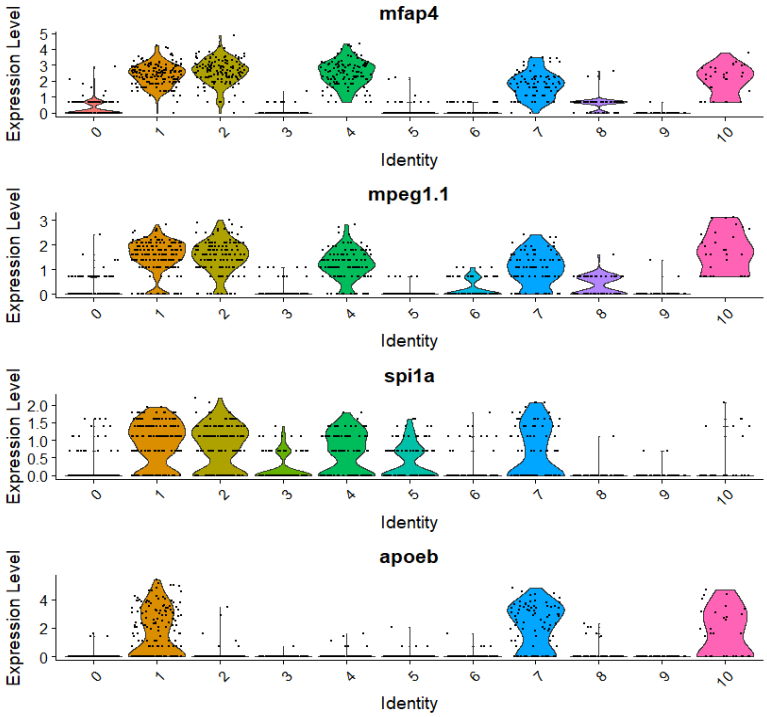

Figure 7. 14: VlnPlot showing expression of *mpeg1.1, mfap4, spi1a* and *apoeb* in specific clusters

7.3.2.2. Cluster Biomarkers

mpeg1.1/mfap4 markers were enriched in Clusters 1,2,4,7 and 10, designating these clusters as microglia/macrophage cells population in zebrafish larva at 72hpf. Expression of *apoeb*, used for identifying matured microglia/macrophage population, was restricted to cluster 1,7 and 10. This suggests that a heterogenous population of microglia exist at 72 hpf with respect to maturation status. To analyze differentially expressed features within five microglia/macrophage clusters, we extracted them from other clusters.

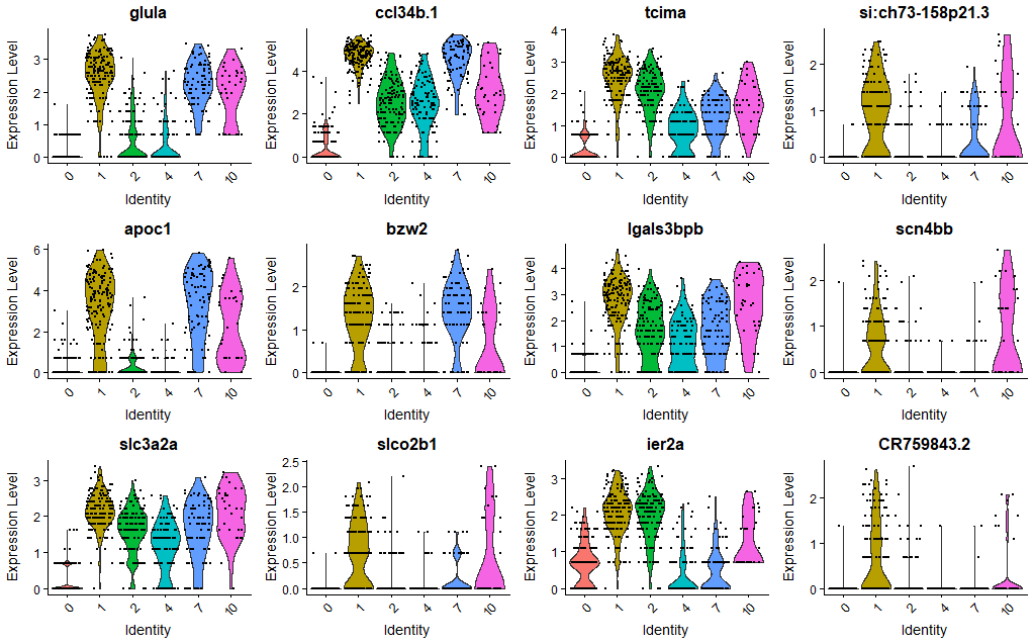

Figure 7. 15: VlnPlot showing differential features across microglia/macrophage clusters

Mature microglia/macrophage marked by *apoeb* expression and represented by cluster in 1,7 and 10 in VlnPlot, showed characteristic gene expression (Fig 7.15). Expression levels of top markers *glula, ccl34b.1, apoc1, bzw2, slcco2b1, scn4bb*. *Glula* and *ccl34b.1,* were high in mature microglia/macrophage cell population, relative to level in immature microglia/macrophage populations. Expression of *apoc1*, *bzw2*, *si-ch73-158p21.3* was limited to cluster 1,7 and 10, suggesting that these markers may be used to identify mature microglia/macrophage population at 72hpf. Marker genes such as *si-ch73-158p21.3*, known to be involved in antigen processing presentation and immune response, were also enriched in mature microglia/macrophage population.

We also identified unique gene expression that distinguish three different populations of differentiated microglia/macrophage (Fig 7.16). *Scn4bb* and *slco2b1,* known mouse/human homeostatic microglia signature were found to be specifically expressed in clusters 1 and 10, but not in cluster 7. These two clusters might represent true mature microglia cluster at 72 hpf. *Mt2* and *gpd1a* were two key markers which were enriched in subset of cells represented by clusters 1 and 7 only. Likewise, a member of pterin family, *pcbd1* was only expressed in cluster 7 (data not shown).

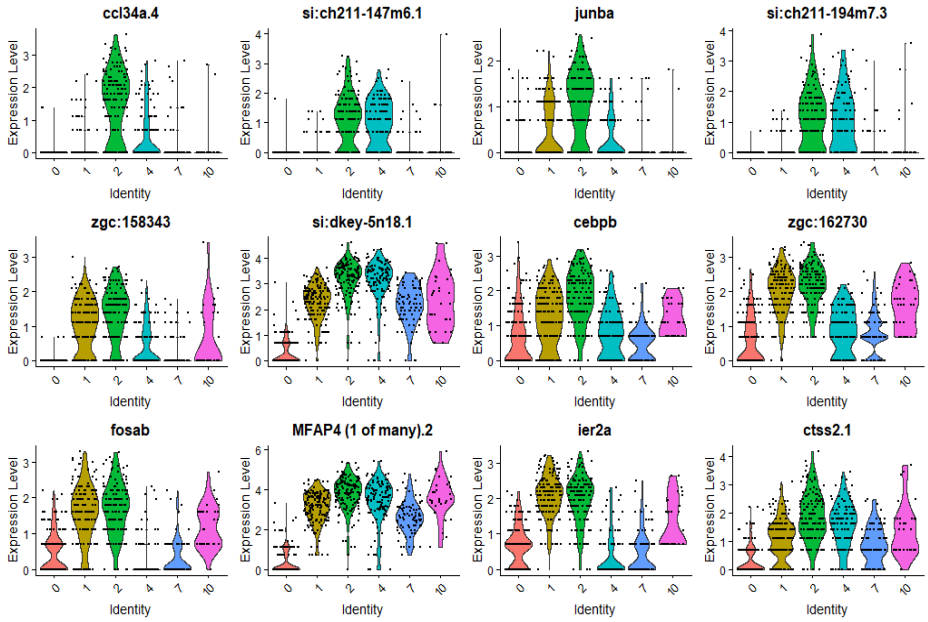

Figure 7. 16: VlnPlot showing differential features across microglia/macrophage clusters

Clusters 2 and 4 represented immature microglia/macrophage population at 72 hpf. VlnPlot (Fig 7.16 and 7.17) shows unique and overlapping gene expression of immature and mature cells. Markers *ccl34a.4*, *si:ch211-147m6.1* ,*f13a1b*, *si:ch211-194m7.4* were only expressed in immature microglia/macrophage population at 72 hpf. *ccl34a.4* which was highly enriched in cluster 2, is a known inflammation effector. Few cells in cluster 4 also expressed *ccl34a.4*, however mature cells seem to had negligible *ccl34a.4* expression. On the contrary immature

microglia/macrophage cell population at 48 hpf lack *ccl34a.4* expression. This indicates that undifferentiated microglia/macrophage population at 2 dpf and 3 dpf differ from one another.

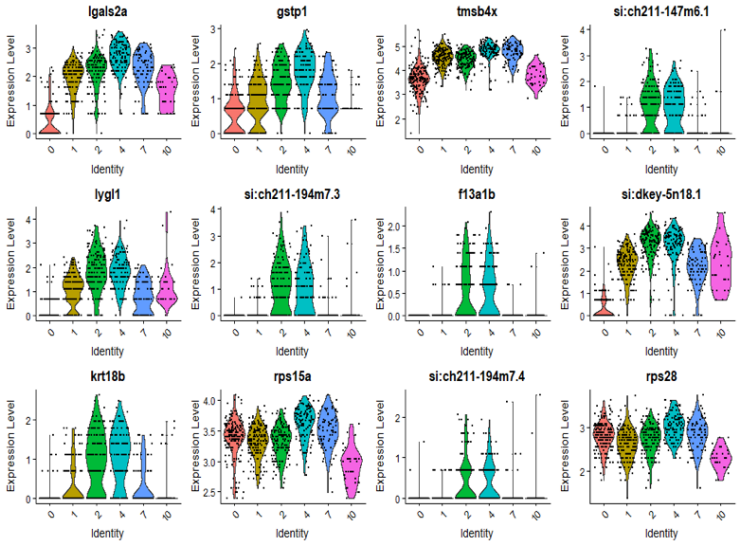

Figure 7. 17: VlnPlot showing differential features across microglia/macrophage clusters

Expression of *zgc158343, fosab, ier2a* in microglia/macrophage Cluster 2 indicates partial overlap in expression pattern with mature microglia/macrophage Cluster 1. Hence, Cluster 2 may represent an intermediate microglia/macrophage population of cells approaching maturation.

7.3.3. Comparative analysis of Single cell transcriptome 2dpf and 3dpf mpeg1.1 cells

To compare the mpeg1.1 positive cells from 2 dpf and 3 dpf, we combined the single-cell transcriptomic data of the two stages. 6 clusters were obtained from the merged data of 48hpf and 72hpf (Fig 7.18). Clusters 0 and 3 represented mature mpeg1.1 positive cells on the basis of *apoeb* expression (Fig 7.19).

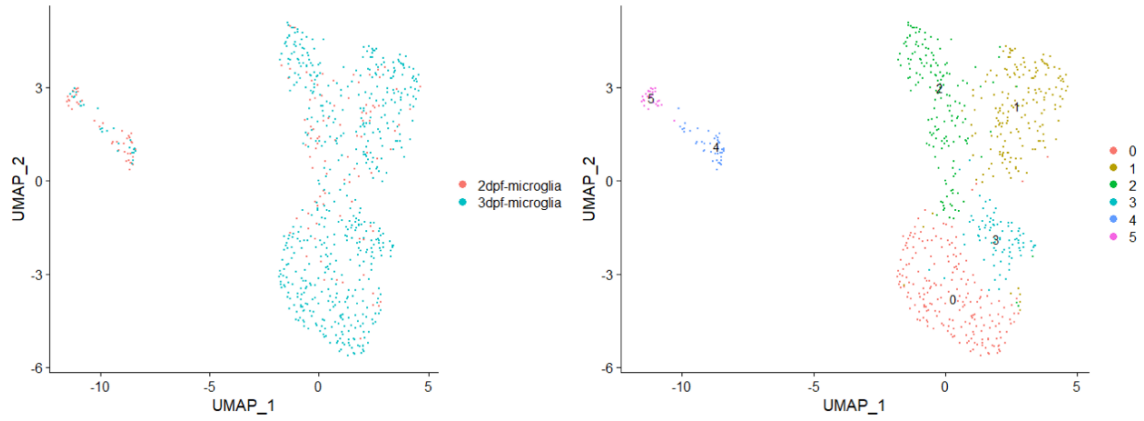

Figure 7. 18: UMAP plot showing microglia/macrophage clusters at 2dpf and 3 dpf

To further illustrate the difference between microglia/macrophage cells at two different time points during zebrafish development, we generated VlnPlot by combining the entire single-cell transcriptomic data, where the two color indicates mpeg1.1 cells from different developmental stages (Fig 7.20). Expression of genes such as *Scn4bb, apoc1, si:ch73-158p21.3, CR759843.2* were limited to and enriched in mpeg1.1 positive cells of 3dpf only. At 3dpf, mature mpeg1.1 cells

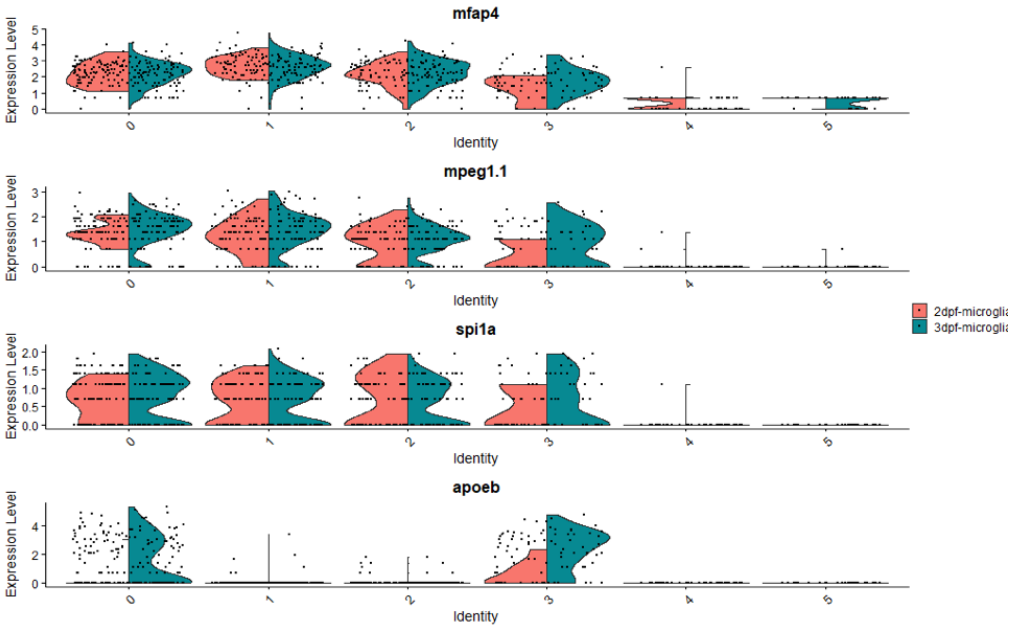

Figure 7. 19: VlnPlot showing microglia/macrophage clusters at 2and 3 dpf

have higher expression of *si:ch73-158p21.3* (an orthologue of mouse CD74a), indicating that these cells have higher ability of antigen processing and representation as compared to their counterparts at 2dpf.

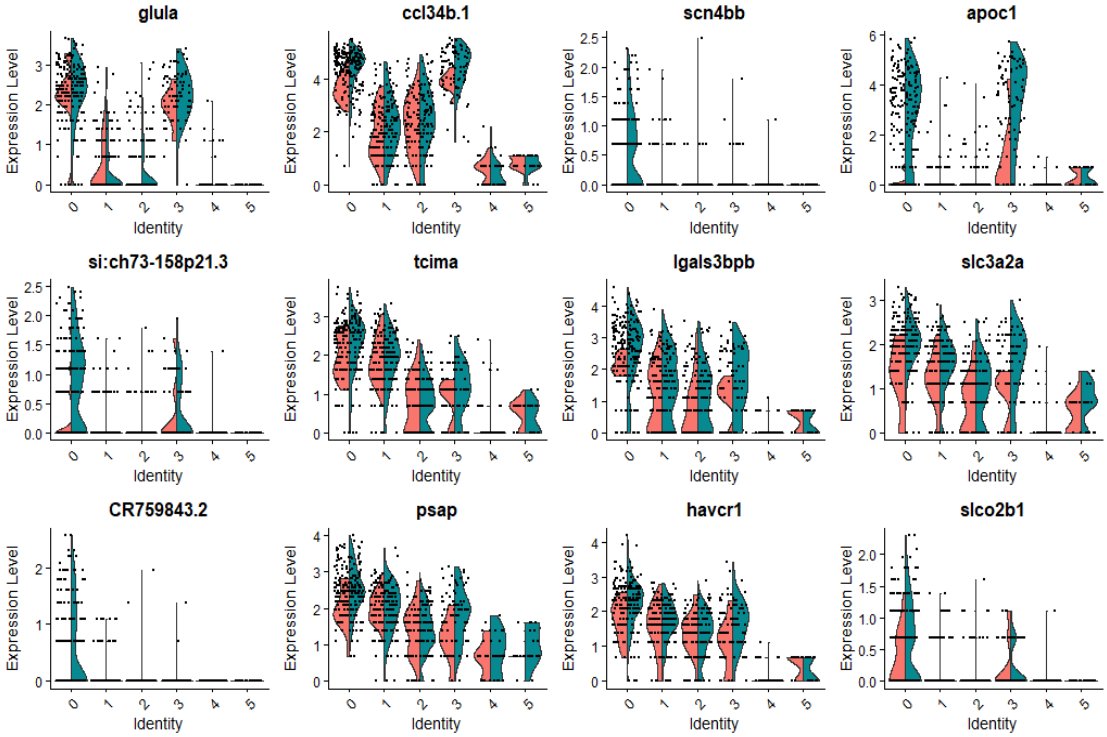

Figure 7. 20: VlnPlot showing microglia/macrophage clusters at 2dpf and 3 dpf

7.4. Discussion

Transgenic larval zebrafish provide an excellent model system to study innate immune cells during development. Embryos develop externally and thereby facilitates easy visualization of fluorescently labelled cells and subsequent isolation during any given timepoint of development. With the advancement in single-cell technology where cells can be separated into individual droplets and characterized based on individual RNA profiles, deciphering the ambiguity underlying the microglia origin and development became realizable.

Mesoderm derived microglia share many features with other myeloid types. In zebrafish, specific markers that can distinguish microglia from peripheral macrophages during early development, are scarce. Hence, in the given scenario, single-cell transcriptomic technologies provides a tool with which a small cell population, like microglial precursors can be encapsulated using high throughput microfluidics into individual droplets and each encapsulated cell can be sequenced. Within 48 hours of development, fluorescently labelled microglial/myeloid precursors can be seen in different regions of brain in larval zebrafish, which can be sorted into distinct clusters depending on differential transcriptome features. Here, we attempted to understand the gene expression profile of microglial/myeloid precursors at 48 hpf and 72 hpf at single-cell level.

Based on the transcriptomic profile of individual cells at 48hpf, *mpeg1.1* positive cells had segregated into two clusters. Presence of two distinctive clusters obtained from the expression profile of individual cells at this early stage of development, signifies the onset of heterogeneity in myeloid cells as early as 48hpf. Analysis of transcriptome in two *mpeg1.1*/*mfap4* double positive cell clusters revealed expression of many microglia specific genes. We observed the expression of microglia-specific chemokine, *ccl34b.1*, in mpeg1.1 clusters of 48 hpf. To our knowledge, this is the first indication that ccl43b.1 is expressed in early zebrafish microglia. This also restate that the two mpeg1.1/mfap4 clusters represent microglia population at 48 hpf. Intriguingly *Slc37a2*, a gene implicated to assist in shrinkage of phagosomes in zebrafish microglia/macrophage (Villani et al., 2019), was enriched only in one cluster of mpeg1.1/mfap4 cells. *Slc37a2* expression may represent a unique cell population of microglia or macrophage. Probing the expression of *Slc37a2* in 48 hpf zebrafish brain might provide insight on the localization of these cells comprising the cluster. One key observation from this analysis is the absence of *apoeb* expression in *mpeg1.1*/*mfap4* clusters. This supports the

previous reports of microglia maturation at 60 hpf (Herbomel et al., 2001b). Other genes that were specifically expressed in microglial clusters were *tcima, tspan36, pasp, slc3a2a, si:dkey-5n18.1* and *selenop*. Deciphering the expression pattern of these genes in 48 hpf zebrafish larval brain may provide valuable understanding of molecular signature of microglia in region specific manner.

Given the huge leap in development of zebrafish larva from 48 hpf to 72 hpf, we obtained five mpeg1.1/mfap4 clusters at 72 hpf. Out of five clusters, three clusters have apoeb expression, suggesting maturation of a fraction of microglia precursors. Presence of three apoeb positive clusters signifies three different populations of matured mpeg1.1/mfap4 cells at a given developmental stage. These three clusters were enriched for expression of *apoc1, bzw2, si-ch73-158p21.3* which was only limited to mature microglia precursors. Known mouse/human microglia signature genes, *Scn4bb* and *slco2b1*, were also enriched in two out of three clusters of matured mpeg1.1/mfap4 cells. Genes like *ccl34a.4, si:ch211-147m6.1 and si:ch211-194m7.3* were only expressed in immature mpeg1.1/mfap4 positive cells distributed into two clusters.

This extensive information of single-cell transcriptome of early microglia/myeloid precursors deepens our understanding of molecular stepping stones in microglia development but also opens up a wide range of questions. As stated before, it's not known whether microglia precursors differ from other peripheral myeloid cells from birth or the environmental cues shape up the identity of these immune cells in brain. As the process of myelopoiesis is conserved across vertebrates, studying myeloid cells at single-cell level in larval zebrafish could answer many outstanding questions in the field. Analyzing microglia/myeloid precursors marked by *mpeg1.1* expression show presence of heterogenous populations since very early

developmental stages. This resolution of gene expression at the single-cell level during microglial/macrophage development in zebrafish larva will enable us to trace the microglia development at molecular level and unravel subtle differences that don't get reflected in morphological and bulk RNA studies. Our data clearly shows that at 48hpf, even before the differentiation of microglia precursors into microglia, brain regions contain two different subpopulations of *mpeg1.1* cells, suggesting that *mpeg1.1* precursors are heterogenous. These two clusters can be interpreted in two ways 1) during the process of myelopoiesis around ~18hpf, a unique subpopulations of microglia precursors arise or 2) over time, during the process of migration a subset of myeloid precursors, adopts microglia fate based on environmental cues.

Analysis of transcripts defining various clusters by in-situ hybridization at 48hpf and 72hpf can throw light on the expression patterns of these genes. Three possible scenarios are 1) genes from both the clusters are also expressed in peripheral *mpeg1.1* positive cells, suggesting no unique microglia subpopulation 2) these genes are only uniformly expressed across the head regions, or 3) the expression pattern is region restricted in head defined by the environment, for instance, early microglia in retina could differ from microglia in midbrain.

Aforementioned experiments for investigating expression pattern of genes in zebrafish larvae, is likely to provide novel microglia specific markers in zebrafish. Such markers would be instrumental in establishing transgenic zebrafish lines that will enable real time monitoring of microglia during development. In addition, inclusion of more time points of development such as 36hpf, 120hpf, 168hpf, help in our understanding of which myeloid precursors commitment to microglia fate during myelopoiesis. This research work has the potential to provide the

extensive transcriptomic information of early microglia in zebrafish which could be used as reference for microglia behavior in early neurodegenerative zebrafish models.

REFERENCES

AARUM, J., SANDBERG, K., HAEBERLEIN, S. L. & PERSSON, M. A. 2003. Migration and differentiation of neural precursor cells can be directed by microglia. *Proc Natl Acad Sci U S A,* 100**,** 15983-8.

AJAMI, B., BENNETT, J. L., KRIEGER, C., TETZLAFF, W. & ROSSI, F. M. V. 2007. Local self-renewal can sustain CNS microglia maintenance and function throughout adult life. *Nature Neuroscience,* 10**,** 1538-1543.

ALLENDE, M. L. & WEINBERG, E. S. 1994. The Expression Pattern of 2 Zebrafish Achaete-Scute Homolog (Ash) Genes Is Altered in the Embryonic Brain of the Cyclops Mutant. *Developmental Biology,* 166**,** 509-530.

ALLIOT, F., GODIN, I. & PESSAC, B. 1999. Microglia derive from progenitors, originating from the yolk sac, and which proliferate in the brain. *Developmental Brain Research,* 117**,** 145-152.

ALVAREZ, Y., CEDERLUND, M. L., COTTELL, D. C., BILL, B. R., EKKER, S. C., TORRES-VAZQUEZ, J., WEINSTEIN, B. M., HYDE, D. R., VIHTELIC, T. S. & KENNEDY, B. N. 2007. Genetic determinants of hyaloid and retinal vasculature in zebrafish. *BMC Dev Biol,* 7**,** 114.

APPEL, B. & CHITNIS, A. 2002. Neurogenesis and specification of neuronal identity. *Results Probl Cell Differ,* 40**,** 237-51.

ARNO, B., GRASSIVARO, F., ROSSI, C., BERGAMASCHI, A., CASTIGLIONI, V., FURLAN, R., GRETER, M., FAVARO, R., COMI, G., BECHER, B., MARTINO, G. & MUZIO, L. 2014. Neural progenitor cells orchestrate microglia migration and positioning into the developing cortex. *Nature Communications,* 5.

ASH, J. D. & OVERBEEK, P. A. 2000. Lens-specific VEGF-A expression induces angioblast migration and proliferation and stimulates angiogenic remodeling. *Dev Biol,* 223**,** 383-98.

ASHWELL, K. W., HOLLANDER, H., STREIT, W. & STONE, J. 1989. The appearance and distribution of microglia in the developing retina of the rat. *Vis Neurosci,* 2**,** 437-48.

BACHSTETTER, A. D., MORGANTI, J. M., JERNBERG, J., SCHLUNK, A., MITCHELL, S. H., BREWSTER, K. W., HUDSON, C. E., COLE, M. J., HARRISON, J. K., BICKFORD, P. C. & GEMMA, C. 2011. Fractalkine and CX 3 CR1 regulate hippocampal neurogenesis in adult and aged rats. *Neurobiol Aging,* 32**,** 2030-44.

BAYE, L. M. & LINK, B. A. 2005. Examining interkinetic nuclear migration during retinal development. *Faseb Journal,* 19**,** A1367-A1367.

BELECKYADAMS, T., COOK, B. & ADLER, R. 1996. Correlations between terminal mitosis and differentiated fate of retinal precursor cells in vivo and in vitro: Analysis with the "window-labeling" technique. *Developmental Biology,* 178**,** 304-315.

BENNETT, C. M., KANKI, J. P., RHODES, J., LIU, T. X., PAW, B. H., KIERAN, M. W., LANGENAU, D. M., DELAHAYE-BROWN, A., ZON, L. I., FLEMING, M. D. & LOOK, A. T. 2001. Myelopoiesis in the zebrafish, Danio rerio. *Blood,* 98**,** 643-651.

BERGHMANS, S., MURPHEY, R. D., WIENHOLDS, E., NEUBERG, D., KUTOK, J. L., FLETCHER, C. D., MORRIS, J. P., LIU, T. X., SCHULTE-MERKER, S., KANKI, J. P., PLASTERK, R., ZON, L. I. & LOOK, A. T. 2005. tp53 mutant zebrafish develop malignant peripheral nerve sheath tumors. *Proc Natl Acad Sci U S A,* 102**,** 407-12.

BERTRAND, J. Y., JALIL, A., KLAINE, M., JUNG, S., CUMANO, A. & GODIN, I. 2005. Three pathways to mature macrophages in the early mouse yolk sac. *Blood,* 106**,** 3004-11.

BERTRAND, J. Y., KIM, A. D., VIOLETTE, E. P., STACHURA, D. L., CISSON, J. L. & TRAVER, D. 2007. Definitive hematopoiesis initiates through a committed erythromyeloid progenitor in the zebrafish embryo. *Development,* 134**,** 4147-56.

BERTRAND, J. Y. & TRAVER, D. 2009. Hematopoietic cell development in the zebrafish embryo. *Current Opinion in Hematology,* 16**,** 243-248.

BLADER, P., FISCHER, N., GRADWOHL, G., GUILLEMOT, F. & STRAHLE, U. 1997. The activity of neurogenin1 is controlled by local cues in the zebrafish embryo. *Development,* 124**,** 4557-4569.

BUTOVSKY, O., JEDRYCHOWSKI, M. P., MOORE, C. S., CIALIC, R., LANSER, A. J., GABRIELY, G., KOEGLSPERGER, T., DAKE, B., WU, P. M., DOYKAN, C. E., FANEK, Z., LIU, L., CHEN, Z., ROTHSTEIN, J. D., RANSOHOFF, R. M., GYGI, S. P., ANTEL, J. P. & WEINER, H. L. 2014. Identification of a unique TGF-beta-dependent molecular and functional signature in microglia. *Nat Neurosci,* 17**,** 131-43.

CASANO, A. M., ALBERT, M. & PERI, F. 2016a. Developmental Apoptosis Mediates Entry and Positioning of Microglia in the Zebrafish Brain. *Cell Rep,* 16**,** 897-906.

CASANO, A. M., ALBERT, M. & PERI, F. 2016b. Developmental Apoptosis Mediates Entry and Positioning of Microglia in the Zebrafish Brain. *Cell Reports,* 16**,** 897-906.

CEPKO, C. L., AUSTIN, C. P., YANG, X., ALEXIADES, M. & EZZEDDINE, D. 1996. Cell fate determination in the vertebrate retina. *Proc Natl Acad Sci U S A,* 93**,** 589-95.

CHECCHIN, D., SENNLAUB, F., LEVAVASSEUR, E., LEDUC, M. & CHEMTOB, S. 2006. Potential role of microglia in retinal blood vessel formation. *Invest Ophthalmol Vis Sci,* 47**,** 3595-602.

CHEN, Q., JIANG, L., LI, C., HU, D., BU, J. W., CAI, D. & DU, J. L. 2012. Haemodynamics-driven developmental pruning of brain vasculature in zebrafish. *PLoS Biol,* 10**,** e1001374.

CHINNAIYAN, A. M. 1999. The apoptosome: heart and soul of the cell death machine. *Neoplasia,* 1**,** 5-15.

CHIU, I. M., MORIMOTO, E. T. A., GOODARZI, H., LIAO, J. T., O'KEEFFE, S., PHATNANI, H. P., MURATET, M., CARROLL, M. C., LEVY, S., TAVAZOIE, S., MYERS, R. M. & MANIATIS, T. 2013. A Neurodegeneration-Specific Gene-Expression Signature of Acutely Isolated Microglia from an Amyotrophic Lateral Sclerosis Mouse Model. *Cell Reports,* 4**,** 385-401.

CORY, S. & ADAMS, J. M. 2002. The Bcl2 family: regulators of the cellular life-or-death switch. *Nat Rev Cancer,* 2**,** 647-56.

CRAIG, S. E. L., THUMMEL, R., AHMED, H., VASTA, G. R., HYDE, D. R. & HITCHCOCK, P. F. 2010. The Zebrafish Galectin Drgal1-L2 Is Expressed by Proliferating Muller Glia and Photoreceptor Progenitors and Regulates the Regeneration of Rod Photoreceptors. *Investigative Ophthalmology & Visual Science,* 51**,** 3244-3252.

CROTTI, A. & RANSOHOFF, R. M. 2016. Microglial Physiology and Pathophysiology: Insights from Genome-wide Transcriptional Profiling. *Immunity,* 44**,** 505-515.

CUADROS, M. A., MARTIN, C., COLTEY, P., ALMENDROS, A. & NAVASCUES, J. 1993. First appearance, distribution, and origin of macrophages in the early development of the avian central nervous system. *J Comp Neurol,* 330**,** 113-29.

DALMAU, I., FINSEN, B., TONDER, N., ZIMMER, J., GONZALEZ, B. & CASTELLANO, B. 1997. Development of microglia in the prenatal rat hippocampus. *J Comp Neurol,* 377**,** 70-84.

DE JONG, J. L. O. & ZON, L. I. 2005. Use of the zebrafish system to study primitive and definitive hematopoiesis. *Annual Review of Genetics,* 39**,** 481-501.

DEL BENE, F., WEHMAN, A. M., LINK, B. A. & BAIER, H. 2008. Regulation of neurogenesis by interkinetic nuclear migration through an apical-basal Notch gradient. *Cell,* 134**,** 1055-1065.

DIEZROUX, G. & LANG, R. A. 1997. Macrophages induce apoptosis in normal cells in vivo. *Development,* 124**,** 3633-3638.

DONIACH, T. & MUSCI, T. J. 1995. Induction of Anteroposterior Neural Pattern in Xenopus - Evidence for a Quantitative Mechanism. *Mechanisms of Development,* 53**,** 403-413.

EIMON, P. M. & ASHKENAZI, A. 2010. The zebrafish as a model organism for the study of apoptosis. *Apoptosis,* 15**,** 331-349.

ELLETT, F. & LIESCHKE, G. J. 2010. Zebrafish as a model for vertebrate hematopoiesis. *Current Opinion in Pharmacology,* 10**,** 563-570.

ELLETT, F., PASE, L., HAYMAN, J. W., ANDRIANOPOULOS, A. & LIESCHKE, G. J. 2011. mpeg1 promoter transgenes direct macrophage-lineage expression in zebrafish. *Blood,* 117**,** E49-E56.

ERIKSSON, P. S., PERFILIEVA, E., BJORK-ERIKSSON, T., ALBORN, A. M., NORDBORG, C., PETERSON, D. A. & GAGE, F. H. 1998. Neurogenesis in the adult human hippocampus. *Nature Medicine,* 4**,** 1313-1317.

FANTIN, A., VIEIRA, J. M., GESTRI, G., DENTI, L., SCHWARZ, Q., PRYKHOZHIJ, S., PERI, F., WILSON, S. W. & RUHRBERG, C. 2010. Tissue macrophages act as cellular chaperones for vascular anastomosis downstream of VEGF-mediated endothelial tip cell induction. *Blood,* 116**,** 829-40.

FERRERO, G., MAHONY, C. B., DUPUIS, E., YVERNOGEAU, L., DI RUGGIERO, E., MISEROCCHI, M., CARON, M., ROBIN, C., TRAVER, D., BERTRAND, J. Y. & WITTAMER, V. 2018. Embryonic Microglia Derive from Primitive Macrophages and Are Replaced by cmyb-Dependent Definitive Microglia in Zebrafish. *Cell Rep,* 24**,** 130-141.

FRIEDMAN, J. R., LACKNER, L. L., WEST, M., DIBENEDETTO, J. R., NUNNARI, J. & VOELTZ, G. K. 2011. ER tubules mark sites of mitochondrial division. *Science,* 334**,** 358-62.

GAUTIER, E. L., SHAY, T., MILLER, J., GRETER, M., JAKUBZICK, C., IVANOV, S., HELFT, J., CHOW, A., ELPEK, K. G., GORDONOV, S., MAZLOOM, A. R., MA'AYAN, A., CHUA, W. J., HANSEN, T. H., TURLEY, S. J., MERAD, M., RANDOLPH, G. J. & CONSORTIUM, I. G. 2012. Gene-expression profiles and transcriptional regulatory pathways that underlie the identity and diversity of mouse tissue macrophages. *Nature Immunology,* 13**,** 1118-1128.

GEBARA, E., SULTAN, S., KOCHER-BRAISSANT, J. & TONI, N. 2013. Adult hippocampal neurogenesis inversely correlates with microglia in conditions of voluntary running and aging. *Front Neurosci,* 7**,** 145.

GINHOUX, F., GRETER, M., LEBOEUF, M., NANDI, S., SEE, P., GOKHAN, S., MEHLER, M. F., CONWAY, S. J., NG, L. G., STANLEY, E. R., SAMOKHVALOV, I. M. & MERAD, M. 2010a. Fate mapping analysis reveals that adult microglia derive from primitive macrophages. *Science,* 330**,** 841-5.

GINHOUX, F., GRETER, M., LEBOEUF, M., NANDI, S., SEE, P., GOKHAN, S., MEHLER, M. F., CONWAY, S. J., NG, L. G., STANLEY, E. R., SAMOKHVALOV, I. M. & MERAD, M. 2010b. Fate Mapping Analysis Reveals That Adult Microglia Derive from Primitive Macrophages. *Science,* 330**,** 841-845.

GOLDMANN, T., WIEGHOFER, P., JORDAO, M. J., PRUTEK, F., HAGEMEYER, N., FRENZEL, K., AMANN, L., STASZEWSKI, O., KIERDORF, K., KRUEGER, M., LOCATELLI, G., HOCHGERNER, H., ZEISER, R., EPELMAN, S., GEISSMANN,

F., PRILLER, J., ROSSI, F. M., BECHMANN, I., KERSCHENSTEINER, M., LINNARSSON, S., JUNG, S. & PRINZ, M. 2016. Origin, fate and dynamics of macrophages at central nervous system interfaces. *Nat Immunol,* 17**,** 797-805.

GOULD, E. 2007. Opinion - How widespread is adult neurogenesis in mammals? *Nature Reviews Neuroscience,* 8**,** 481-488.

GRAHAM, D. K., DERYCKERE, D., DAVIES, K. D. & EARP, H. S. 2014. The TAM family: phosphatidylserine sensing receptor tyrosine kinases gone awry in cancer. *Nat Rev Cancer,* 14**,** 769-85.

HARMS, A. S., CAO, S. W., ROWSE, A. L., THOME, A. D., LI, X. R., MANGIERI, L. R., CRON, R. Q., SHACKA, J. J., RAMAN, C. & STANDAERT, D. G. 2013. MHCII Is Required for alpha-Synuclein-Induced Activation of Microglia, CD4 T Cell Proliferation, and Dopaminergic Neurodegeneratione. *Journal of Neuroscience,* 33**,** 9592-9600.

HARTSOCK, A., LEE, C., ARNOLD, V. & GROSS, J. M. 2014. In vivo analysis of hyaloid vasculature morphogenesis in zebrafish: A role for the lens in maturation and maintenance of the hyaloid. *Developmental Biology,* 394**,** 327-339.

HASHIURA, T., KIMURA, E., FUJISAWA, S., OIKAWA, S., NONAKA, S., KUROSAKA, D. & HITOMI, J. 2017. Live imaging of primary ocular vasculature formation in zebrafish. *PLoS One,* 12**,** e0176456.

HERBOMEL, P., THISSE, B. & THISSE, C. 2001a. Zebrafish early macrophages colonize cephalic mesenchyme and developing brain, retina, and epidermis through a M-CSF receptor-dependent invasive process. *Dev Biol,* 238**,** 274-88.

HERBOMEL, P., THISSE, B. & THISSE, C. 2001b. Zebrafish early macrophages colonize cephalic mesenchyme and developing brain, retina, and epidermis through, a M-CSF receptor-dependent invasive process. *Developmental Biology,* 238**,** 274-288.

HICKMAN, S. E., KINGERY, N. D., OHSUMI, T. K., BOROWSKY, M. L., WANG, L. C., MEANS, T. K. & EL KHOURY, J. 2013. The microglial sensome revealed by direct RNA sequencing. *Nat Neurosci,* 16**,** 1896-905.

HILL, M. M., ADRAIN, C., DURIEZ, P. J., CREAGH, E. M. & MARTIN, S. J. 2004. Analysis of the composition, assembly kinetics and activity of native Apaf-1 apoptosomes. *EMBO J,* 23**,** 2134-45.

HU, M. & EASTER, S. S. 1999. Retinal neurogenesis: the formation of the initial central patch of postmitotic cells. *Dev Biol,* 207**,** 309-21.

HUANG, T., CUI, J., LI, L., HITCHCOCK, P. F. & LI, Y. 2012. The role of microglia in the neurogenesis of zebrafish retina. *Biochem Biophys Res Commun,* 421**,** 214-20.

IMAI, F., YOSHIZAWA, A., MATSUZAKI, A., OGURI, E., ARARAGI, M., NISHIWAKI, Y. & MASAI, I. 2014. Stem-loop binding protein is required for retinal cell proliferation, neurogenesis, and intraretinal axon pathfinding in zebrafish. *Dev Biol,* 394**,** 94-109.

INOHARA, N. & NUNEZ, G. 2000. Genes with homology to mammalian apoptosis regulators identified in zebrafish. *Cell Death Differ,* 7**,** 509-10.

ISHIZUKA, K., FUJITA, Y., KAWABATA, T., KIMURA, H., IWAYAMA, Y., INADA, T., OKAHISA, Y., EGAWA, J., USAMI, M., KUSHIMA, I., UNO, Y., OKADA, T., IKEDA, M., ALEKSIC, B., MORI, D., SOMEYA, T., YOSHIKAWA, T., IWATA, N., NAKAMURA, H., YAMASHITA, T. & OZAKI, N. 2017. Rare genetic variants in CX3CR1 and their contribution to the increased risk of schizophrenia and autism spectrum disorders. *Transl Psychiatry,* 7**,** e1184.

ISOGAI, S., HORIGUCHI, M. & WEINSTEIN, B. M. 2001. The vascular anatomy of the developing zebrafish: an atlas of embryonic and early larval development. *Dev Biol,* 230**,** 278-301.

JAGASIA, R., GROTE, P., WESTERMANN, B. & CONRADT, B. 2005. DRP-1-mediated mitochondrial fragmentation during EGL-1-induced cell death in C. elegans. *Nature,* 433**,** 754-60.

JAHANI-ASL, A. & SLACK, R. S. 2007. The phosphorylation state of Drp1 determines cell fate. *EMBO Rep,* 8**,** 912-3.

JAZAYERI, A., FALCK, J., LUKAS, C., BARTEK, J., SMITH, G. C., LUKAS, J. & JACKSON, S. P. 2006. ATM- and cell cycle-dependent regulation of ATR in response to DNA double-strand breaks. *Nat Cell Biol,* 8**,** 37-45.

JIA, W., LIANG, D., LI, N., LIU, M., DONG, Z., LI, J., DONG, X., YUE, Y., HU, P., YAO, J. & ZHAO, Q. 2019. Zebrafish microRNA miR-210-5p inhibits primitive myelopoiesis by silencing foxj1b and slc3a2a mRNAs downstream of gata4/5/6 transcription factor genes. *J Biol Chem,* 294**,** 2732-2743.

JIN, H., SOOD, R., XU, J., ZHEN, F. H., ENGLISH, M. A., LIU, P. P. & WEN, Z. L. 2009. Definitive hematopoietic stem/progenitor cells manifest distinct differentiation output in the zebrafish VDA and PBI (vol 136, pg 647, 2009). *Development,* 136**,** 1397-1397.

JIN, S. W., BEIS, D., MITCHELL, T., CHEN, J. N. & STAINIER, D. Y. 2005. Cellular and molecular analyses of vascular tube and lumen formation in zebrafish. *Development,* 132**,** 5199-209.

JING, L. L. & ZON, L. I. 2011. Zebrafish as a model for normal and malignant hematopoiesis. *Disease Models & Mechanisms,* 4**,** 433-438.

JOBLING, A. I., WAUGH, M., VESSEY, K. A., PHIPPS, J. A., TROGRLIC, L., GREFERATH, U., MILLS, S. A., TAN, Z. L., WARD, M. M. & FLETCHER, E. L. 2018. The Role of the Microglial Cx3cr1 Pathway in the Postnatal Maturation of Retinal Photoreceptors. *J Neurosci,* 38**,** 4708-4723.

KAUFMAN, R., WEISS, O., SEBBAGH, M., RAVID, R., GIBBS-BAR, L., YANIV, K. & INBAL, A. 2015. Development and origins of zebrafish ocular vasculature. *BMC Dev Biol,* 15**,** 18.

KAY, J. N., FINGER-BAIER, K. C., ROESER, T., STAUB, W. & BAIER, H. 2001. Retinal ganglion cell genesis requires lakritz, a Zebrafish atonal Homolog. *Neuron,* 30**,** 725-36.

KEREN-SHAUL, H., SPINRAD, A., WEINER, A., MATCOVITCH-NATAN, O., DVIR-SZTERNFELD, R., ULLAND, T. K., DAVID, E., BARUCH, K., LARA-ASTAISO, D., TOTH, B., ITZKOVITZ, S., COLONNA, M., SCHWARTZ, M. & AMIT, I. 2017. A Unique Microglia Type Associated with Restricting Development of Alzheimer's Disease. *Cell,* 169**,** 1276-+.

KIERDORF, K., ERNY, D., GOLDMANN, T., SANDER, V., SCHULZ, C., PERDIGUERO, E. G., WIEGHOFER, P., HEINRICH, A., RIEMKE, P., HOLSCHER, C., MULLER, D. N., LUCKOW, B., BROCKER, T., DEBOWSKI, K., FRITZ, G., OPDENAKKER, G., DIEFENBACH, A., BIBER, K., HEIKENWALDER, M., GEISSMANN, F., ROSENBAUER, F. & PRINZ, M. 2013. Microglia emerge from erythromyeloid precursors via Pu.1- and Irf8-dependent pathways. *Nat Neurosci,* 16**,** 273-80.

KISSA, K., MURAYAMA, E., ZAPATA, A., CORTES, A., PERRET, E., MACHU, C. & HERBOMEL, P. 2008. Live imaging of emerging hematopoietic stem cells and early thymus colonization. *Blood,* 111**,** 1147-1156.

KITAMBI, S. S., MCCULLOCH, K. J., PETERSON, R. T. & MALICKI, J. J. 2009. Small molecule screen for compounds that affect vascular development in the zebrafish retina. *Mechanisms of Development,* 126**,** 464-477.

KORZH, V. & STRAHLE, U. 2002. Proneural, prosensory, antiglial: the many faces of neurogenins. *Trends in Neurosciences,* 25**,** 603-605.

KOUSHIK, S. V., WANG, J., ROGERS, R., MOSKOPHIDIS, D., LAMBERT, N. A., CREAZZO, T. L. & CONWAY, S. J. 2001. Targeted inactivation of the sodium-calcium exchanger (Ncx1) results in the lack of a heartbeat and abnormal myofibrillar organization. *FASEB J,* 15**,** 1209-11.

KRATZ, E., EIMON, P. M., MUKHYALA, K., STERN, H., ZHA, J., STRASSER, A., HART, R. & ASHKENAZI, A. 2006. Functional characterization of the Bcl-2 gene family in the zebrafish. *Cell Death Differ,* 13**,** 1631-40.

KUBBUTAT, M. H., JONES, S. N. & VOUSDEN, K. H. 1997. Regulation of p53 stability by Mdm2. *Nature,* 387**,** 299-303.

KUBOTA, Y., TAKUBO, K., SHIMIZU, T., OHNO, H., KISHI, K., SHIBUYA, M., SAYA, H. & SUDA, T. 2009. M-CSF inhibition selectively targets pathological angiogenesis and lymphangiogenesis. *J Exp Med,* 206**,** 1089-102.

KUHN, H. G., DICKINSONANSON, H. & GAGE, F. H. 1996. Neurogenesis in the dentate gyrus of the adult rat: Age-related decrease of neuronal progenitor proliferation. *Journal of Neuroscience,* 16**,** 2027-2033.

LAVIN, Y., WINTER, D., BLECHER-GONEN, R., DAVID, E., KEREN-SHAUL, H., MERAD, M., JUNG, S. & AMIT, I. 2014. Tissue-resident macrophage enhancer landscapes are shaped by the local microenvironment. *Cell,* 159**,** 1312-26.

LAWSON, N. D. & WEINSTEIN, B. M. 2002. In vivo imaging of embryonic vascular development using transgenic zebrafish. *Dev Biol,* 248**,** 307-18.

LEE, J. E., LIANG, K. J., FARISS, R. N. & WONG, W. T. 2008. Ex vivo dynamic imaging of retinal microglia using time-lapse confocal microscopy. *Investigative Ophthalmology & Visual Science,* 49**,** 4169-4176.

LIANG, K. J., LEE, J. E., WANG, Y. D., MA, W., FONTAINHAS, A. M., FARISS, R. N. & WONG, W. T. 2009. Regulation of dynamic behavior of retinal microglia by CX3CR1 signaling. *Invest Ophthalmol Vis Sci,* 50**,** 4444-51.

LIESCHKE, G. J., OATES, A. C., PAW, B. H., THOMPSON, M. A., HALL, N. E., WARD, A. C., HO, R. K., ZON, L. I. & LAYTON, J. E. 2002. Zebrafish SPI-1 (PU.1) marks a site of myeloid development independent of primitive erythropoiesis: Implications for axial patterning. *Developmental Biology,* 246**,** 274-295.

LING, E. A. 1982. A light microscopic demonstration of amoeboid microglia and microglial cells in the retina of rats of various ages. *Arch Histol Jpn,* 45**,** 37-44.

LIVESEY, F. J. & CEPKO, C. L. 2001. Vertebrate neural cell-fate determination: lessons from the retina. *Nat Rev Neurosci,* 2**,** 109-18.

LOBOV, I. B., RAO, S., CARROLL, T. J., VALLANCE, J. E., ITO, M., ONDR, J. K., KURUP, S., GLASS, D. A., PATEL, M. S., SHU, W. G., MORRISEY, E. E., MCMAHON, A. P., KARSENTY, G. & LANG, R. A. 2005. WNT7b mediates macrophage-induced programmed cell death in patterning of the vasculature. *Nature,* 437**,** 417-421.

LOIS, C. & ALVAREZBUYLLA, A. 1993. Proliferating Subventricular Zone Cells in the Adult Mammalian Forebrain Can Differentiate into Neurons and Glia. *Proceedings of the National Academy of Sciences of the United States of America,* 90**,** 2074-2077.

LUMSDEN, A. & KRUMLAUF, R. 1996. Patterning the vertebrate neuraxis. *Science,* 274**,** 1109-1115.

MACDOUGALL, C. A., BYUN, T. S., VAN, C., YEE, M. C. & CIMPRICH, K. A. 2007. The structural determinants of checkpoint activation. *Genes Dev,* 21**,** 898-903.

MARINI, F., PELLICIOLI, A., PACIOTTI, V., LUCCHINI, G., PLEVANI, P., STERN, D. F. & FOIANI, M. 1997. A role for DNA primase in coupling DNA replication to DNA damage response. *EMBO J,* 16**,** 639-50.

MARTINEZ-MORALES, J. R., DEL BENE, F., NICA, G., HAMMERSCHMIDT, M., BOVOLENTA, P. & WITTBRODT, J. 2005. Differentiation of the vertebrate retina is coordinated by an FGF signaling center. *Dev Cell,* 8**,** 565-74.

MARZLUFF, W. F. 1992. Histone 3' ends: essential and regulatory functions. *Gene Expr,* 2**,** 93-7.

MASAI, I., LELE, Z., YAMAGUCHI, M., KOMORI, A., NAKATA, A., NISHIWAKI, Y., WADA, H., TANAKA, H., NOJIMA, Y., HAMMERSCHMIDT, M., WILSON, S. W. & OKAMOTO, H. 2003. N-cadherin mediates retinal lamination, maintenance of forebrain compartments and patterning of retinal neurites. *Development,* 130**,** 2479-94.

MASAI, I., STEMPLE, D. L., OKAMOTO, H. & WILSON, S. W. 2000. Midline signals regulate retinal neurogenesis in zebrafish. *Neuron,* 27**,** 251-63.

MASAI, I., YAMAGUCHI, M., TONOU-FUJIMORI, N., KOMORI, A. & OKAMOTO, H. 2005. The hedgehog-PKA pathway regulates two distinct steps of the differentiation of retinal ganglion cells: the cell-cycle exit of retinoblasts and their neuronal maturation. *Development,* 132**,** 1539-53.

MASUDA, T., TSUDA, M., YOSHINAGA, R., TOZAKI-SAITOH, H., OZATO, K., TAMURA, T. & INOUE, K. 2012. IRF8 Is a Critical Transcription Factor for Transforming Microglia into a Reactive Phenotype. *Cell Reports,* 1**,** 334-340.

MATCOVITCH-NATAN, O., WINTER, D. R., GILADI, A., VARGAS AGUILAR, S., SPINRAD, A., SARRAZIN, S., BEN-YEHUDA, H., DAVID, E., ZELADA GONZALEZ, F., PERRIN, P., KEREN-SHAUL, H., GURY, M., LARA-ASTAISO, D., THAISS, C. A., COHEN, M., BAHAR HALPERN, K., BARUCH, K., DECZKOWSKA, A., LORENZO-VIVAS, E., ITZKOVITZ, S., ELINAV, E., SIEWEKE, M. H., SCHWARTZ, M. & AMIT, I. 2016. Microglia development follows a stepwise program to regulate brain homeostasis. *Science,* 353**,** aad8670.

MATHYS, H., ADAIKKAN, C., GAO, F., YOUNG, J. Z., MANET, E., HEMBERG, M., DE JAGER, P. L., RANSOHOFF, R. M., REGEV, A. & TSAI, L. H. 2017. Temporal Tracking of Microglia Activation in Neurodegeneration at Single-Cell Resolution. *Cell Reports,* 21**,** 366-380.

MAZZOLINI, J., LE CLERC, S., MORISSE, G., COULONGES, C., KUIL, L. E., VAN HAM, T. J., ZAGURY, J. F. & SIEGER, D. 2020. Gene expression profiling reveals a conserved microglia signature in larval zebrafish. *Glia,* 68**,** 298-315.

MCCABE, K. L., GUNTHER, E. C. & REH, T. A. 1999. The development of the pattern of retinal ganglion cells in the chick retina: mechanisms that control differentiation. *Development,* 126**,** 5713-5724.

MCCARTHY, C. A., WIDDOP, R. E., DELIYANTI, D. & WILKINSON-BERKA, J. L. 2013. Brain and retinal microglia in health and disease: an unrecognized target of the renin-angiotensin system. *Clin Exp Pharmacol Physiol,* 40**,** 571-9.

MCKERCHER, S. R., TORBETT, B. E., ANDERSON, K. L., HENKEL, G. W., VESTAL, D. J., BARIBAULT, H., KLEMSZ, M., FEENEY, A. J., WU, G. E., PAIGE, C. J. & MAKI, R. A. 1996. Targeted disruption of the PU.1 gene results in multiple hematopoietic abnormalities. *EMBO J,* 15**,** 5647-58.

MCLEOD, D. S., HASEGAWA, T., BABA, T., GREBE, R., GALTIER D'AURIAC, I., MERGES, C., EDWARDS, M. & LUTTY, G. A. 2012. From blood islands to blood vessels: morphologic observations and expression of key molecules during hyaloid vascular system development. *Invest Ophthalmol Vis Sci,* 53**,** 7912-27.

MEDVINSKY, A., RYBTSOV, S. & TAOUDI, S. 2011. Embryonic origin of the adult hematopoietic system: advances and questions. *Development,* 138**,** 1017-31.
MEEK, D. W. 1997. Post-translational modification of p53 and the integration of stress signals. *Pathol Biol (Paris),* 45**,** 804-14.
MILDNER, A., SCHMIDT, H., NITSCHE, M., MERKLER, D., HANISCH, U. K., MACK, M., HEIKENWALDER, M., BRUCK, W., PRILLER, J. & PRINZ, M. 2007. Microglia in the adult brain arise from Ly-6ChiCCR2+ monocytes only under defined host conditions. *Nat Neurosci,* 10**,** 1544-53.
MITCHELL, C. A., RUTLAND, C. S., WALKER, M., NASIR, M., FOSS, A. J., STEWART, C., GERHARDT, H., KONERDING, M. A., RISAU, W. & DREXLER, H. C. 2006. Unique vascular phenotypes following over-expression of individual VEGFA isoforms from the developing lens. *Angiogenesis,* 9**,** 209-24.
MITCHELL, D. M., SUN, C., HUNTER, S. S., NEW, D. D. & STENKAMP, D. L. 2019. Regeneration associated transcriptional signature of retinal microglia and macrophages. *Sci Rep,* 9**,** 4768.
MOCHIZUKI, T., SUZUKI, S. & MASAI, I. 2014. Spatial pattern of cell geometry and cell-division orientation in zebrafish lens epithelium. *Biol Open,* 3**,** 982-94.
MOSHER, K. I., ANDRES, R. H., FUKUHARA, T., BIERI, G., HASEGAWA-MORIYAMA, M., HE, Y., GUZMAN, R. & WYSS-CORAY, T. 2012. Neural progenitor cells regulate microglia functions and activity. *Nat Neurosci,* 15**,** 1485-7.
MULLEN, T. E. & MARZLUFF, W. F. 2008. Degradation of histone mRNA requires oligouridylation followed by decapping and simultaneous degradation of the mRNA both 5' to 3' and 3' to 5'. *Genes Dev,* 22**,** 50-65.
MYERS, J. S. & CORTEZ, D. 2006. Rapid activation of ATR by ionizing radiation requires ATM and Mre11. *J Biol Chem,* 281**,** 9346-50.
NEUMANN, C. J. & NUESSLEIN-VOLHARD, C. 2000. Patterning of the zebrafish retina by a wave of sonic hedgehog activity. *Science,* 289**,** 2137-2139.
O'KOREN, E. G., YU, C., KLINGEBORN, M., WONG, A. Y. W., PRIGGE, C. L., MATHEW, R., KALNITSKY, J., MSALLAM, R. A., SILVIN, A., KAY, J. N., BOWES RICKMAN, C., ARSHAVSKY, V. Y., GINHOUX, F., MERAD, M. & SABAN, D. R. 2019. Microglial Function Is Distinct in Different Anatomical Locations during Retinal Homeostasis and Degeneration. *Immunity,* 50**,** 723-737 e7.
OKUDA, Y., OGURA, E., KONDOH, H. & KAMACHI, Y. 2010. B1 SOX Coordinate Cell Specification with Patterning and Morphogenesis in the Early Zebrafish Embryo. *Plos Genetics,* 6.
OOSTERHOF, N., HOLTMAN, I. R., KUIL, L. E., VAN DER LINDE, H. C., BODDEKE, E. W., EGGEN, B. J. & VAN HAM, T. J. 2017. Identification of a conserved and acute neurodegeneration-specific microglial transcriptome in the zebrafish. *Glia,* 65**,** 138-149.
PERDIGUERO, E. G., KLAPPROTH, K., SCHULZ, C., BUSCH, K., AZZONI, E., CROZET, L., GARNER, H., TROUILLET, C., DE BRUIJN, M., GEISSMANN, F. & RODEWALD, H. R. 2015. Tissue-Resident Macrophages Originate from Yolk Sac-Derived Erythro-Myeloid Progenitors. *Experimental Hematology,* 43**,** S64-S64.
PETTMANN, B. & HENDERSON, C. E. 1998. Neuronal cell death. *Neuron,* 20**,** 633-47.
POGGI, L., VITORINO, M., MASAI, I. & HARRIS, W. A. 2005. Influences on neural lineage and mode of division in the zebrafish retina in vivo. *J Cell Biol,* 171**,** 991-9.
PRIETO, D. & ZOLESSI, F. R. 2017. Functional Diversification of the Four MARCKS Family Members in Zebrafish Neural Development. *Journal of Experimental Zoology Part B-Molecular and Developmental Evolution,* 328**,** 119-138.

PROULX, K., LU, A. & SUMANAS, S. 2010. Cranial vasculature in zebrafish forms by angioblast cluster-derived angiogenesis. *Dev Biol,* 348**,** 34-46.

RAPAPORT, D. H., WONG, L. L., WOOD, E. D., YASUMURA, D. & LAVAIL, M. M. 2004. Timing and topography of cell genesis in the rat retina. *Journal of Comparative Neurology,* 474**,** 304-324.

RATHNASAMY, G., FOULDS, W. S., LING, E. A. & KAUR, C. 2019. Retinal microglia - A key player in healthy and diseased retina. *Prog Neurobiol,* 173**,** 18-40.

REIM, G. & BRAND, M. 2006. Maternal control of vertebrate dorsoventral axis formation and epiboly by the POU domain protein Spg/Pou2/Oct4. *Development,* 133**,** 2757-2770.

RENTZSCH, F., BAKKERS, J., KRAMER, C. & HAMMERSCHMIDT, M. 2004. Fgf signaling induces posterior neuroectoderm independently of Bmp signaling inhibition. *Developmental Dynamics,* 231**,** 750-757.

RIGATO, C., BUCKINX, R., LE-CORRONC, H., RIGO, J. M. & LEGENDRE, P. 2011. Pattern of Invasion of the Embryonic Mouse Spinal Cord by Microglial Cells at the Time of the Onset of Functional Neuronal Networks. *Glia,* 59**,** 675-695.

ROSENBAUER, F. & TENEN, D. G. 2007. Transcription factors in myeloid development: balancing differentiation with transformation. *Nat Rev Immunol,* 7**,** 105-17.

ROSSI, F., CASANO, A. M., HENKE, K., RICHTER, K. & PERI, F. 2015. The SLC7A7 Transporter Identifies Microglial Precursors prior to Entry into the Brain. *Cell Reports,* 11**,** 1008-1017.

RUTLAND, C. S., MITCHELL, C. A., NASIR, M., KONERDING, M. A. & DREXLER, H. C. 2007. Microphthalmia, persistent hyperplastic hyaloid vasculature and lens anomalies following overexpression of VEGF-A188 from the alphaA-crystallin promoter. *Mol Vis,* 13**,** 47-56.

SAELENS, X., FESTJENS, N., VANDE WALLE, L., VAN GURP, M., VAN LOO, G. & VANDENABEELE, P. 2004. Toxic proteins released from mitochondria in cell death. *Oncogene,* 23**,** 2861-74.

SAINT-GENIEZ, M. & D'AMORE, P. A. 2004. Development and pathology of the hyaloid, choroidal and retinal vasculature. *Int J Dev Biol,* 48**,** 1045-58.

SANTOS, A. M., CALVENTE, R., TASSI, M., CARRASCO, M. C., MARTIN-OLIVA, D., MARIN-TEVA, J. L., NAVASCUES, J. & CUADROS, M. A. 2008. Embryonic and postnatal development of microglial cells in the mouse retina. *J Comp Neurol,* 506**,** 224-39.

SASAI, Y. 1998. Identifying the missing links: Genes that connect neural induction and primary neurogenesis in vertebrate embryos. *Neuron,* 21**,** 455-458.

SASAI, Y. & DEROBERTIS, E. M. 1997. Ectodermal patterning in vertebrate embryos. *Developmental Biology,* 182**,** 5-20.

SAVILL, J., FADOK, V., HENSON, P. & HASLETT, C. 1993. Phagocyte recognition of cells undergoing apoptosis. *Immunol Today,* 14**,** 131-6.

SCHMIDT, R., STRAHLE, U. & SCHOLPP, S. 2013. Neurogenesis in zebrafish - from embryo to adult. *Neural Development,* 8.

SCHULER, M. & GREEN, D. R. 2001. Mechanisms of p53-dependent apoptosis. *Biochem Soc Trans,* 29**,** 684-8.

SEHNERT, A. J., HUQ, A., WEINSTEIN, B. M., WALKER, C., FISHMAN, M. & STAINIER, D. Y. R. 2002. Cardiac troponin T is essential in sarcomere assembly and cardiac contractility. *Nature Genetics,* 31**,** 106-110.

SIDI, S., SANDA, T., KENNEDY, R. D., HAGEN, A. T., JETTE, C. A., HOFFMANS, R., PASCUAL, J., IMAMURA, S., KISHI, S., AMATRUDA, J. F., KANKI, J. P., GREEN, D. R., D'ANDREA, A. A. & LOOK, A. T. 2008. Chk1 suppresses a

caspase-2 apoptotic response to DNA damage that bypasses p53, Bcl-2, and caspase-3. *Cell,* 133**,** 864-77.

SIEGER, D., MORITZ, C., ZIEGENHALS, T., PRYKHOZHIJ, S. & PERI, F. 2012a. Long-range Ca2+ waves transmit brain-damage signals to microglia. *Dev Cell,* 22**,** 1138-48.

SIEGER, D., MORITZ, C., ZIEGENHALS, T., PRYKHOZHIJ, S. & PERI, F. 2012b. Long-Range Ca2+ Waves Transmit Brain-Damage Signals to Microglia. *Developmental Cell,* 22**,** 1138-1148.

SOROKIN, S. P., HOYT, R. F., JR., BLUNT, D. G. & MCNELLY, N. A. 1992. Macrophage development: II. Early ontogeny of macrophage populations in brain, liver, and lungs of rat embryos as revealed by a lectin marker. *Anat Rec,* 232**,** 527-50.

SOULES, K. A. & LINK, B. A. 2005. Morphogenesis of the anterior segment in the zebrafish eye. *Bmc Developmental Biology,* 5.

SPEMANN, H. & MANGOLD, H. 2001. Induction of embryonic primordia by implantation of organizers from a different species. 1923. *Int J Dev Biol,* 45**,** 13-38.

STENKAMP, D. L. & FREY, R. A. 2003. Extraretinal and retinal hedgehog signaling sequentially regulate retinal differentiation in zebrafish. *Developmental Biology,* 258**,** 349-363.

STREIT, A., BERLINER, A. J., PAPANAYOTOU, C., SIRULNIK, A. & STERN, C. D. 2000. Initiation of neural induction by FGF signalling before gastrulation. *Nature,* 406**,** 74-78.

STREIT, A., SOCKANATHAN, S., PEREZ, L., REX, M., SCOTTING, P. J., SHARPE, P. T., LOVELLBADGE, R. & STERN, C. D. 1997. Preventing the loss of competence for neural induction: HGF/SF, L5 and Sox-2. *Development,* 124**,** 1191-1202.

TANAKA, S., SUZUKI, K., WATANABE, M., MATSUDA, A., TONE, S. & KOIKE, T. 1998. Upregulation of a new microglial gene, mrf-1, in response to programmed neuronal cell death and degeneration. *J Neurosci,* 18**,** 6358-69.

TANG, Y. & LE, W. D. 2016. Differential Roles of M1 and M2 Microglia in Neurodegenerative Diseases. *Molecular Neurobiology,* 53**,** 1181-1194.

UNOKI, N., MURAKAMI, T., NISHIJIMA, K., OGINO, K., VAN ROOIJEN, N. & YOSHIMURA, N. 2010. SDF-1/CXCR4 contributes to the activation of tip cells and microglia in retinal angiogenesis. *Invest Ophthalmol Vis Sci,* 51**,** 3362-71.

VAN LOO, G., SAELENS, X., VAN GURP, M., MACFARLANE, M., MARTIN, S. J. & VANDENABEELE, P. 2002. The role of mitochondrial factors in apoptosis: a Russian roulette with more than one bullet. *Cell Death and Differentiation,* 9**,** 1031-1042.

VILLANI, A., BENJAMINSEN, J., MORITZ, C., HENKE, K., HARTMANN, J., NORLIN, N., RICHTER, K., SCHIEBER, N. L., FRANKE, T., SCHWAB, Y. & PERI, F. 2019. Clearance by Microglia Depends on Packaging of Phagosomes into a Unique Cellular Compartment. *Developmental Cell,* 49**,** 77-+.

WALSH, C. E. & HITCHCOCK, P. F. 2017. Progranulin regulates neurogenesis in the developing vertebrate retina. *Developmental Neurobiology,* 77**,** 1114-1129.

WALTON, E. M., CRONAN, M. R., BEERMAN, R. W. & TOBIN, D. M. 2015. The Macrophage-Specific Promoter mfap4 Allows Live, Long-Term Analysis of Macrophage Behavior during Mycobacterial Infection in Zebrafish. *Plos One,* 10.

WESSELY, O., AGIUS, E., OELGESCHLAGER, M., PERA, E. M. & DE ROBERTIS, E. M. 2001. Neural induction in the absence of mesoderm: beta-catenin-dependent expression of secreted BMP antagonists at the blastula stage in Xenopus. *Developmental Biology,* 234**,** 161-173.

WESTERFIELD, M. 1993. *The zebrafish book : a guide for the laboratory use of zebrafish (Brachydanio rerio),* Eugene, OR, M. Westerfield.

WILSON, P. A., LAGNA, G., SUZUKI, A. & HEMMATIBRIVANLOU, A. 1997. Concentration-dependent patterning of the Xenopus ectoderm by BMP4 and its signal transducer smad1. *Development,* 124**,** 3177-3184.

WILSON, S. I., RYDSTROM, A., TRIMBORN, T., WILLERT, K., NUSSE, R., JESSELL, T. M. & EDLUND, T. 2001. The status of Wnt signalling regulates neural and epidermal fates in the chick embryo. *Nature,* 411**,** 325-330.

WITTING, A., MULLER, P., HERRMANN, A., KETTENMANN, H. & NOLTE, C. 2000. Phagocytic clearance of apoptotic neurons by Microglia/Brain macrophages in vitro: involvement of lectin-, integrin-, and phosphatidylserine-mediated recognition. *J Neurochem,* 75**,** 1060-70.

WU, S., XUE, R., HASSAN, S., NGUYEN, T. M. L., WANG, T., PAN, H., XU, J., LIU, Q., ZHANG, W. & WEN, Z. 2018. Il34-Csf1r Pathway Regulates the Migration and Colonization of Microglial Precursors. *Dev Cell,* 46**,** 552-563.e4.

XU, J., WANG, T., WU, Y., JIN, W. & WEN, Z. 2016. Microglia Colonization of Developing Zebrafish Midbrain Is Promoted by Apoptotic Neuron and Lysophosphatidylcholine. *Dev Cell,* 38**,** 214-22.

XU, J., ZHU, L., HE, S. C., WU, Y., JIN, W., YU, T., QU, J. Y. & WEN, Z. L. 2015. Temporal-Spatial Resolution Fate Mapping Reveals Distinct Origins for Embryonic and Adult Microglia in Zebrafish. *Developmental Cell,* 34**,** 632-641.

YAMAGUCHI, M., FUJIMORI-TONOU, N., YOSHIMURA, Y., KISHI, T., OKAMOTO, H. & MASAI, I. 2008. Mutation of DNA primase causes extensive apoptosis of retinal neurons through the activation of DNA damage checkpoint and tumor suppressor p53. *Development,* 135**,** 1247-57.

YAMAGUCHI, M., TONOU-FUJIMORI, N., KOMORI, A., MAEDA, R., NOJIMA, Y., LI, H., OKAMOTO, H. & MASAI, I. 2005. Histone deacetylase 1 regulates retinal neurogenesis in zebrafish by suppressing Wnt and Notch signaling pathways. *Development,* 132**,** 3027-43.

YUAN, Z. M., HUANG, Y., WHANG, Y., SAWYERS, C., WEICHSELBAUM, R., KHARBANDA, S. & KUFE, D. 1996. Role for c-Abl tyrosine kinase in growth arrest response to DNA damage. *Nature,* 382**,** 272-4.

ZHANG, X. M. & YANG, X. J. 2001. Regulation of retinal ganglion cell production by Sonic hedgehog. *Development,* 128**,** 943-957.

ZUSSO, M., METHOT, L., LO, R., GREENHALGH, A. D., DAVID, S. & STIFANI, S. 2012. Regulation of Postnatal Forebrain Amoeboid Microglial Cell Proliferation and Development by the Transcription Factor Runx1. *Journal of Neuroscience,* 32**,** 11285-11298.